Magnetic and Dielectric Properties of $Cu_{3-x}Ni_xWO_6$ and $Cu_3W_{1-x}Mo_xO_6$

Dan Xu

A THESIS SUBMITTED TO THE FACULTY OF GRADUATE STUDIES IN PARTIAL FULFILMENT OF THE REQUIREMENTS
FOR THE DEGREE OF
MASTER OF SCIENCE OF PHYSICS
In
The Faculty of Mathematics and Sciences
Department of Physics

Brock University
St. Catharines, Ontario
November 2017

Abstract

Cu_3WO_6 is a compound with an interesting coordination chemistry for both Cu and W. In this research, all samples were made by using the standard Solid Phase Reaction method with and without any doping. Using Powder x-ray diffraction and Rietveld analysis, we did not observe any distortion of the cubic crystal. Ni substitution for Cu, and Mo substitution for W, will act as a negative pressure on the lattice parameter of Cu_3WO_6. Magnetization measurements of $Cu_{3-x}Ni_xWO_6$ indicate that all compounds undergo an antiferromagnetic phase transition at the Néel temperature. However, a significant change was observed in Néel temperature with Ni's concentration. All compounds show Curie–Weiss antiferromagnetic behavior at high temperatures. The value of the μ_{eff} is close to the theoretical calculation in Cu_3WO_6. And the magnitude of μ_{eff} (exp) increases with Ni's concentration. A spin-singlet ground state with energy gap at low temperatures was observed for all compounds. The energy gap Δ is decreasing with the increasing concentration of Ni.

The dielectric permittivity as a function of temperature and different frequency from1 kHz to 20 kHz for all samples, were investigated. A peak in dielectric loss ε'' appears between 150 K to 260 K in all samples of $Cu_{3-x}Ni_xWO_6$. The peak position has a linear relationship with $\log_{10}(f)$ as a function of temperaure. The doping of Ni causes a gradual shift in the peak position. The activation energy E_a is decreasing with the increasing of Ni's concentration.

Contents

List of Figures

List of Tables

Acknowledgements

I would like to thank everybody that has helped me during this research, especially the members of my committee Dr. Maureen Reedyk, Dr. David A. Crandles and Dr. Fereidoon S. Razavi, my thesis supervisor. Dr. Razavi is not only a wonderful, patient teacher and effective supervisor, but he also taught me numerous, invaluable key skills during my graduate study.

Also, I would like to thank Biljana Indovski and Darren Hicks for the productive discussions and their help during this research.

A thank you to the whole Physics Department, all the faculty members and all the students for making this experience as significant and memorable as it should be. A heartfelt thank you to Ms. Eléonore Reinéry for her diligent proof-reading of this thesis.

Lastly, I would like to express a big thank you to my husband, Frank and my parents for their strong, continuing support and enduring encouragement these past two years of my studies.

Chapter 1

Introduction

Transition metal oxides represent many compounds with properties such as being good insulators, semiconductors, metals, or superconductors. An external control parameter, for example, temperature, pressure or chemical composition, may cause substantial changes in properties in these compounds such as a metal-to-insulator transition (MIT). The change of physical properties may cause changes in the electronic structure and electronic properties. The electrical, magnetic and optical properties of transition metal oxides have important technical applications, for example, a widespread use of ferrite in electronic equipment such as ferromagnetic insulators in electrical circuits, the core of coils in microwave frequency devices and computer memory core elements [1].

Copper-Tungsten-Oxide systems have been reported since 1957.Materials that have been investigated include $CuWO_4$, Cu_xWO_3 and $Cu_xWO_{3+\delta}$ [2-5]. Cu_3WO_6 is a compound with an interesting coordination chemistry for both Cu and W.

There have been few reports on electronic and magnetic properties of Cu_3WO_6 [6-9]. In 1969, Elizabeth Gebert and Lars Kihlborg were the first to synthesize this compound (Cu_3WO_6) and characterize and refine its structure [6]. They found that the symmetry of Cu_3WO_6 is cubic, with space group $Pa\bar{3}(T_h^6)$ and that the unit cell parameter a is 9.797(±3) Å. The structure of Cu_3WO_6 is illustrated in Figure 1.1. They described the structure as being composed of distorted WO_6

octahedra and CuO_5 triangular bi-pyramids, which share corners and edges in a rather complicated way (Figure 1.2). Each octahedron is linked to twelve (12) bi-pyramids and each bi-pyramid to four (4) octahedra and six (6) other CuO_5 bi-pyramids. Six CuO_5 bi-pyramids sharing edges, form a staggered ring and a WO_6 group on either side of the ring closed the hole in the center [6].

Frank Benko and Frans Koffyberg by using photo-electrochemical measurement [7], reported that Cu_3WO_6 is an n-type semiconductor with a band gap of the order of 1.85eV.

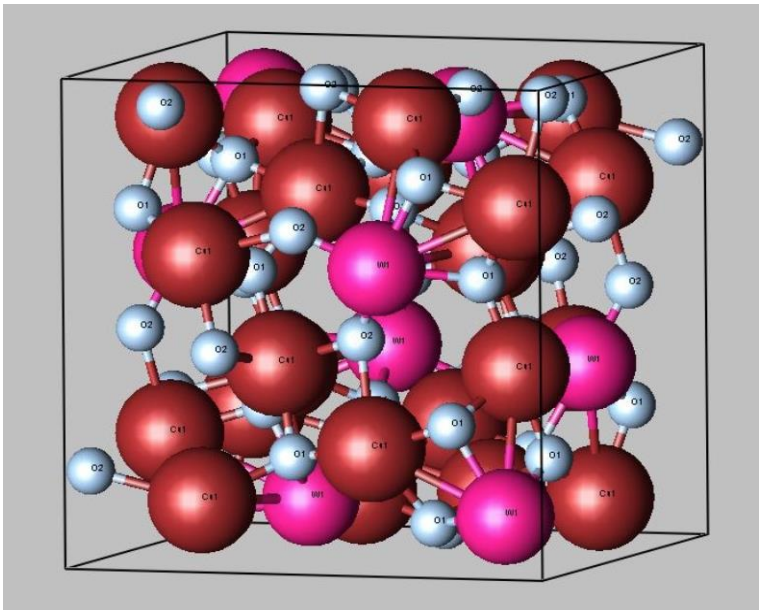

Fig. 1.1 A stereo pair showing the unit cell of Cu_3WO_6.

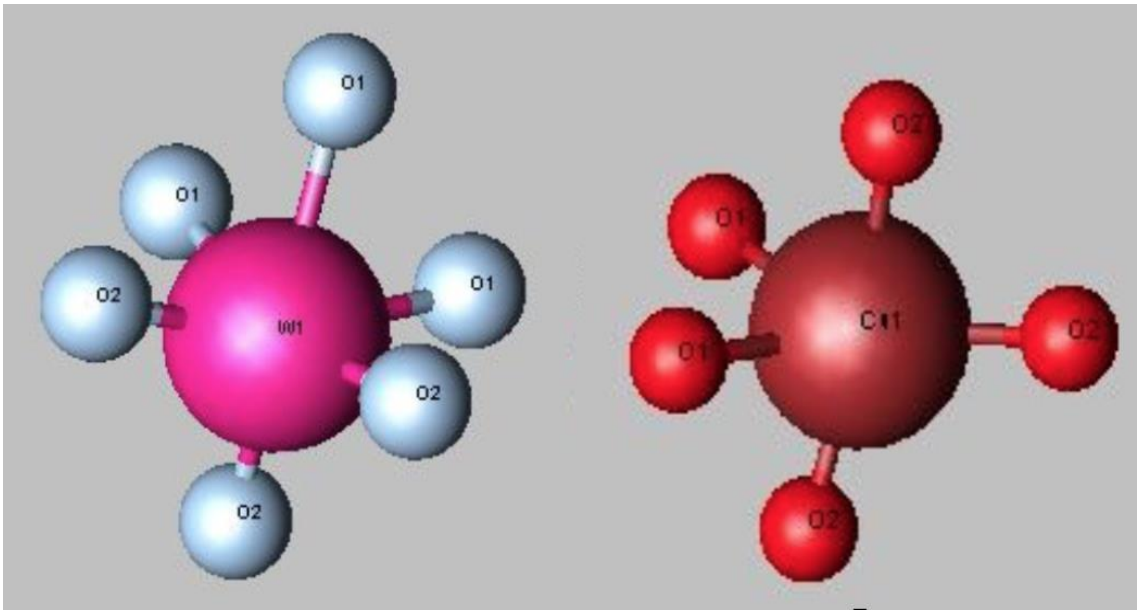

Fig. 1.2 Distorted WO_6 octahedra and CuO_5 triangular bi-pyramids.

In 1995, Muneaki Hase and Kunimitsu Uchinokura noted that a new kind of magnetic system with a spin gap might exist in Cu_3WO_6 [8]. They measured the magnetic susceptibility using a Superconducting Quantum Interference Device (SQUID) magnetometer. The magnetic susceptibility of polycrystalline Cu_3WO_6 exhibits a sharp reduction at low temperatures. The spin susceptibility is nearly equal to 0 near 0K, since a typical value of an orbital part of χ (T) is about 1×10^{-4} emu/Cu^{2+} mol. They interpreted their results based on the existence of a spin-singlet ground state with the gap energy of about 110 K [8] (Figure 1.3). No phase transition was observed in the specific heat [10], therefore, this ground state is not caused by any transition, but it is intrinsic to Cu_3WO_6. The broad maximum was around 130 K and is associated to a low-dimensional antiferromagnetic (AF) system, with an AF exchange interaction.

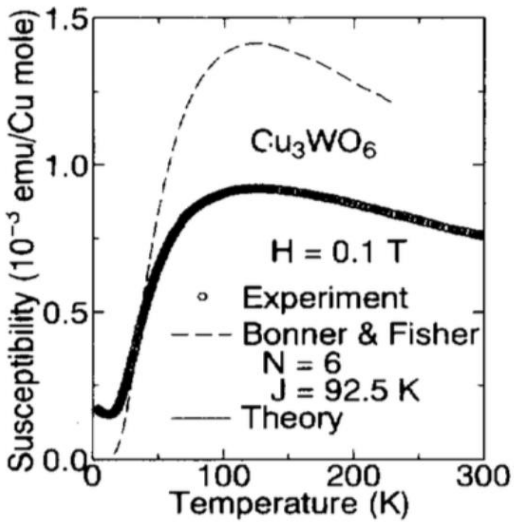

Fig. 1.3 The temperature dependence of the magnetic susceptibility of polycrystalline Cu_3WO_6 in 0.1T (open circle). The dashed curve denotes the susceptibility of the AF ring with 6 spins (S=1/2) calculated by Bonner and Fisher [11].

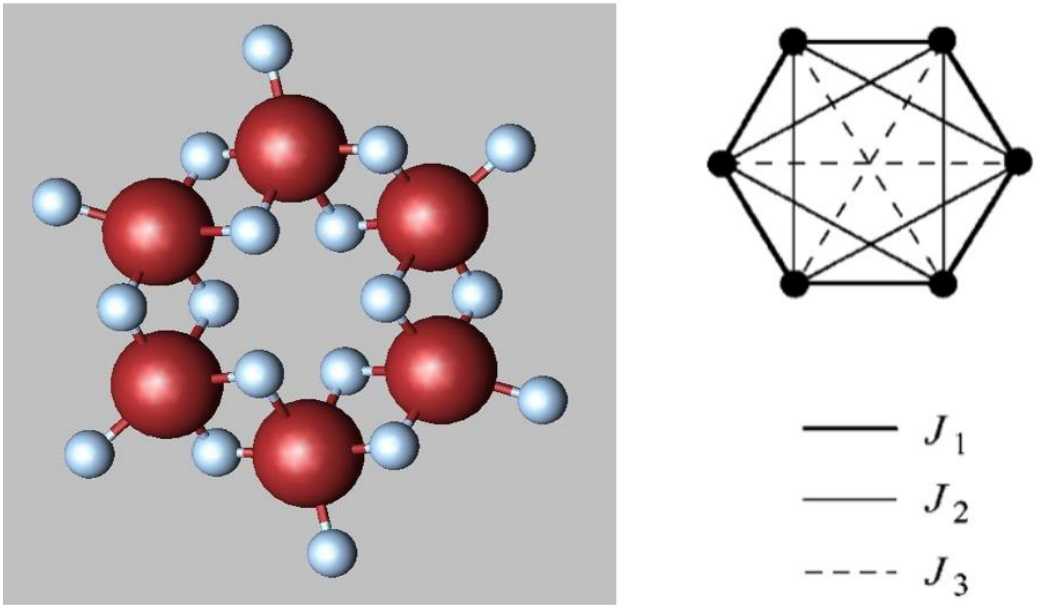

Fig. 1.4 (Left) A six-spin ring in Cu_3WO_6, formed by CuO_5 bi-pyramids, red and white ball represent Cu^{2+} and O^{2-} ions, respectively. Cu^{2+} ions in the ring are coupled by the nearest-neighbour interactions. (Right) The first (J1), the second (J2) and the third (J3) nearest-neighbour interactions are within the ring [8].

Later on, Hase and Uchinokura carried out neutron scattering studies of magnetic excitation in Cu_3WO_6 [9]. The neutron scattering results confirmed that Cu_3WO_6 is a spin-gap system containing magnetic rings, which consist of six *S=1/2* nearest neighbour spins coupling antiferromagnetically (Figure 1.4). They reported that the distance between two Cu^{2+} ions located in the two edge-sharing bi-pyramids is 2.99Å, while the distance in the two corner-sharing bi-pyramids is 3.22 or 3.53Å [6]. They considered that the edge sharing interaction is significantly stronger than the corner-sharing ones. This would lead to the dominant nearest-neighbour coupling of six *S=1/2* Cu^{2+} spins in the ring. These six-spin rings, however, are not isolated perfectly since Cu^{2+} ions in a ring are also coupled with those in other rings by the corner-sharing coupling. At 11 K, the Neutron results show three peak positions at 11, 14, and 18 meV [9]; these peaks are associated with the spin gaps as they were temperature independent up to 40 K; above 60 K, the peaks become negligible and they disappeared completely above 80 K. Hase and Uchinokura also observed a strong presence of phonon vibrations. They associated the 18 meV peak with a phonon vibration. They were able to fit their data obtained by neutron scattering to a model that considered exchange interaction for the first and second and third nearest neighbour for the Cu S=1/2 ring. However, this model failed to account for the experimental susceptibility data, see Figure 1.3.

The Muon spin relaxation in the Cu_3WO_6 experiment failed to observe an energy gap in contrast to what was observed in neutron scattering as well as in the susceptibility measurement [9]. The Muon spin relaxation measurements indicate only spin freezing at 7 K which it disappeared upon doping with only 1% of non-magnetic Zn. Fudamoto et al also reported a similarity between the observations of charge ordering of $Na_xV_2O_5$ by the Muon spin relaxation experiment to that of Cu_3WO_6.

For a better understanding of the properties of Cu_3WO_6 and to shed some light on some of the discrepancies observed previously, we examined the effect of two different types of doping on electronic and magnetic properties of this compound. First, we substituted Ni with S=1 for Cu, and second, we substituted Mo with a slightly different electronic configuration for W (tungsten). We examined their magnetic susceptibility and dielectric properties as a function of temperatures and magnetic fields from 1.7 K to 400 K.

In Chapter 2, preparation of samples and x-ray results are discussed.

In Chapter 3, the results of measurements of the magnetic properties are discussed.

In Chapter 4, the results of measurements of the dielectric properties are presented.

In Chapter 5, the conclusion, and possible future work on this compound are proposed.

Chapter 2

Samples Preparation and X-Ray Measurements and Results

2.1 Samples Preparation

The samples were prepared by the standard Solid Phase Reaction Method. High purity WO_3, CuO, NiO and MoO_3, powders (all≥99.9%) were thoroughly mixed in an alumina mortar (Figure 2.1) according to the chemical reaction equation 2.1 and 2.2.

$$(3-x)\mathrm{CuO} + x\mathrm{NiO} + \mathrm{WO_3} \rightarrow \mathrm{Cu_{3-x}Ni_xWO_6} \quad (2.1)$$

$$3\mathrm{CuO} + (1-x)\mathrm{WO_3} + x\mathrm{MoO_3} \rightarrow \mathrm{Cu_3W_{1-x}Mo_xO_6} \quad (2.2)$$

The powders were calcined at 800^{o}C for 60 hours (h). After grinding, these pellets were pressed under a pressure of 1.8 Kbar and sintered at 800^{o}C for 60h with intermediate grinding and repressing. All samples were quenched in ambient air at the end of sintering treatments. In total, 8 samples were made by using the standard Solid Phase Reaction Method with and without any doping, Cu_3WO_6, $Cu_{3-x}Ni_xWO_6$ (x=0.01 to 0.1) and $Cu_3W_{1-x}Mo_xO_6$ (x=0.01 to 0.05).

Fig. 2.1 The powder of Cu_3WO_6 in alumina mortar.

2.2 X-Ray Measurements

The Rigaku powder X-Ray diffractometer (XRD) with SmartLab software (Figure 2.2) was used for measuring X-ray diffraction patterns of the samples. Its most novel feature is the SmartLab Guidance software, which provides the user with an intelligent interface that gives guidance through the intricacies of each experiment [12]. The phase content of the pellets was checked after each heat treatment by X-ray powder diffraction in Precise Theta/2-Theta Scan (Bragg-Brentano focusing) using CuKα radiation. The scattered X-rays were counted at the angle range of 2θ=10°- 90° with 0.01 increments for all samples.

Fig. 2.2 The internal structure of the Rigaku powder X-ray diffractometer.

2.3 X-Ray Results of Cu_3WO_6

The powder diffraction pattern of Cu_3WO_6 is shown in Figure 2.3. XRD patterns were analyzed by using PDLX software (Rigaku), an application software package which includes crystal structure analysis, Rietveld and phase identification. Crystal structure parameters were obtained using CIF (crystal information file) and ICSD (Inorganic crystal structure database).

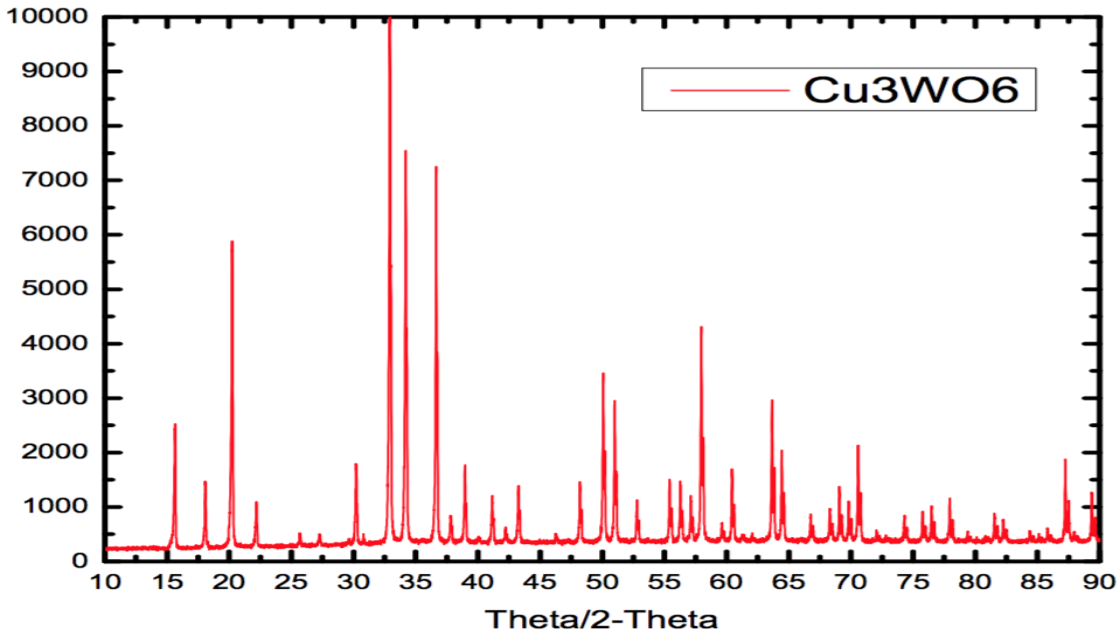

Fig. 2.3 X-Ray diffraction of Cu_3WO_6 powder at the angle range of 2θ=10°- 90°.

The report of Cu_3WO_6 can be seen in the Appendix and it was indexed on the basis of a cubic unit cell (Table 2.1). The lattice constant of Cu_3WO_6 was calculated from the powder patterns and was found to be 9.7962(3)Å with the space group $Pa\bar{3}(T_h^6)$. And the volume of unit cell is 940.0975 $Å^3$. From Rietveld analysis of the X-Ray data, the coordinates of atoms is given by fraction in Table 2.2 where B is temperature factor. The crystal structure is shown in Figure 2.4. Our results agree well with the published experimental results.

Table 2.1 The crystal structure parameters for Cu_3WO_6.

Phase name	**Formula**	**Space group**	**Phase reg. detail**	**DB card number**
Copper Tungsten Oxide	Cu_3WO_6	205 : Pa-3	ICDD (PDF2.DAT)	01-071-2208

a(Å) = **b**(Å) = **c**(Å)	**α** (deg) = **β** (deg) = **γ** (deg)	V(Å^3)
9.7962(3)	90.00	940.0975

Table 2.2 Position of atoms in cubic crystal of Cu_3WO_6.

Atom Position	***x***	***y***	***z***	**B**
W *8c*	0.6167	0.1167	0.3833	0
Cu *24d*	0.7840	0.3616	0.5955	0
O (1) *24d*	0.2245	-0.5479	0.4404	1.975
O (2) *24d*	0.5850	0.2986	0.6691	1.575

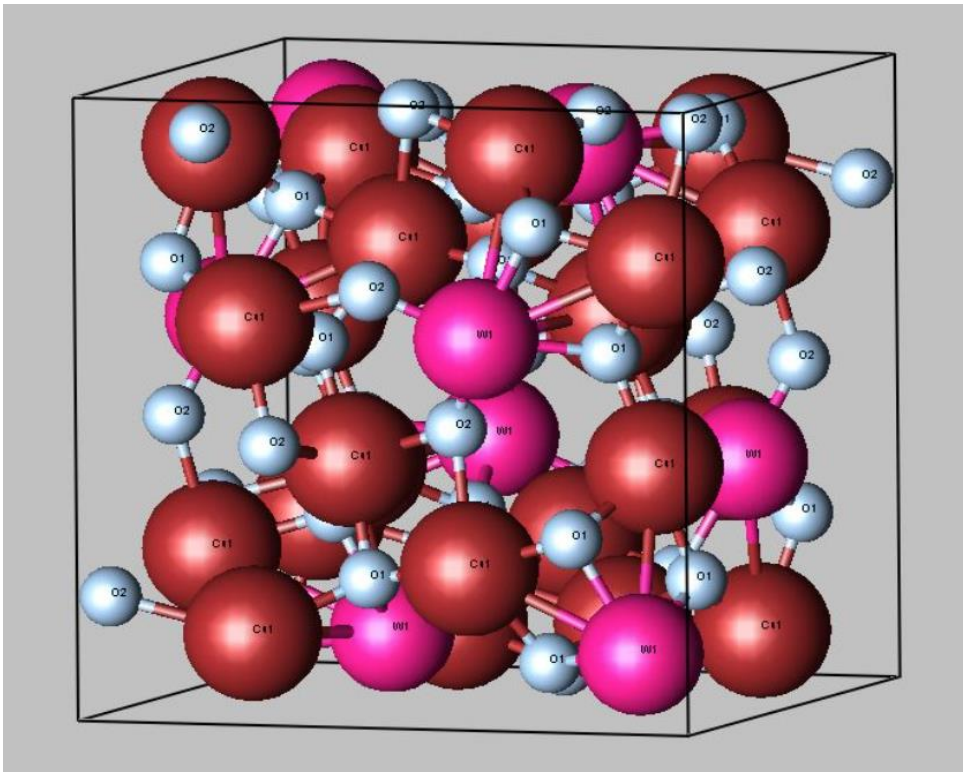

Fig. 2.4 Cu_3WO_6 unit cell, all atoms are labeled with red balls for Cu^{2+}, magenta balls for W^{6+} and gray balls for O^{2-}.

2.4 X-Ray Results of $Cu_{3-x}Ni_xWO_6$

The X-ray patterns of $Cu_{3-x}Ni_xWO_6$ (x=0.01 to 0.1) were measured under the same conditions as used for Cu_3WO_6. Figure 2.5 shows the X-Ray diffraction patterns of $Cu_{3-x}Ni_xWO_6$ powders with CuKα at room temperature. The difference between Cu_3WO_6 and the doped samples, for the range of 2θ from 15° to 45°, is shown in Figure 2.6 and Figure 2.7. The results showed that substitution of Ni for Cu causes a gradual shift in the X-Ray diffraction patterns. Figure 2.6 and Figure 2.7 show the superimposed patterns of Cu_3WO_6 and $Cu_{3-x}Ni_xWO_6$, which indicate the presence of two impurity phases. Using PDLX software and Rietveld analysis, it was

found that the impurity phases belong to CuO and $Cu_{1-\delta}Ni_{\delta}WO_4$ by matching data from the database.

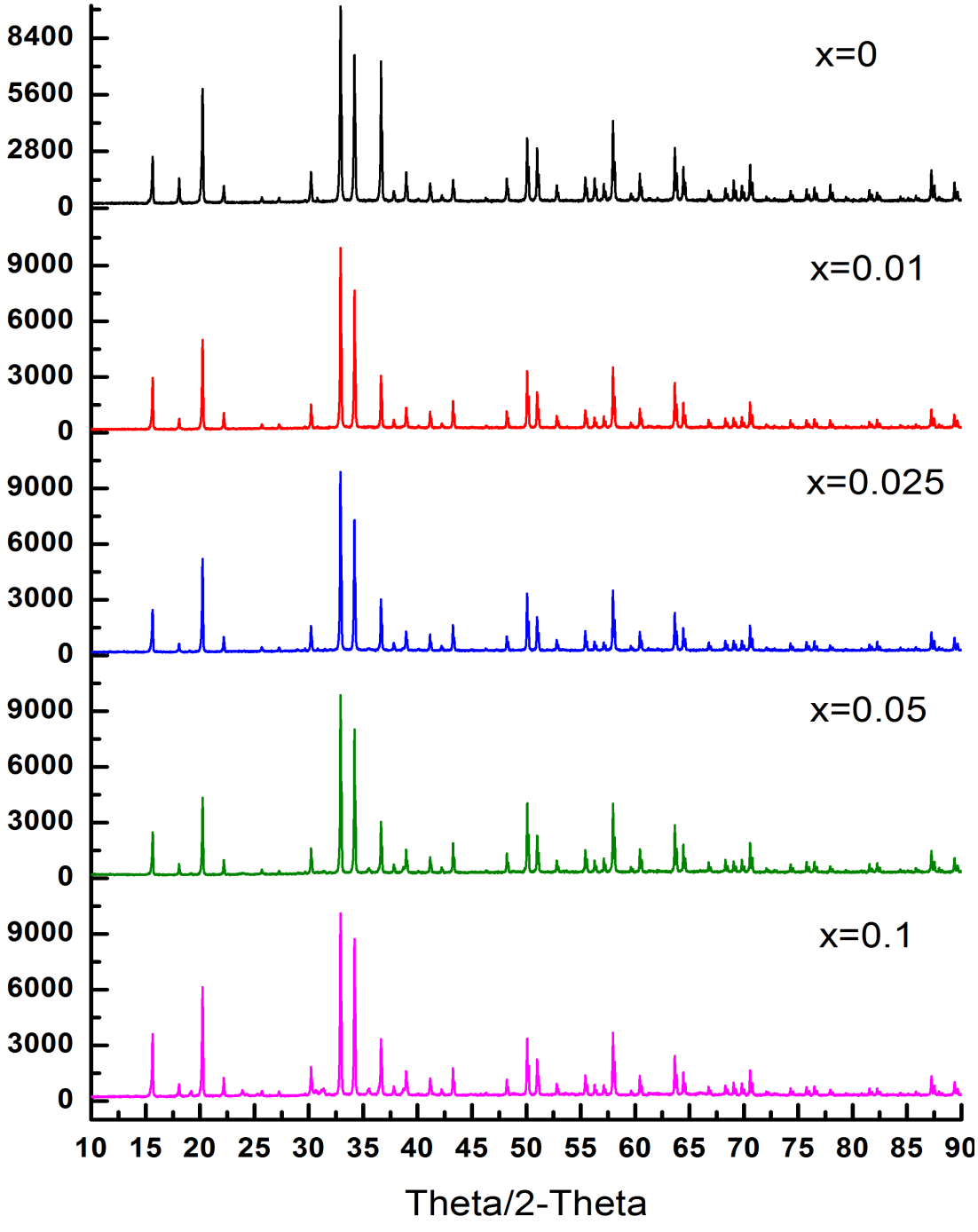

Fig. 2.5 X-Ray diffraction patterns of $Cu_{3-x}Ni_xWO_6$ (x=0.01 to 0.1) powder for 2θ between 10° to 90°.

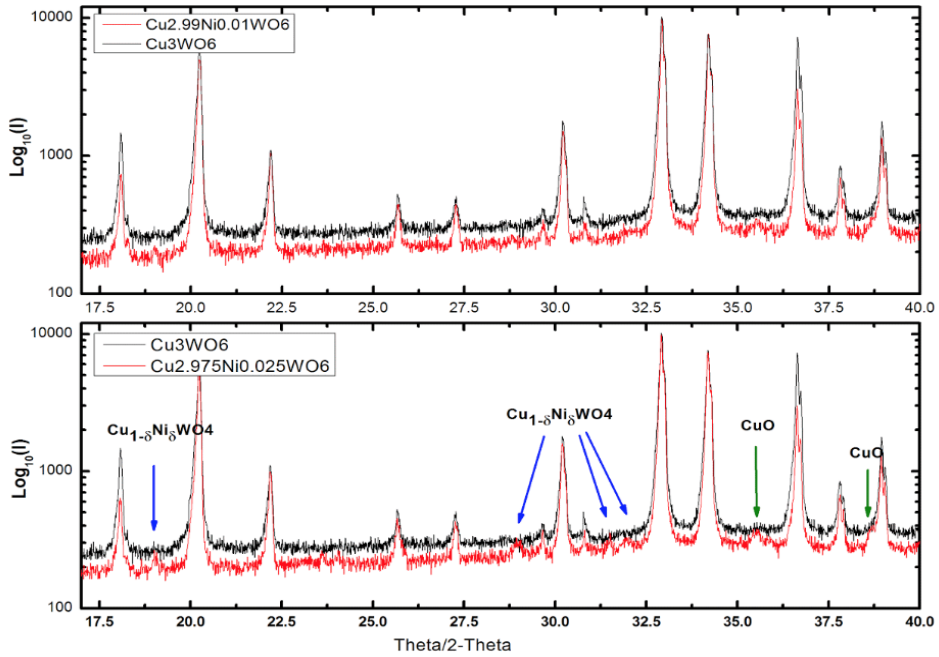

Fig. 2.6 Superposition of the patterns of Cu_3WO_6 with $Cu_{2.99}Ni_{0.01}WO_6$ & $Cu_{2.975}Ni_{0.025}WO_6$ in the 2θ range of 15° to 45°.

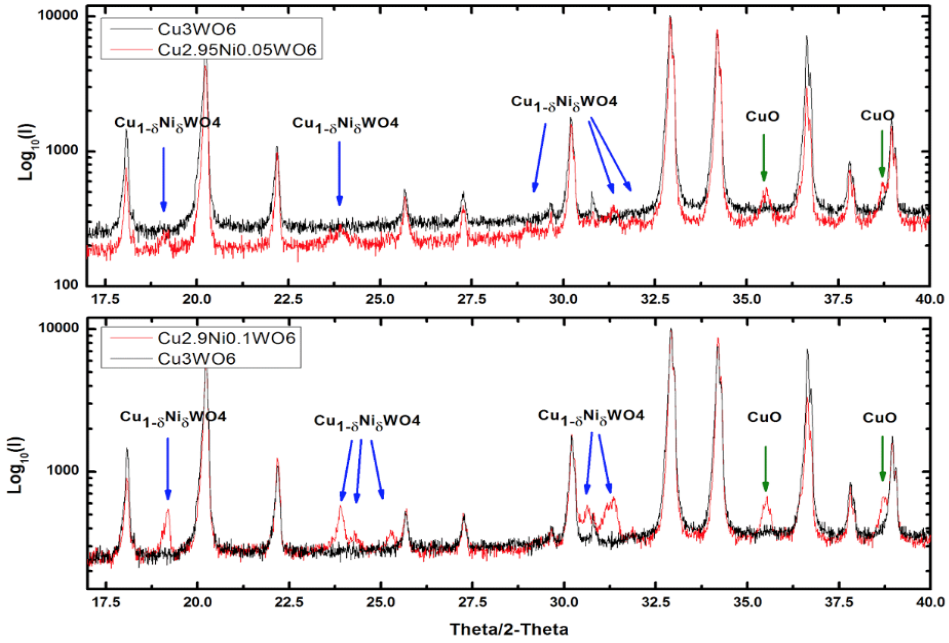

Fig. 2.7 Superposition of the patterns of Cu_3WO_6 with $Cu_{2.95}Ni_{0.05}WO_6$ & $Cu_{2.9}Ni_{0.1}WO_6$ in the 2θ range of 15° to 45°.

Table 2.3 The crystal parameters of $Cu_{3-x}Ni_xWO_6$ (x=0 to 0.1).

$Cu_{3-x}Ni_xWO_6$	**a (Å)**	**Volume (Å^3)**
① x=0	9.7962(3)	940.09(5)
② x=0.01	9.7959(2)	940.02(4)
③ x=0.025	9.79564(19)	939.94(3)
④ x=0.05	9.79532(17)	939.84(3)
⑤ x=0.10	9.7944(2)	939.58(4)

The X-ray analysis reports of $Cu_{3-x}Ni_xWO_6$ can be found in the Appendix. Substituting Ni (nickel) for Cu (copper) causes a gradual decrease of the crystal lattice constant (see Table 2.3). The ionic radius of Cu^{2+} is 73pm and for Ni^{2+} is 70pm. Thus, it is expected that the Ni substitution for Cu will act as a negative pressure on the lattice parameter of Cu_3WO_6.

The results of Table 2.3 indicate that initially all Ni was substituted for the missing Cu. However, afterwards, the substitution was minimal as can be seen in Figure 2.8. The variation of the lattice parameter as a function of Cu concentration is minimal. We did not observe any distortion of the cubic crystal. If Ni was completely substituted for the missing Cu, and approximating a linear relation between lattice parameter change and Ni concentration the size of the lattice parameter would follow the red line in Figure 2.8. Comparing the experimental data and theoretical data, the experimental lattice parameters varied to a lesser extent with the addition of Ni compared to the theoretical prediction. This implies is that Ni is not completely substituted for Cu. With the doping of Ni, Ni^{2+}, Cu^{2+} and WO_4^{2-} form into a $Cu_{\delta}Ni_{1-\delta}WO_4$

compound, and some excess of copper oxide CuO is also left in the solid solution. As a result, some impurity peaks belonging to $Cu_{\delta}Ni_{1-\delta}WO_4$ and CuO are found in the $Cu_{3-x}Ni_xWO_6$ powder X-Ray diffraction. Using the change of volume, Table 2.3**,** we can estimate the amount of Ni in each sample of $Cu_{3-x}Ni_xWO_6$ (see Table 2.4). The concentrations of different phases calculated from the Rietveld analysis, are also given in Table 2.4.

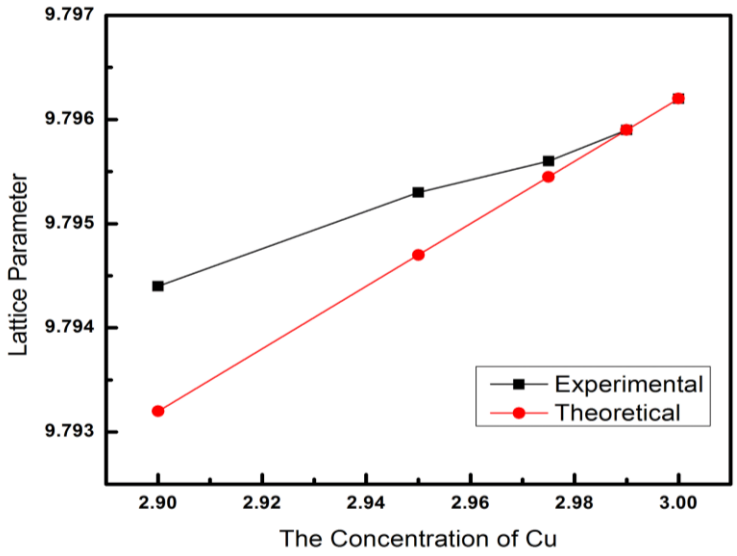

Fig. 2.8 Lattice parameter of $Cu_{3-x}Ni_xWO_6$ (x=0 to 0.1) depends on the concentration of Cu.

Table 2.4 The Content of $Cu_{3-x}Ni_xWO_6$ (x=0 to 0.1).

$Cu_{3-x}Ni_xWO_6$	**Content (%) from Rietveld analysis for different phases**	
① x=0	Cu_3WO_6	100%
② x=0.01	$Cu_{2.99}Ni_{0.01}WO_6$	100%
③ x=0.025	$Cu_{2.98}Ni_{0.02}WO_6$ CuO $Cu_{0.93}Ni_{.070}WO_4$	90(2)% 3.4(12)% 6.6(6)%
④ x=0.05	$Cu_{2.97}Ni_{0.03}WO_6$ CuO $Cu_{0.85}Ni_{0.15}WO_4$	83(699)% 5(499)% 10(778)%
⑤ x=0.1	$Cu_{2.94}Ni_{0.06}WO_6$ CuO $Cu_{0.73}Ni_{0.27}WO_4$	80.8160% 6.5297% 12.71418%

2.5 X-Ray Results of $Cu_3W_{1-x}Mo_xO_6$

The XRD patterns of $Cu_3W_{1-x}Mo_xO_6$ (x=0.01 to 0.05) were measured under the same conditions as Cu_3WO_6. Figure 2.9 shows the X-Ray diffraction patterns of $Cu_3W_{1-x}Mo_xO_6$ powders using CuKα at room temperature. The differences between Cu_3WO_6 and the doped samples, for the range of 2θ from 15° to 45°, are shown in Figure 2.10 and Figure 2.11. The results show that the substitution of Mo for W causes a gradual shift in the X-Ray diffraction patterns. Figure 2.10 and Figure 2.11 show the superimposed patterns of Cu_3WO_6 and Cu_3W_{1-}

$_xMo_xO_6$, which indicate the presence of two impurity phases. Using PDLX software, and Rietveld analysis, it was found that the impurity phases are CuO and $CuW_{1-\delta}Mo_\delta O_4$ from the matching database.

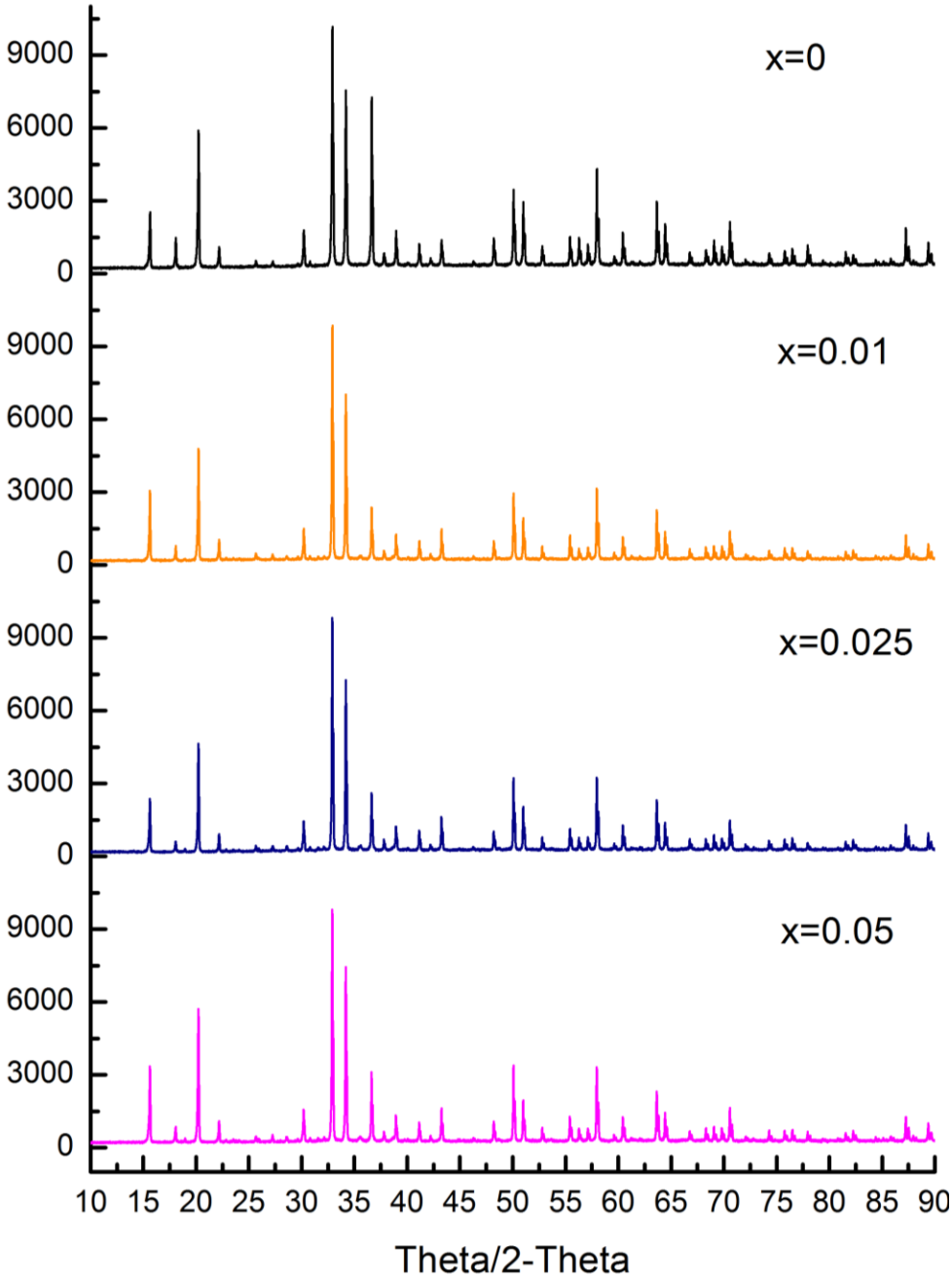

Fig. 2.9 X-Ray diffraction of $Cu_3W_{1-x}Mo_xO_6$ (x=0.01 to 0.05) powder at the angle range of 2θ=10°- 90°.

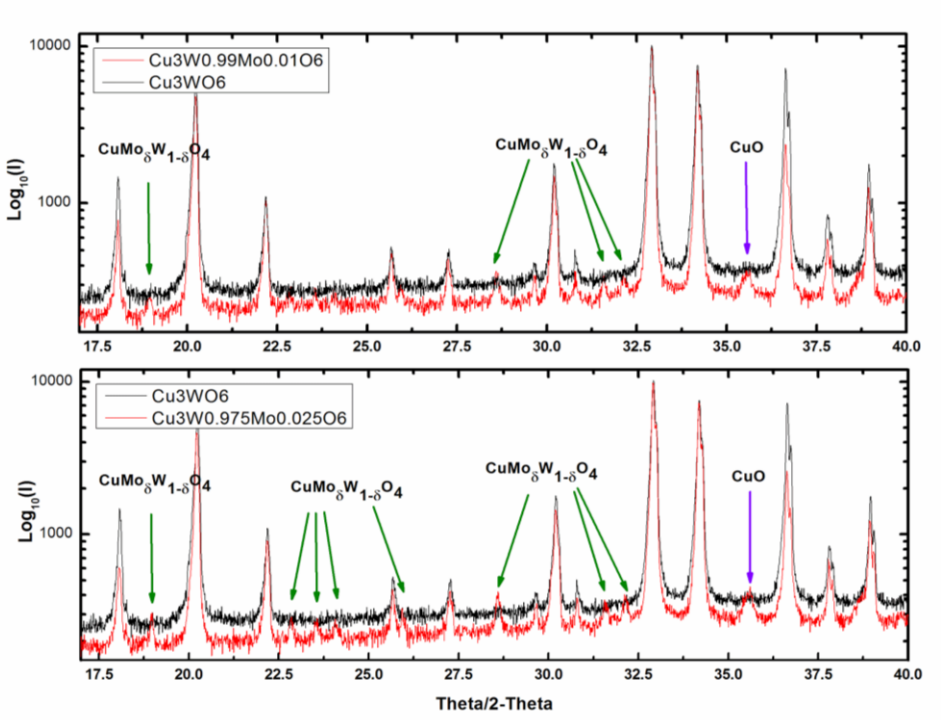

Fig. 2.10 Superposition of the patterns of Cu_3WO_6 with that of $Cu_3W_{0.99}Mo_{0.01}O_6$ & $Cu_3W_{0.975}Mo_{0.025}O_6$ in the angle range of 2θ=15°- 45°.

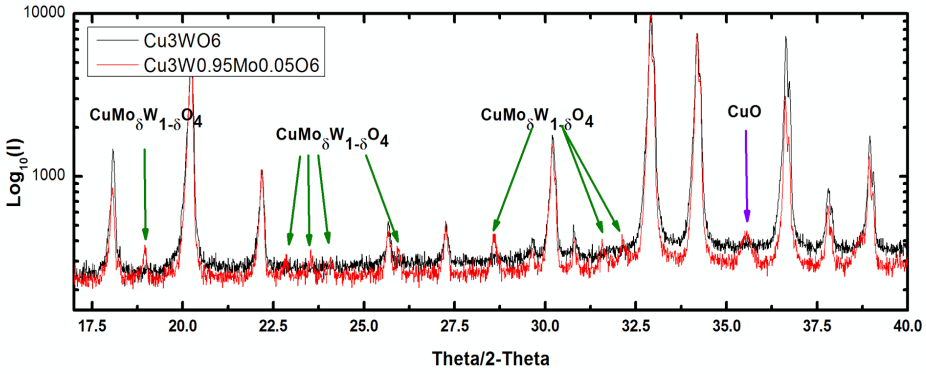

Fig. 2.11 Superposition of the patterns of Cu_3WO_6 with that of $Cu_3W_{0.95}Mo_{0.05}O_6$ in the angle range of 2θ=15°- 45°.

Table 2.5 The crystal parameters of $Cu_3W_{1-x}Mo_xO_6$ (x=0 to 0.05).

$Cu_3W_{1-x}Mo_xO_6$	a(Å)	V(Å^3)
① x=0	9.7962(3)	940.09(5)
② x=0.01	9.79439(15)	939.58(3)
③ x=0.025	9.7936(2)	939.36(4)
④ x=0.05	9.7933(2)	939.26(4)

Substitution of W (Tungsten) with Mo causes a gradual decrease of the lattice parameter (Table 2.5). The substitution of Mo for W is minimal as can be seen by the small amount of change in the lattice parameter of Cu_3WO_6. From the X-ray analysis, it is clear that Mo cannot replace W with complete efficacy in Cu_3WO_6 since CuO as well as $CuW_{1-\delta}Mo_\delta O_4$ are also formed as obtained from the Rietveld analyses of XRD patterns. Table 2.6 shows the composition analyses of each sintered sample. The small changes of the lattice parameter in Table 2.5 indicate that, either small amounts of Mo replace the W vacancies or that there are some vacancies generated by reduction of Cu atoms.

Table 2.6 The Content of $Cu_3W_{1-x}Mo_xO_6$ (x=0 to 0.05).

$Cu_3W_{1-x}Mo_xO_6$	Content (%)	
① x=0	Cu_3WO_6	100%
② x=0.01	$Cu_3W_{0.988}Mo_{0.012}O_6$ CuO $CuWO_4$	85.8(14)% 4.8(6)% 9.3(8)%
③ x=0.025	$Cu_3W_{0.983}Mo_{0.017}O_6$ CuO $CuW_{0.869}Mo_{0.131}O_4$	93(2)% 2.4(4)% 4.6(11)%
④ x=0.05	$Cu_3W_{0.981}Mo_{0.019}O_6$ CuO $CuW_{0.637}Mo_{0.363}O_4$	91(3)% 3.3(19)% 5.7(11)%

Chapter 3

Magnetic Measurements and Results

3.1 Overview of Magnetic Properties

Magnetism is a very important physical property of materials and is widely used in modern science and technology. In the magnetic field the material exhibits a certain magnetization $\vec{M}$, where $\vec{M} = \sum_i \frac{\vec{\mu_i}}{V}$. In a linear material $\vec{M} = \chi_m \vec{H}$, where $\vec{H}$ is the applied field. Diamagnetic materials have χ<0; Paramagnetic materials have χ>0; In ferromagnetic materials, χ has a singularity. That is $\vec{M} \neq 0$ even when $\vec{H} = 0$. Any substance is composed of atoms, and atoms are composed of nuclei and electrons. Modern physics proves that each electron has intrinsic $(\vec{S})$ and orbital angular momentum $(\vec{L})$, and the magnetism is due to the connection of magnetic moment to angular momentum.

The nucleus also has a magnetic moment, but its magnetic moment is very small, about 1/2000 of the electronic magnetic moment, which be ignored generally. The theory proves that when an electron orbital in the atom is filled, the sum of the magnetic moments of the electron is zero, and they do not contribute to the atomic magnetic moment. If all electron orbitals in the atom are filled, the atom has no magnetic moment (an atom with an even number of electrons). If the sum of the electron magnetic moments of the electron orbitals is not zero, then the atom has a magnetic moment (an atom with an odd number of electrons). This magnetic moment is called the intrinsic magnetic moment of the atom.

Paramagnetism

The main characteristic of paramagnetic materials is that there is a net electronic magnetic moment. However, there is no strong interaction between the atomic (or molecular) magnetic moments, so the atomic moments are in disordered orientation under the hot commotion, and the atomic magnetic moments cancel each other without coercivity. However, when subjected to the applied magnetic field, these irregularly arranged atomic magnetic moments are arranged in the direction of the applied magnetic field. Therefore, the total effect is to have a certain magnetic moment component in the direction of the applied magnetic field. This brings the magnetic susceptibility χ (the ratio of magnetization strength $\vec{M}$ and magnetic field strength $\vec{H}$ [13]) to a positive value, but the value is very small. χ is about 10^{-5} to 10^{-3}, and it increases with decreasing temperature, following Curie's Law.

Diamagnetism

In diamagnetic materials the atomic moments are zero. However, when subjected to an applied magnetic field, the electronic orbital movement changes which produces a small magnetization in the opposite direction to the applied magnetic field. So the magnetic susceptibility χ of diamagnetism is a small negative number which is near -10^{-6}. An important feature of the diamagnetism is that the magnetic susceptibility χ does not vary with temperature. The Langevin diamagnetic theory can be used to explain the diamagnetism of materials with electron shells.

Ferromagnetism

Ferromagnetism is a magnetic state of a material characterized by a spontaneous magnetization. Some materials are magnetized in an external magnetic field. Even if the external magnetic field is removed, ferromagnetic materials can still maintain their non-zero magnetization state.

In 1907, the French physicist Pierre-Ernest Weiss put forward the domain theory of ferromagnetism, where the main contents are as follows: there is a strong "molecular field" in ferromagnetic materials. Under the action of the molecular field, an atom's magnetic moments tend to be parallel to the same direction. Small areas of spontaneous magnetization are called magnetic domains. In the absence of an external magnetic field, the magnetization directions of the magnetic domains are different and the net magnetization is zero.

The magnetic properties of ferromagnetic materials are spontaneous. The process of magnetization is not caused by an external magnetic field. Like atomic paramagnetism, it is a necessary condition in order to generate ferromagnetism that there is a partially filled electronic shell. The hysteresis loop represents the closed magnetization curve of the hysteresis when the magnetic field changes periodically (Figure 3.1[15]). Hysteresis loops are an important feature of ferromagnetic materials, and there is no such phenomenon in paramagnetic and diamagnetic materials.

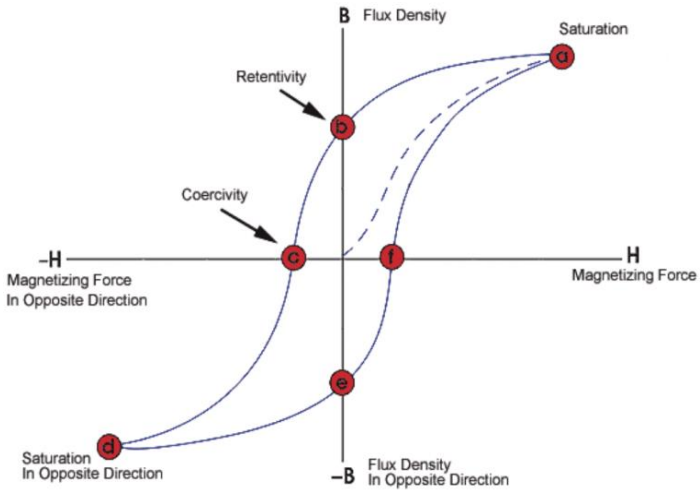

Fig. 3.1 The hysteresis loop [15].

Anti-ferromagnetism

If the adjacent atomic magnetic moments are equal, and the atomic magnetic moments are in an antiparallel arrangement, the atomic magnetic moments will cancel each other out, so that the spontaneous magnetization is zero. This is called anti-ferromagnetism. When the temperature is very high, the magnetic susceptibility χ is very small. As the temperature decreases, χ increases and at a certain temperature, χ reaches a maximum value. When we continue to lower the temperature, χ is reduced. The temperature point at which χ is a maximum is called the Néel Temperature, denoted by T_N. When the temperature is higher than T_N, the magnetic susceptibility χ obeys the Curie - Weiss Law $\chi = \frac{C}{T+\theta}$. The Néel point delineates the boundary between the anti-ferromagnetic phase and the paramagnetic phase. Figure 3.2 shows the temperature dependence of the magnetic susceptibility χ for paramagnetism, ferromagnetism, and antiferromagnetism [16].

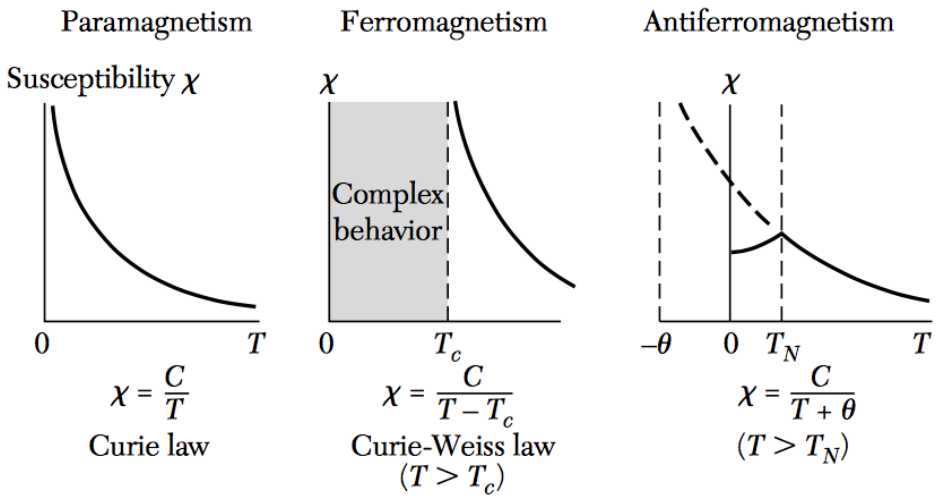

Fig. 3.2 Temperature dependence of the magnetic susceptibility in paramagnetism, ferromagnetism, and antiferromagnetism [16].

3.2 Magnetic properties of Cu_3WO_6

Masashi Hase and Kunimitsu Uchinokura [8] found that Cu_3WO_6 consists of the six Cu's on a plane that form a hexagonal ring where the distance of each Cu from the center is about 2.988 Å and their positions above the plane is 0.120 Å. They also reported that a spin singlet ground state with a spin gap is formed in this six spin ring system. The interaction between each Cu (spin=1/2) nearest neighbor is a Heisenberg antiferromagnetic exchange interaction. However, there are strong interactions that also exist between the 2nd and the 3rd nearest neighbors as their separation, especially for the 2nd nearest neighbors is 3.219 Å which is comparable to the 1st nearest neighbor separation. These interactions affect the magnetic properties of Cu_3WO_6. Therefore, there are three Heisenberg exchange interactions J_1 between 1st nearest neighbors J_2 between 2nd nearest neighbors and J_3 between 3rd nearest neighbors where $J_1 > J_2 > J_3$ (See Figure 1.4).

The origin of the spin-singlet ground state with the energy gap in Cu_3WO_6 can be described through the magnetic susceptibility. The reported results [8] indicate that the magnetic susceptibility should be explained by considering Heisenberg exchange interactions J_1 and J_2, and J_3. The calculation results show that these interactions lead to the AF spin ring with 6 spins, which has a spin-singlet ground state with a gap [11]. The theoretical curve of the AF spin ring with 6 spins does not agree with that of the experimental results (see Figure 1.3). Results of neutron scattering [9] as well as Muon spin relaxation also could not explain the discrepancy between the experimental and the theoretical results.

At the present time, the origin of the spin-singlet ground state with the spin gap in Cu_3WO_6 has not been resolved completely [8-9].

The Cu_3WO_6 consists only of magnetic Cu^{2+} ions (S=1/2, L=2, J=5/2), which contribute to the magnetic moment of the compound as W^{6+} ions do not contribute any magnetic moments to Cu_3WO_6. In most cases, the magnetic moment of the molecule is mainly produced by spin magnetic moments. But sometimes, we need also to consider the orbital magnetic moment as well. The theoretical value of the magnetic moment $\boldsymbol{\mu}$ for pure copper with the Cu^{2+} ions can be calculated by the following formula (3.1)

$$\mu = 2\mu_B\sqrt{J(J+1)} = 1.73\,\mu_B \tag{3.1}$$

where, J is total angular momentum (for Cu one should use J = S although J = S+L =5/2), and μ_B is the Bohr magneton. The question here is whether or not the orbital angular moment plays a factor in the properties of Cu_3WO_6**.**

3.3 Measurements of Magnetic Properties

There are many ways to measure magnetic properties of materials. The magnetic Property Measurement System (MPMS Quantum Design) (Figure 3.3) has been widely used to study magnetic properties of materials. The MPMS system is equipped with a superconducting magnet and liquid helium temperature control system. It can provide for measurements with a high magnetic field (up to 5.5 T) and temperatures from 400 K to a minimum of about 1.7 K. The MPMS system uses the SQUID (Superconducting Quantum Interference Device) to detect magnetic signals, and the entire measurement process (including data collection and analysis) is highly automated.

The ZFC-FC (Zero Field Cooling - Field Cooling) sequence was chosen to measure the magnetization of all samples. At the beginning, the system is cooled from a high temperature at T = 300 K to the minimum temperature T_{min} = 1.7 K in the absence of Magnetic Field (H=0). Then, the magnetic field is turned on at 1.7 K and subsequently ZFC magnetization M_{ZFC} is measured as a function of temperature with an increasing temperature from 1.7 K to 300 K in a magnetic field of H = 5000 Oe. Finally, the sample is cooled slowly from a high temperature at 300 K to 1.7 K again in the presence of the same Magnetic Field. Then, the field cooled magnetization (M_{FC}) is measured as a function of temperature with increasing temperature from 1.7 K to 300 K at H = 5000 Oe.

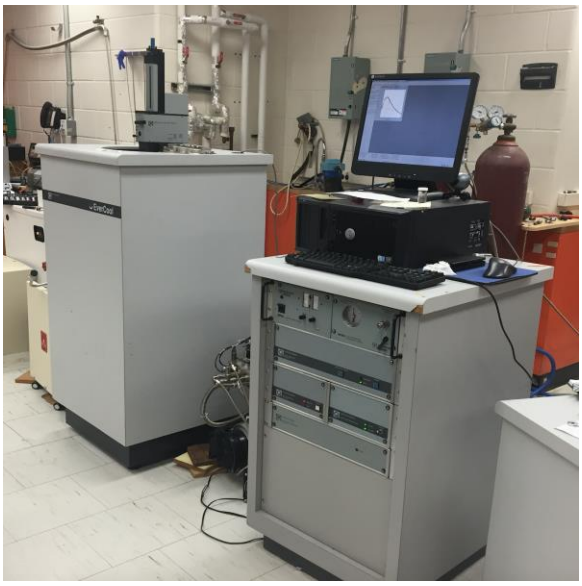

Fig. 3.3 The Magnetic Property Measurement System (MPMS) in the lab of Dr. F.S. Razavi at Brock University

3.4 Magnetic Results of Cu_3WO_6

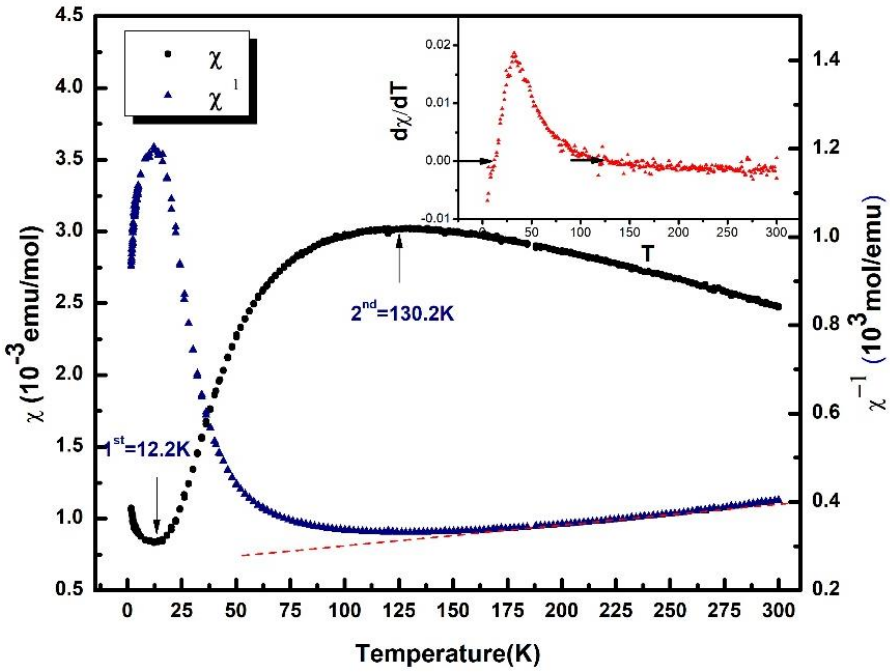

Fig. 3.4 The temperature dependence of the magnetic susceptibility χ and χ^{-1} of Cu_3WO_6

Fig. 3.4 shows the temperature dependence of the magnetic susceptibility χ(T) measured in a magnetic field of 5000Oe (solid circle). Note that the susceptibility shows no hysteresis in ZFC-FC processes. The solid up triangle curve is the temperature dependence of $1/\chi$.

With the temperature rising from 1.7 K, the susceptibility χ reduces to a minimum value which is about 8.28×10^{-4} emu/mol at 12.2 K. As the temperature continues to rise, a broad maximum value of χ was observed at 130.2K, which is about 3.0×10^{-3} emu/mol. The value of χ decreases again with increasing temperature above 130.2 K. By fitting the susceptibility to the Curie–Weiss law ($\chi = C/(T-\theta)$) for temperatures between 225K to 300 K, the following parameters were found the Curie Constant C is 1.72 and the Weiss Constant θ is -392.17 K. Cu_3WO_6 undergoes an antiferromagnetic phase transition at the Néel temperature T_N = 130.2 K.

The $\boldsymbol{\mu}_{eff}$(exp) is calculated using the following formula (3.2).

$$\chi = \frac{C}{T} = \frac{\mu^2 \mu_0 N_A}{3K_B T}$$

$$\mu_{eff}(exp) = \sqrt{\frac{3K_B C}{\mu_0 N_A}} = 2.84\mu_B\sqrt{C} = 3.72\mu_B \tag{3.2}$$

$$\mu^* = 2\mu_B\sqrt{(3-x)S_{Cu}(S_{Cu}+1) + xS_{Ni}(S_{Ni}+1)} = 3\mu_B \tag{3.3}$$

This value of the $\boldsymbol{\mu}_{eff}$ is $3.72\boldsymbol{\mu}_B$, which is close to the theoretical calculation for $\boldsymbol{\mu}^* = 3\boldsymbol{\mu}_B$ in Cu_3WO_6. Our result can be compared to that derived from the magnetic data of Masashi Hase and Kunimitsu Uchinokura[8] in Figure 1.3, which yields a value of $\boldsymbol{\mu}_{eff}$ of $3.56\boldsymbol{\mu}_B$.

3.5 Magnetic Results of $Cu_{3-x}Ni_xWO_6$

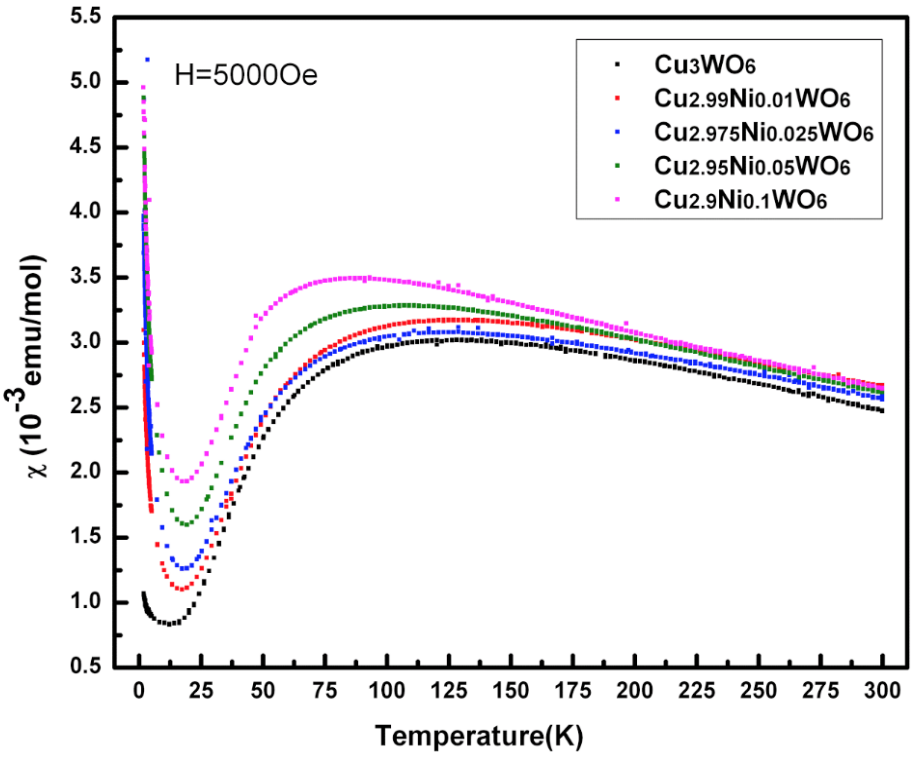

Fig. 3.5 The temperature dependence of the magnetic susceptibility χ of Cu3-xNixWO6 (x=0 to 0.1) in 5000Oe.

The temperature dependence of the magnetic susceptibility χ of $Cu_{3-x}Ni_xWO_6$ (x=0 to 0.1) in 5000Oe is given in Figure 3.5 for five $Cu_{3-x}Ni_xWO_6$ (x=0 to 0.1) compounds. The magnetic susceptibility data of the doped samples was analyzed in Figures 3.6 to 3.9.

The first derivative $d\chi/dT$ is shown in inset of the figures 3.4 and 3.6 to 3.9. The 1st and 2nd transition temperatures are the minimum and maximum value of the magnetic susceptibility χ, respectively, where the Néel temperature T_N is the 2nd transition temperature. All compounds show Curie–Weiss antiferromagnetic behavior at high temperatures. The values of C and θ are

calculated using the χ(T)'s curves by fitting the data to the Curie–Weiss law $\chi = C/(T - \theta)$ for a temperature range between 225 K-300 K for each compound.

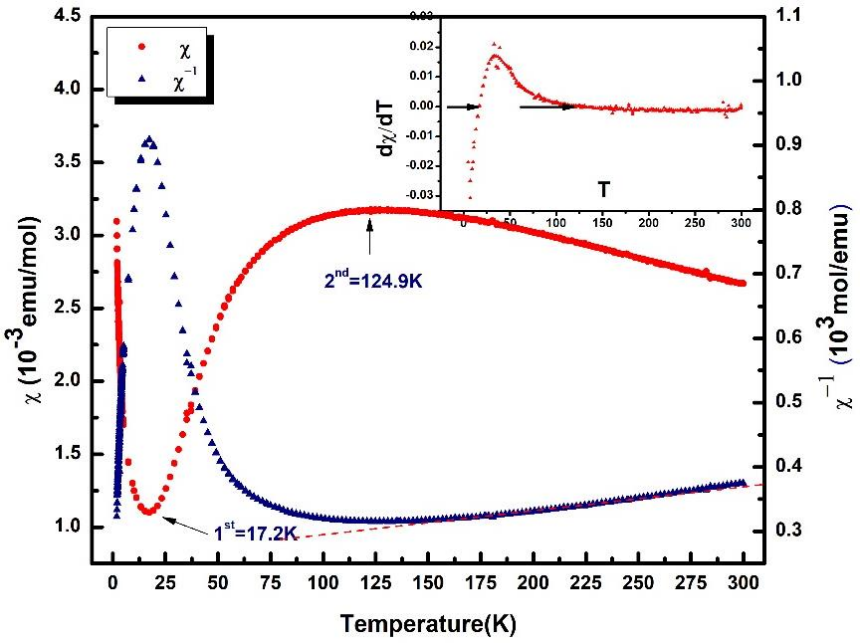

Fig. 3.6 The temperature dependence of the magnetic susceptibility χ and χ^{-1} of $Cu_{2.99}Ni_{0.01}WO_6$.

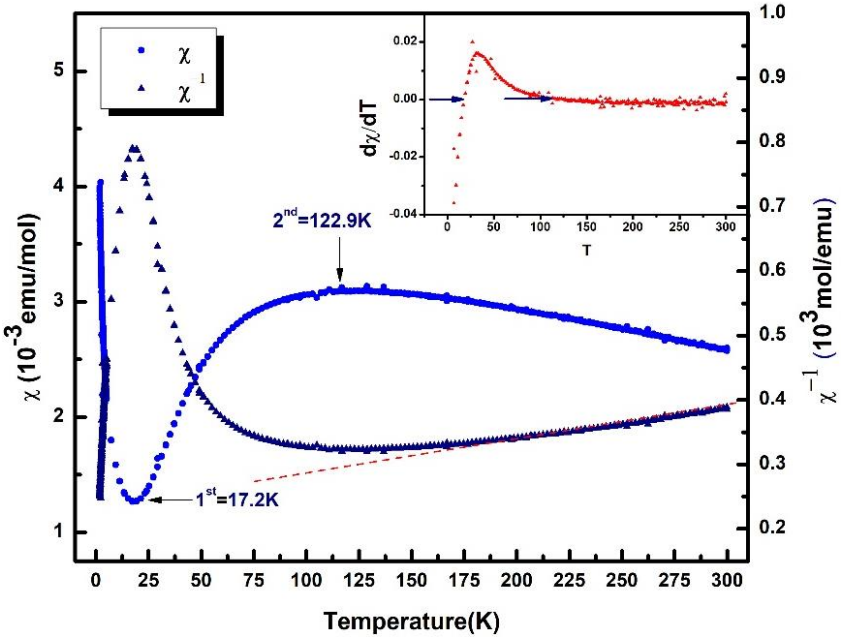

Fig. 3.7 The temperature dependence of the magnetic susceptibility χ and χ^{-1} of $Cu_{2.975}Ni_{0.025}WO_6$.

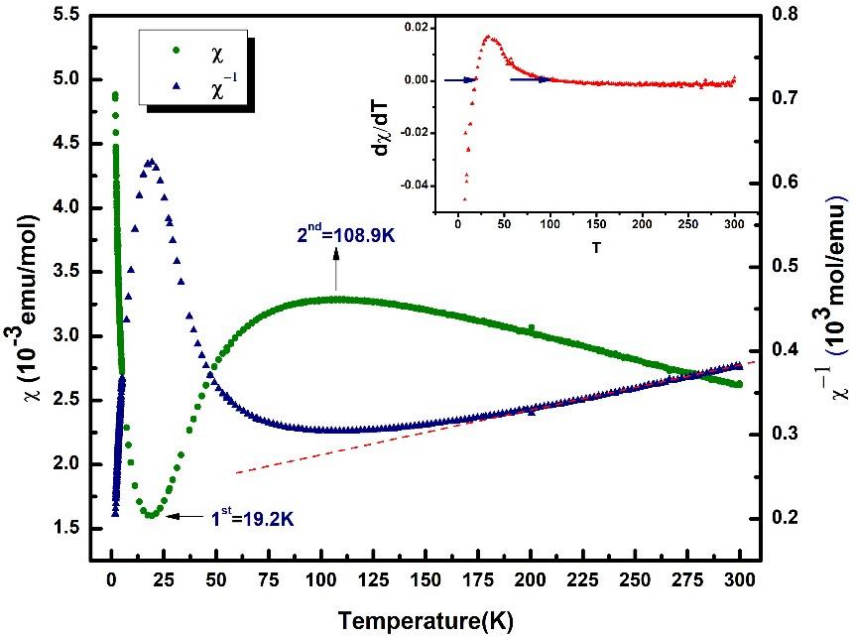

Fig. 3.8 The temperature dependence of the magnetic susceptibility χ and χ^{-1} of $Cu_{2.95}Ni_{0.05}WO_6$.

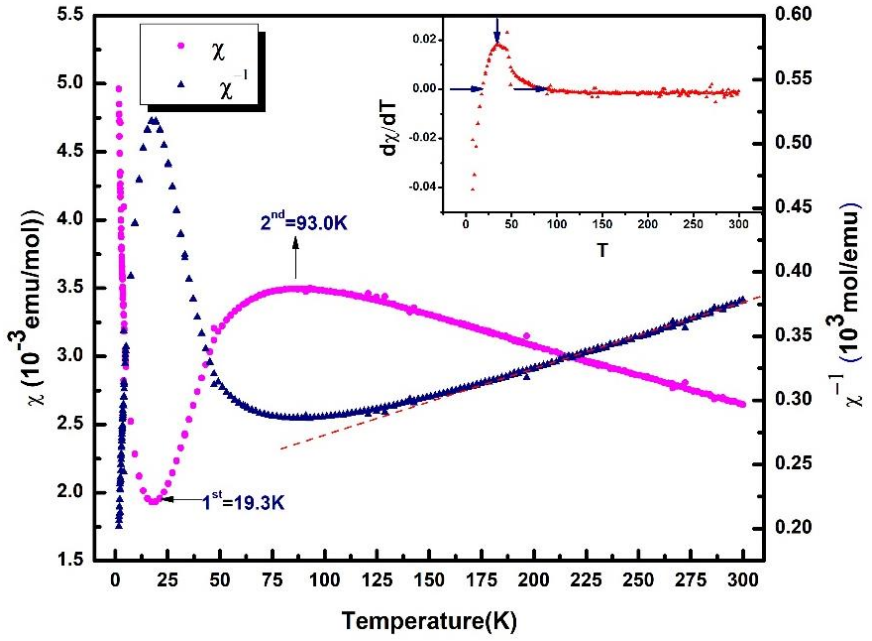

Fig. 3.9 The temperature dependence of the magnetic susceptibility χ and χ^{-1} of $Cu_{2.9}Ni_{0.1}WO_6$.

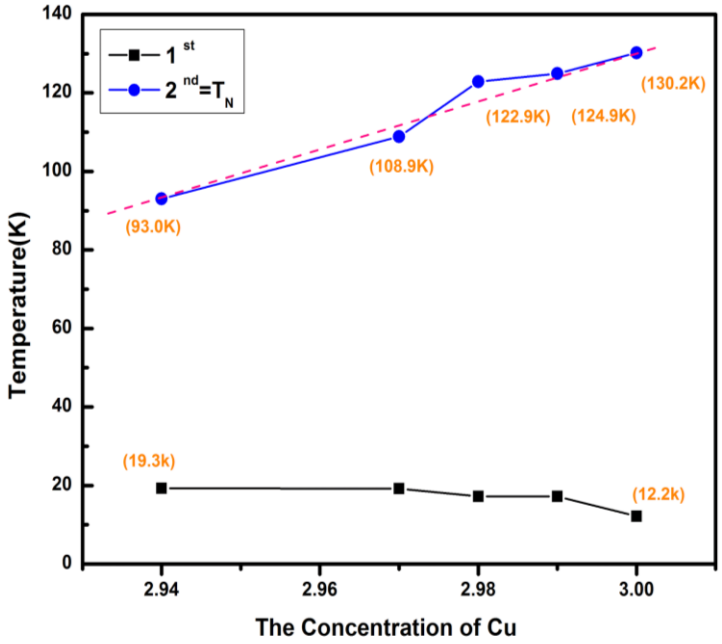

Fig. 3.10 Two transition temperatures for $Cu_{3-x}Ni_xWO_6$ (x=0 to 0.06).

As the concentration of Ni increases in $Cu_{3-x}Ni_xWO_6$, the maximum of the susceptibility χ increases from 3.0×10^{-3}emu/mol for Cu_3WO_6 to 3.48×10^{-3}emu/mol for $Cu_{2.9}Ni_{0.1}WO_6$.

We observed no significant change in the temperature of the minimum in the susceptibility data (the 1st transition) as shown in Figure 3.10. However, a significant change was observed in the Néel temperature as the concentration of Ni is increased (Figure 3.10). By substituting Ni for Cu, we are inducing a chemical pressure on $Cu_{3-x}Ni_xWO_6$ which resulted in a reduction of the antiferromagnetic Heisenberg exchange interaction. The linear variation of the Néel temperature T_N with the Cu concentration is an indication that our calculations of the concentration, x, obtained from X-ray results are correct.

As all compounds show a Curie–Weiss antiferromagnetic behavior at high temperatures, the effective magnetic moment $\boldsymbol{\mu}_{eff}$(exp) was determined for all compounds. According to the results

of X-Ray measurements, there are some impurity compounds in $Cu_{3-x}Ni_xWO_6$(x=0.025 to 0.1). When we calculate the Curie Constant C and Weiss Constant θ at high temperature, we should remove the effect of CuO and $Cu_{1-\delta}Ni_\delta WO_4$ on $Cu_{3-x}Ni_xWO_6$ first. The range of χ for CuO is 1.82 to 2.15 $\times 10^{-4}$ emu/mol [26]. Considering the content of CuO which is 6.5% at most, we ignored the effect of CuO. Because there is no literature data for $Cu_{1-\delta}Ni_\delta WO_4$, we used the magnetic data of $CuWO_4$ [27]. The range of χ for $CuWO_4$ is 1.2 to 2.2 $\times 10^{-3}$ emu/mol. and the Curie Constant C is 0.611 and the Weiss Constant θ is -152K in high temperature. Depending on the content in the X-Ray report, we calculated the approximate value of the Curie Constant C and the Weiss Constant θ for each compound. All parameters obtained from the analysis of the susceptibility data are given in Table 3.1.

Table 3.1 Listing of parameters obtained from the susceptibility.

$Cu_{3-x}Ni_xWO_6$ (using X-ray results)	**C_{obs}**	**$\mu_{eff}(exp)/\mu_B$**	**θ(K)**	**$\chi \times 10^{-3}$(emu/mol)**
① x=0	1.72	3.72	-392.17	0.828~3.0
② x=0.01	2.16	4.18	-510.51	1.1~3.17
③ x=0.02	2.20	4.21	-494.16	1.26~3.094
④ x=0.03	2.22	4.23	-449.22	1.59~3.27
⑤ x=0.06	2.26	4.27	-413.38	1.94~3.48

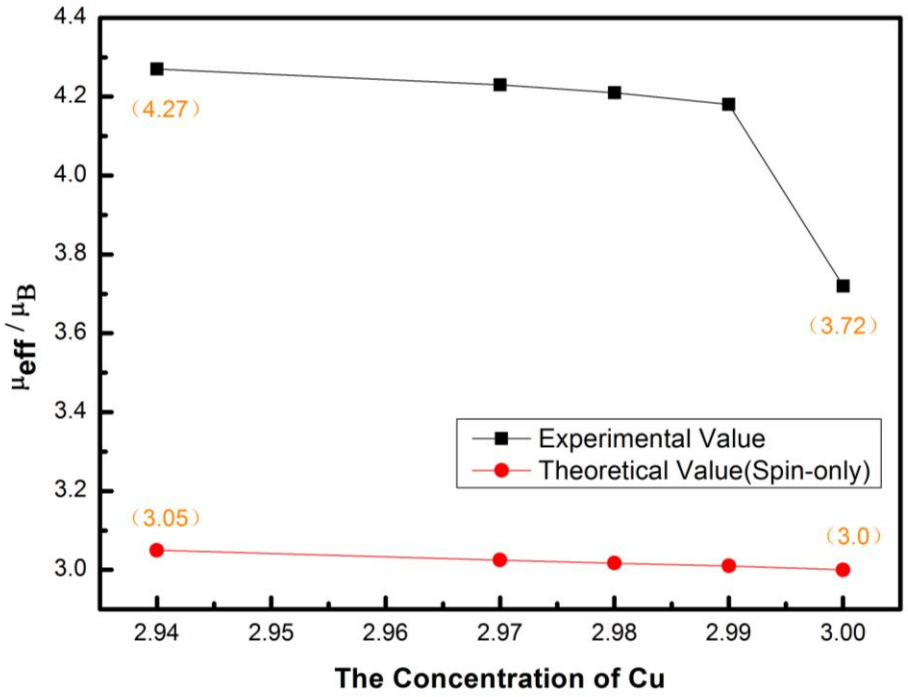

Fig. 3.11 Trends in $\boldsymbol{\mu}_{eff}$(exp) of $Cu_{3-x}Ni_xWO_6$ (x=0 to 0.06).

The Figure shows the comparison between experimental value and theoretical value of magnetic moment. The theoretical $\boldsymbol{\mu}^*$ is calculated using the following formula 3.3 for each compound. The results show that the magnitude of the effective magnetic moment $\boldsymbol{\mu}_{eff}$(exp) increases from 3.72$\boldsymbol{\mu}_B$ for Cu_3WO_6 to 4.27$\boldsymbol{\mu}_B$ for $Cu_{2.94}Ni_{0.06}WO_6$. Even with a small amount of Ni's doping is doped, the value of $\boldsymbol{\mu}_{eff}$(exp) increases significantly. This growth is contributed by orbit angular moment. But with for the doping, $\boldsymbol{\mu}_{eff}$(exp)'s growth is not as great.

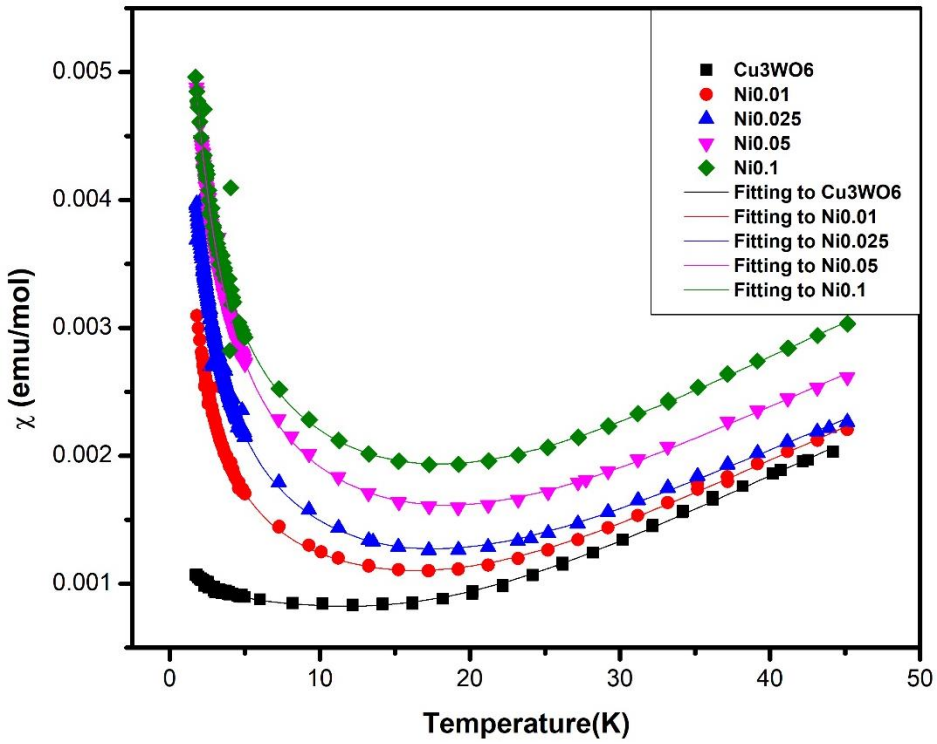

Fig. 3.12 Magnetic Susceptibility χ of $Cu_{3-x}Ni_xWO_6$ (x=0 to 0.1) at low temperature(1.7-45K) along with fits to equation 3.4.

Hase and Uchinokura [9] have fitted the low temperature results of the susceptibility data to equation (3.4) to argue for the existence of a spin-singlet ground state with an energy gap:

$$\chi(\mathrm{T}) = \frac{C}{T-\theta} + Aexp(-\frac{\Delta}{K_B T}) + \chi_0 \qquad (3.4)$$

Although this equation is phenomenological, they nevertheless found a good fit to χ(T). Their argument for using this equation was that $Aexp\left(-\frac{\Delta}{K_B T}\right)$ reflects the excited states of the small spin density which are almost isolated. This term is produced this along with the Curie–Weiss law Term. The constant term can be as a consequence of the orbital part of the susceptibility.

Fig.3.12 shows the magnetic susceptibility of each sample at temperatures below 45 K. The Equation 3.4 can be fitted to the susceptibility χ(T) for $Cu_{3-x}Ni_xWO_6$ (x=0 to 0.1) as shown in Figure 3.12. All parameters obtained from the best fit are presented in Table 3.2. The energy gap **Δ** decreases from 6.80meV(x=0) to 6.63meV(x=0.06). The value of the Curie Constant C increases from 8.96×10^{-4} for Cu_3WO_6 to 98.5×10^{-4} for $Cu_{2.94}Ni_{0.06}WO_6$. It can be obvious that the value of susceptibility χ has a big value with the Ni concentration at a low temperature of 1.7K to 5K. Zinc substitution for Cu causes the same phenomenon[9]. Both Ni and Zn doping causes the susceptibility χ to have big value in low temperatures.

Table 3.2 List of parameters obtained from the best fit the susceptibility to Equation (3.4).

$Cu_{3-x}Ni_xWO_6$ **(using X-ray results)**	$C\times10^{-4}$	$\boldsymbol{\theta}$(K)	$A\times10^{-3}$	$\boldsymbol{\Delta}$(meV)	$\chi_0\times10^{-4}$
① x=0	8.96	-1.06	7.67	6.80±0.22	7.4
② x=0.01	54.3	-0.48	8.03	6.76±0.10	7.2
③ x=0.02	82.9	-0.75	8.03	6.72±0.36	7.2
④ x=0.03	104.6	-0.87	8.12	6.65±0.16	9.5
⑤ x=0.6	98.5	-0.97	8.47	6.63±0.73	13

3.5 Magnetic Results of $Cu_3W_{1-x}Mo_xO_6$

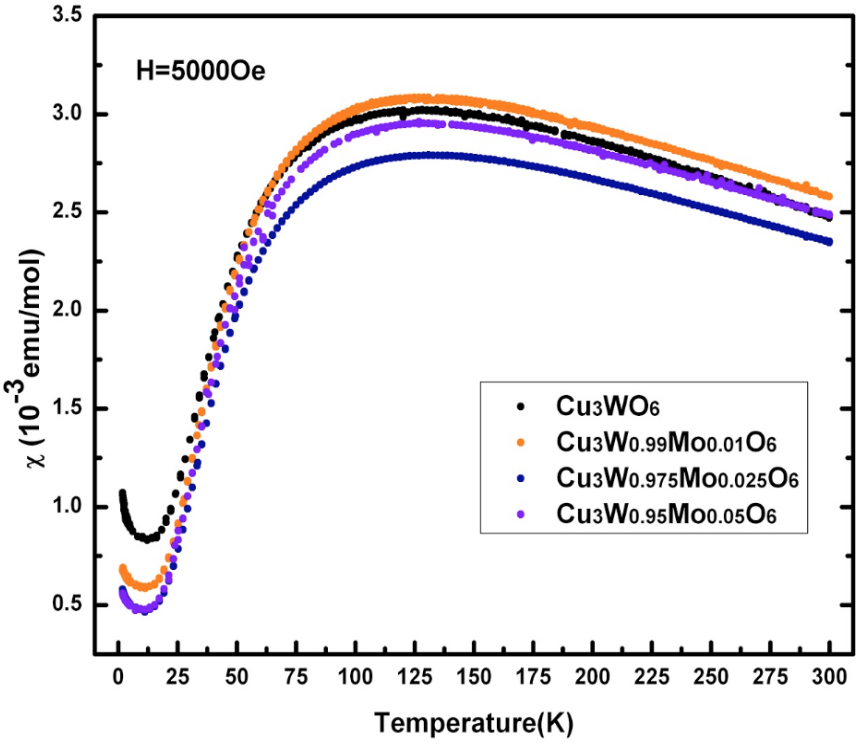

Fig. 3.13 The temperature dependence of magnetic susceptibility χ of $Cu_3W_{1-x}Mo_xO_6$.

The XRD results for $Cu_3W_{1-x}Mo_xO_6$ (x=0 to 0.05) indicate that only minute amounts of Mo might replace W in Cu_3WO_6. As a result, there were only small changes in the magnetic susceptibility χ as x increases as shown in Fig. 3.13 for $Cu_3W_{1-x}Mo_xO_6$ (x=0 to 0.05).

Chapter 4

Dielectric Measurements and Results for $Cu_{3-x}Ni_xWO_6$

4.1 Overview of Dielectric properties

Materials whose resistivity is more than 10**Ω**·cm are called a dielectrics. The charged particles of the dielectric are tightly bound by the internal force of the molecules or atoms, so that charged particles are bound charges. Under an external electric field, these charged particles only move in the microscopic range, resulting in polarization. In an electrostatic field, there can be a large electric field inside the dielectric material, which is the basic difference between a dielectric and a conductor. Dielectric materials have many uses such the substrates for integrated circuits, and capacitors in the electronics industry. When the external electric field is applied, the dielectric will generate induced charges which weakens the external electric field. The ratio of the external electric field to the induced electric field inside the dielectric is the dielectric constant. The dielectric constant has a real part and the imaginary part.

The real part ε' of the complex permittivity, the imaginary part ε'' of the complex permittivity, loss tangent, tan δ, and ac electrical conductivity σ_{ac} as a function of temperature have been studied widely. The complex permittivity can be defined in the following complex formula [17,18]:

$$\varepsilon^* = \varepsilon' - j\varepsilon'' \tag{4.1}$$

where *j* is the imaginary root of -1. The complex permittivity formula has been used to describe the electrical and dielectric properties. In the formulation of ε^*, in case of admittance measurements (C-V and G/*w*-V), the following relation is obeyed:

$$\varepsilon^* = \frac{Y}{j\omega C_0} = \frac{C}{C_0} - \mathrm{j}\frac{G}{\omega C_0} \tag{4.2}$$

where Y, C and G are the measured admittance, capacitance and conductance of the dielectric, respectively and ω is the angular frequency ($\omega=2\pi f$) of the applied electric field [18]. The dielectric constant (ε'), at various temperatures was calculated by using the measured capacitance values at the strong accumulation region by the formula [19,20]:

$$\varepsilon' = \frac{C}{C_0} \tag{4.3}$$

where C_o is capacitance of an empty capacitor.Define $C_0 = \varepsilon_0 \frac{A}{d}$; where A is the rectifier contact area in m^{-2}, d is the sample thickness and ε_o is the permittivity of free space charge (ε_o = 8.85×10^{-12} F/m). The dielectric loss ε'', at various temperatures was calculated by using the measured conductance values from the equation below:

$$\varepsilon'' = \frac{G}{\omega C_0} \tag{4.4}$$

The loss tangent (tanδ) can be expressed as follows [17-20], $\tan\delta = \varepsilon''/\varepsilon'$. The ac electrical conductivity σ_{ac} of the dielectric materials can be calculated from the dielectric loss according to the relation [21-24]:

$$\sigma_{ac} = \omega C \tan\delta \frac{d}{A} = \varepsilon''\omega\varepsilon_0 \tag{4.5}$$

The motion of the charges in the dielectric gives rise to the conduction current and additionally polarizes the dielectric [25]. The ac conductivity σ_{ac} of the material depends on the dielectric nature of the sample. There is a strong correlation between the frequency response and the temperature dependence of the electrical conductivity of the materials. The temperature dependence of σ_{ac} shows the presence of a single or multiple relaxations in the material. In polar materials the conduction mechanism can be ionic and/or electronic in nature. Depending upon the purity and temperature of the materials, the proportion of ionic to electronic conduction in the materials varies. Usually polar dielectric materials show an increasing trend in conductivity with a rise in temperature. The variation of electrical conductivity with temperature is explained by the equation [25]:

$$\sigma = \mathrm{A}\exp\left(-\frac{E_a}{K_B T}\right) + \mathrm{B}\exp\left(-\frac{E_B}{K_B T}\right) \tag{4.6}$$

where E_a and E_b are the activation energy for the intrinsic and extrinsic conduction process respectively and A and B are constants. At higher temperatures the intrinsic conduction process dominates, and eq 4.6 reduces to [25]:

$$\sigma = \mathrm{A}\exp\left(-\frac{E_a}{K_B T}\right) \tag{4.7}$$

where A is the pre-exponential factor, E_a is the activation energy and K_B is Boltzmann's constant.

4.2 Dielectric Results of Cu_3WO_6

The dielectric constant ε' and dielectric loss ε'' of Cu_3WO_6 were measured as the function of f=1kHz to 20kHz and as a function of T=5K to 400K, using the MPMS system with AH2700A

Ultra-precision capacitor bridge (Figure 4.1). Typical dimensions of samples were area≈10mm^2 and thickness≈0.1mm. The samples were cut in a rectangular shape, the two large surfaces were covered by two components silver epoxy and two gold wires contacted to them as electrodes.

Fig. 4.1 AH 2700A Ultra-precision capacitor in the lab at Brock University.

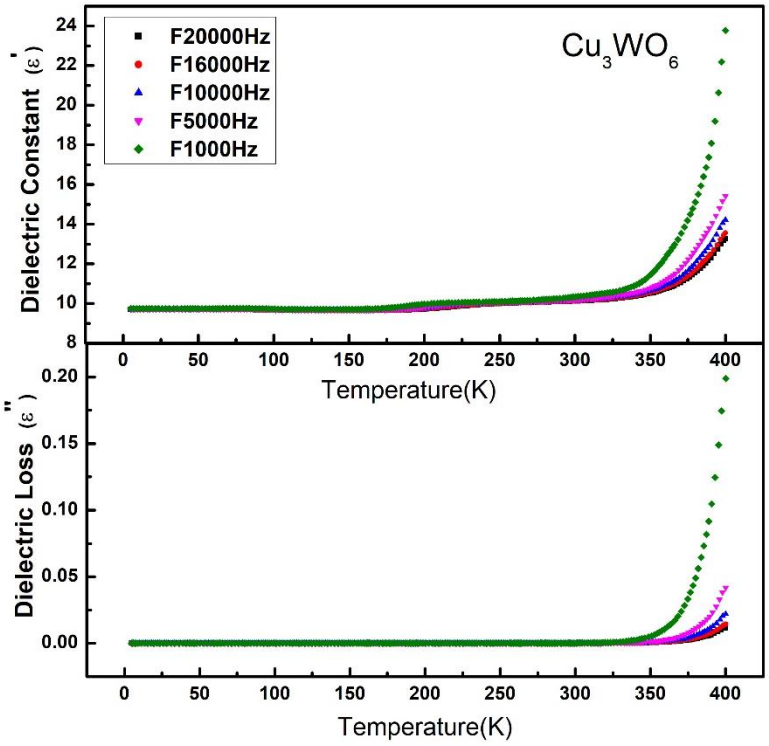

Fig. 4.2 Dielectric constant ε' and dielectric loss ε" of Cu_3WO_6.

Figure 4.2 shows the variation of dielectric constant ε' and dielectric loss ε'' with temperatures and frequencies for Cu_3WO_6. The relative dielectric constant ε' increases from 9.7 to 24 at f = 1 kHz and from 9.7 to 13 at f = 20 kHz as a function of temperature, respectively. The dielectric loss ε'' increases from 0 to 0.2 at f=1 kHz and from 0 to 0.01 at f = 20 kHz as a function of temperature, respectively.

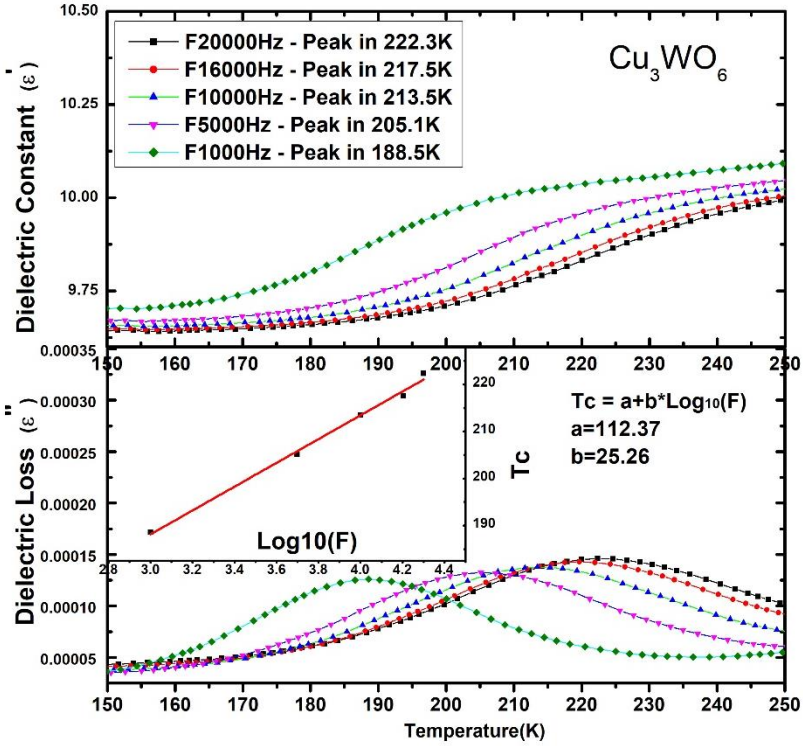

Fig. 4.3 Appearance of a change of the slope in ε' and a peak in ε'' as a function of temperatures between 150 K to 260 K. The inset in the lower Figure shows the peak position as a function of frequency.

The slope of dielectric constant ε' starts changing at 260 K and levels off at 150 K. This change corresponds to the appearance of a peak in the dielectric loss ε'' at about 188.56 K which moves to higher temperatures as the frequency increases (see the inset of Figure 4.3). The linear fit to the data indicates that at f = 0 the corresponding peak temperature is 112 K.

Hase et al. reported [9] neutron-scattering results of magnetic excitations in Cu_3WO_6. They observed three peaks in the constant Q spectra at Q = 1.7 $Å^{-1}$ corresponding to peak positions at energies 11, 14, and 18 meV. The integrated intensity of the neutron scattered beam between 5 to 16 meV shows a temperature dependance which vanishes above 80 K . Thus they attribute the observed peaks at 11 meV (128 K) and 14 meV (162 K) to be due to magnetic excitations. However, the peak at 18 meV (208.8 K) was found to be independent of temperature and it is thus attributed to phonon excitations. By comparing the Cu_3WO_6 dielectric results and that of neutron scattering it can be concluded that the peak observed in the ε'' originates from phonon excitations which affect the ionic conductivities. The sharp bend in the curve for the dielectric loss ε'' suggests a transition taking place in Cu_3WO_6. The results presented above are phenomena which are characteristic of ionic relaxation which comprises ionic conductivity and interfacial and space charge relaxation due to structural changes.

Figure 4.4 presents ac conductivity (σ_{ac}) as a function of temperature for frequencies f = 1 kHz to 20 kHz. The ac conductivity σ_{ac} and activation energy E_a were calculated from the dielectric data collected at different temperatures using Equation 4.5 and 4.7, respectively. $\ln\sigma_{ac}$ is plotted as a function $10^3/T$ (Figure 4.4 low figure). The value of the activation energy E_a obtained from the slope of the curve $\ln\sigma_{ac}$ vs. $10^3/T$ at high temperature was 0.84eV for f = 1 kHz and 0.7eV for f = 20 kHz, respectively. The activation energy E_a decreases with an increase in frequency.

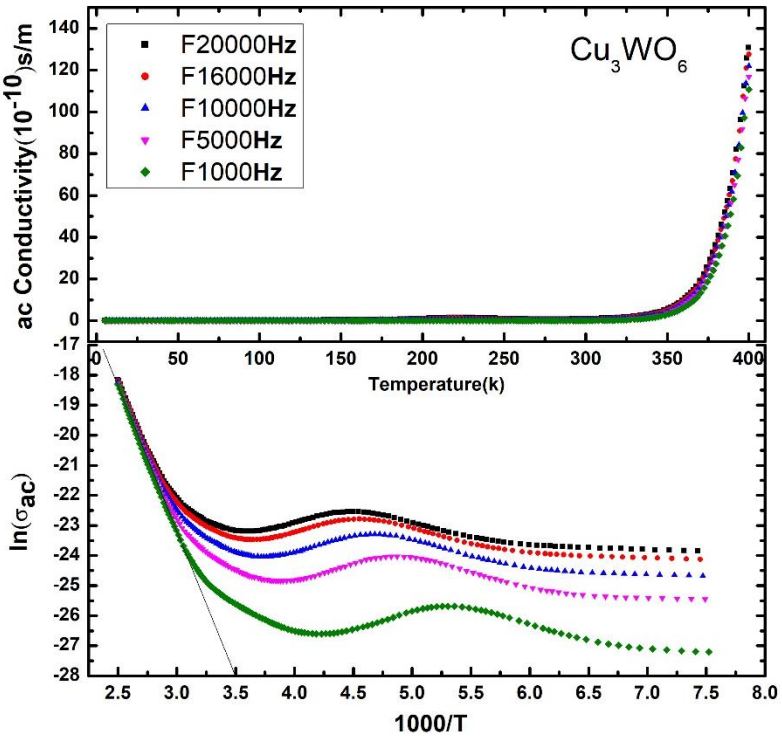

Fig. 4.4 Ac conductivity σ_{ac} ($\ln\sigma_{ac}$) vs. temperature (10^3/T) of Cu_3WO_6.

4.3 Dielectric Experiment Results of $Cu_{3-x}Ni_xWO_6$

Using the same conditions as above, the dielectric constant ε' and dielectric loss ε'' of $Cu_{3-x}Ni_xWO_6$ (x=0.01 to 0.1) were measured as a function of temperature (5K to 400K) with f=1kHz to 20kHz.

Figures 4.5 to 4.18 show the variation of dielectric constant ε', dielectric loss ε'' and ac conductivity σ_{ac} as a function of temperature for f = 1 kHz to 20 kHz for $Cu_{3-x}Ni_xWO_6$ (x=0.01 to 0.06). Figure 4.19 demonstrates that the temperature and $\log_{10}(f)$ have a linear relationship for each phase transition. The peak in dielectric loss ε'' shifts from 188.5 K for Cu_3WO_6 to 121.44 K for $Cu_{2.94}Ni_{0.06}WO_6$ at f = 1 kHz. An anamoly appeared at high temperature, which shifts from 279.89K for $Cu_{2.97}Ni_{0.03}WO_6$ to 286.19K for $Cu_{2.94}Ni_{0.06}WO_6$ at f =1 kHz which might be due to

an impurity phase in the higher doped compounds or a structural instability caused by the Ni doping in Cu_3WO_6. In each graph of the ac conductivity (σ_{ac}) (Figure 4.5 to Figure 4.18), the two anamolies can easily be observed. Activation energies E_a for each compound are calculated (Eq. 4.6). The E_a value is found to decrease with increasing concentration of Ni (Figure 4.20).

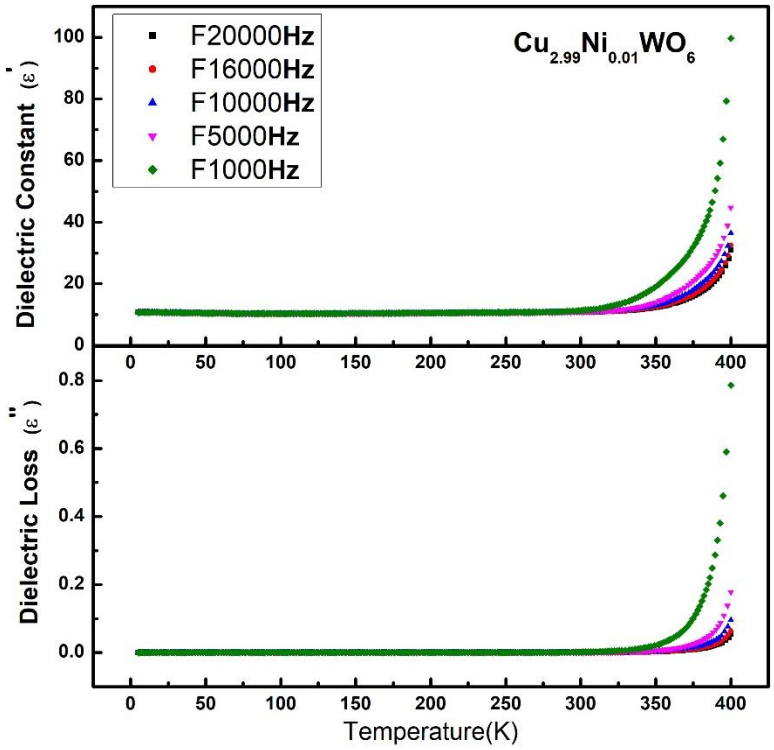

Fig. 4.5 Dielectric constant ε' and dielectric loss ε'' of $Cu_{2.99}Ni_{0.01}WO_6$.

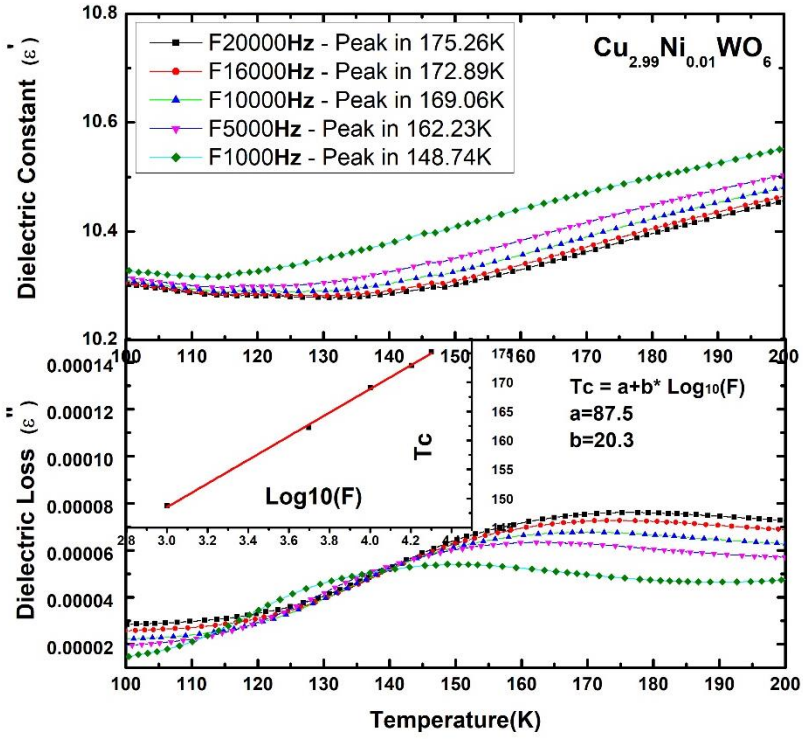

Fig. 4.6 1st phase transition with frequency of $Cu_{2.99}Ni_{0.01}WO_6$.

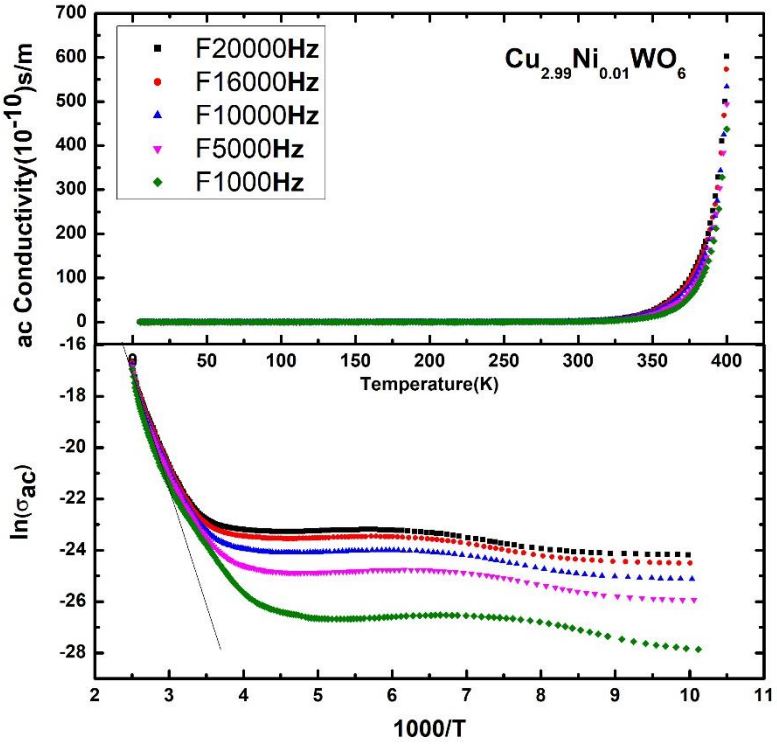

Fig. 4.7 Ac conductivity σ_{ac} ($\ln\sigma_{ac}$) vs. temperature (10^3/T) of $Cu_{2.99}Ni_{0.01}WO_6$.

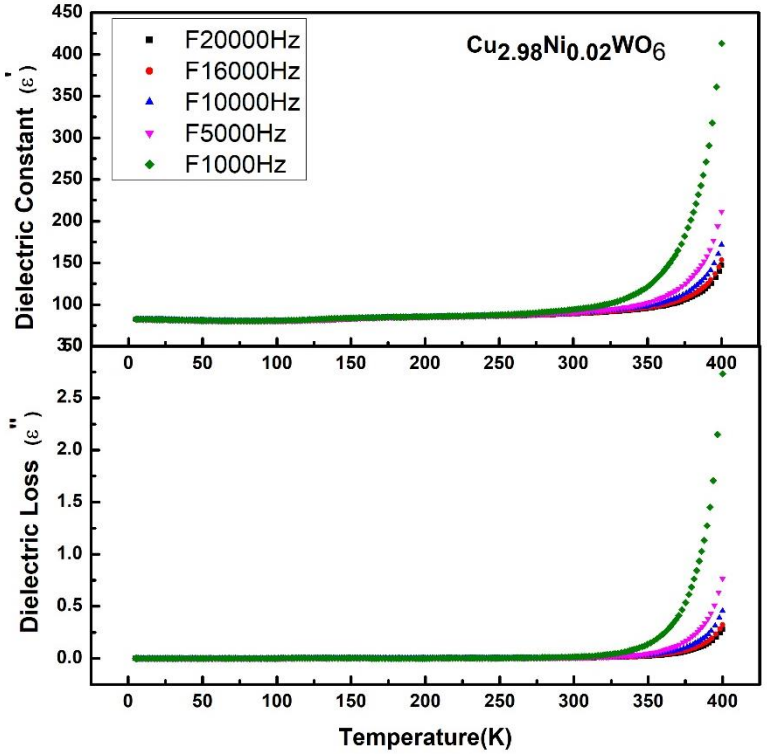

Fig. 4.8 Dielectric constant ε' and dielectric loss ε" of $Cu_{2.98}Ni_{0.02}WO_6$.

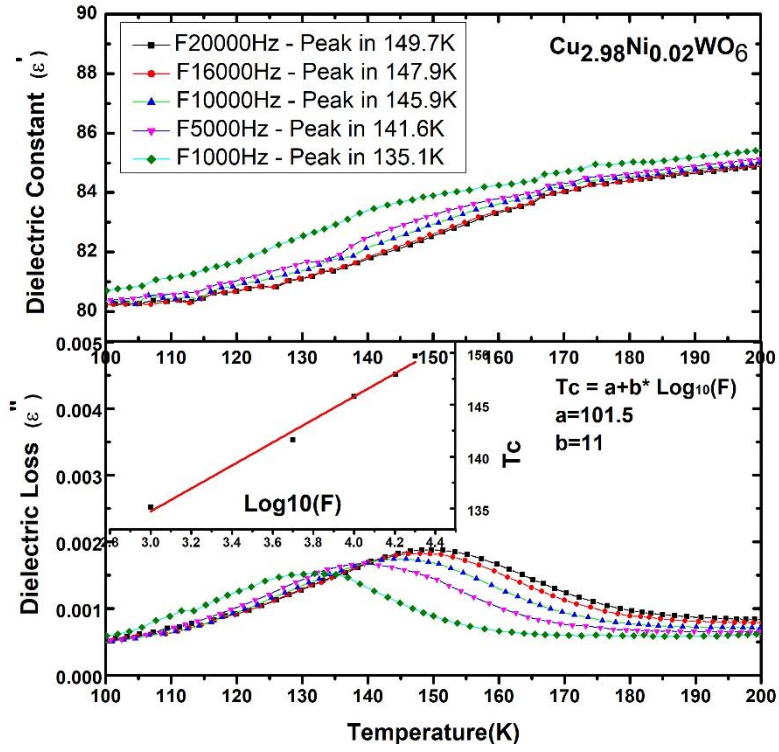

Fig. 4.9 1st phase transition of $Cu_{2.98}Ni_{0.02}WO_6$.

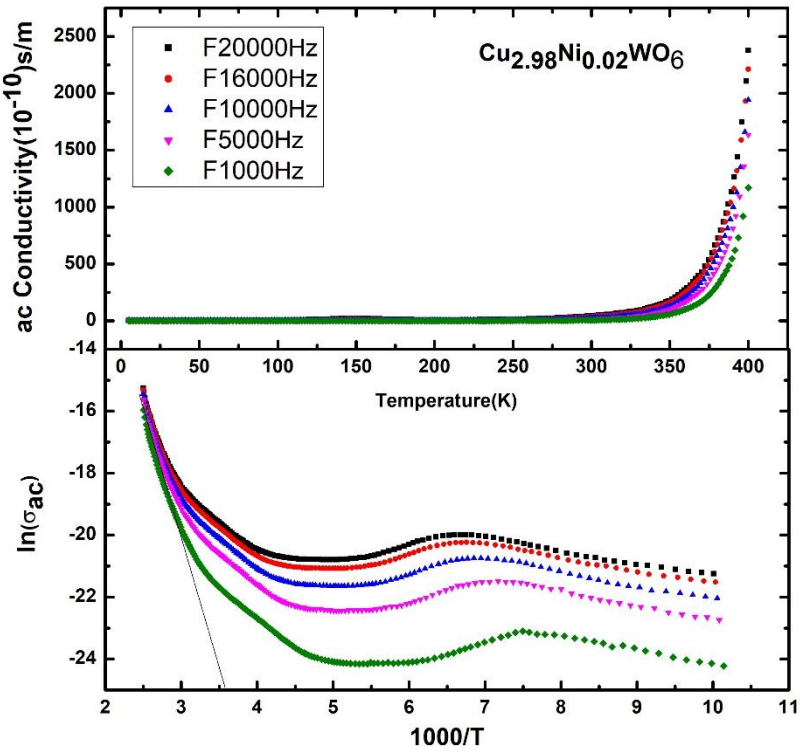

Fig. 4.10 Ac conductivity σ_{ac} ($\ln\sigma_{ac}$) vs. temperature (10^3/T) of $Cu_{2.98}Ni_{0.02}WO_6$.

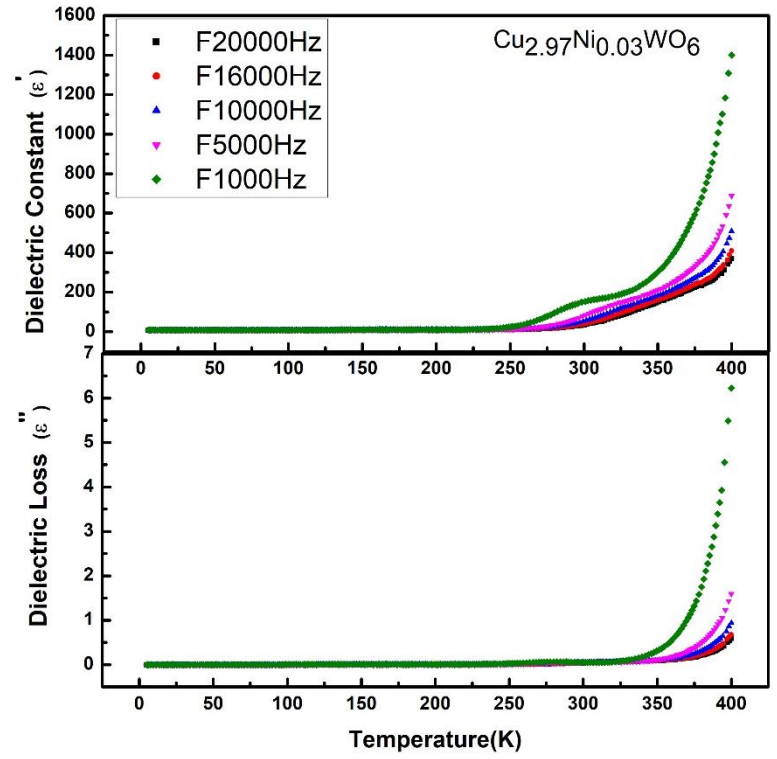

Fig. 4.11 Dielectric constant ε' and dielectric loss ε'' of $Cu_{2.97}Ni_{0.03}WO_6$.

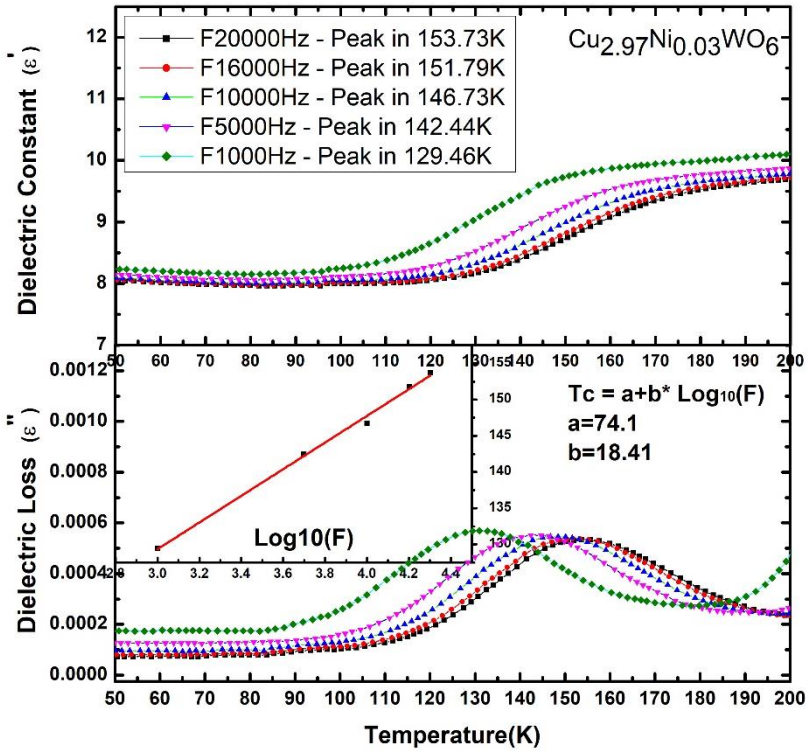

Fig. 4.12 1st phase transition of $Cu_{2.97}Ni_{0.03}WO_6$.

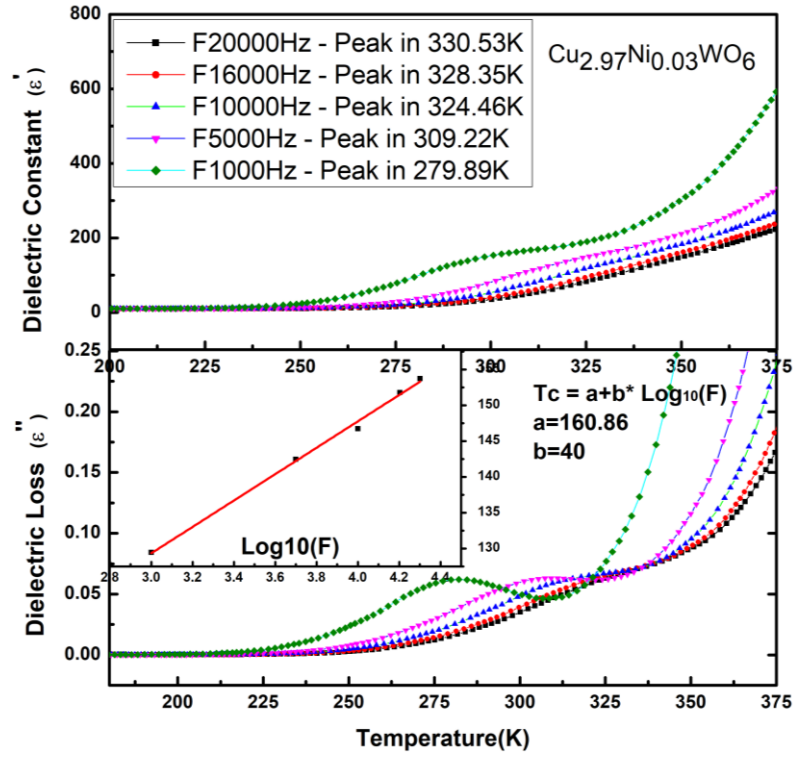

Fig. 4.13 2nd phase transition of $Cu_{2.97}Ni_{0.03}WO_6$.

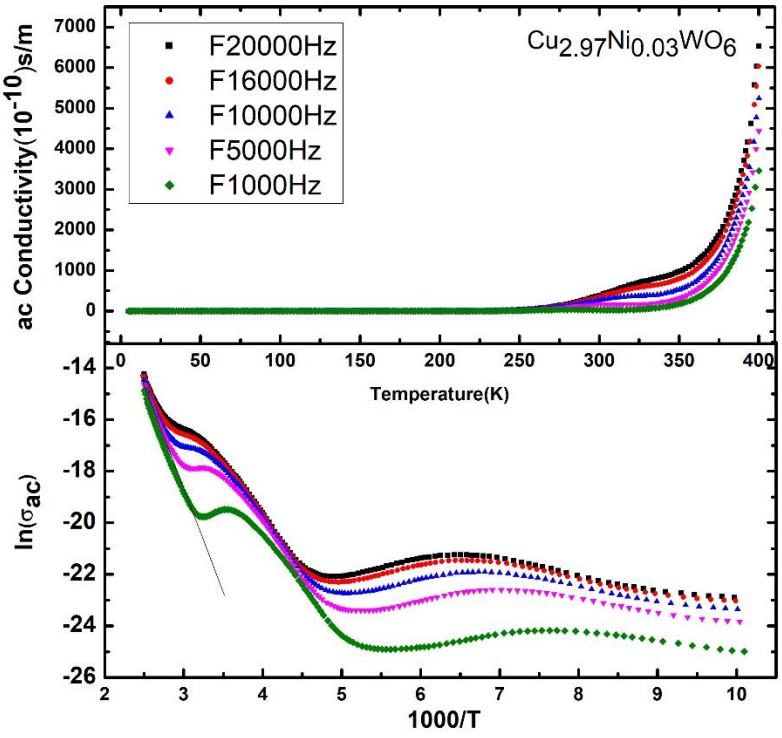

Fig. 4.14 Ac conductivity σ_{ac} ($\ln\sigma_{ac}$) vs. temperature (10^3/T) of $Cu_{2.93}Ni_{0.03}WO_6$.

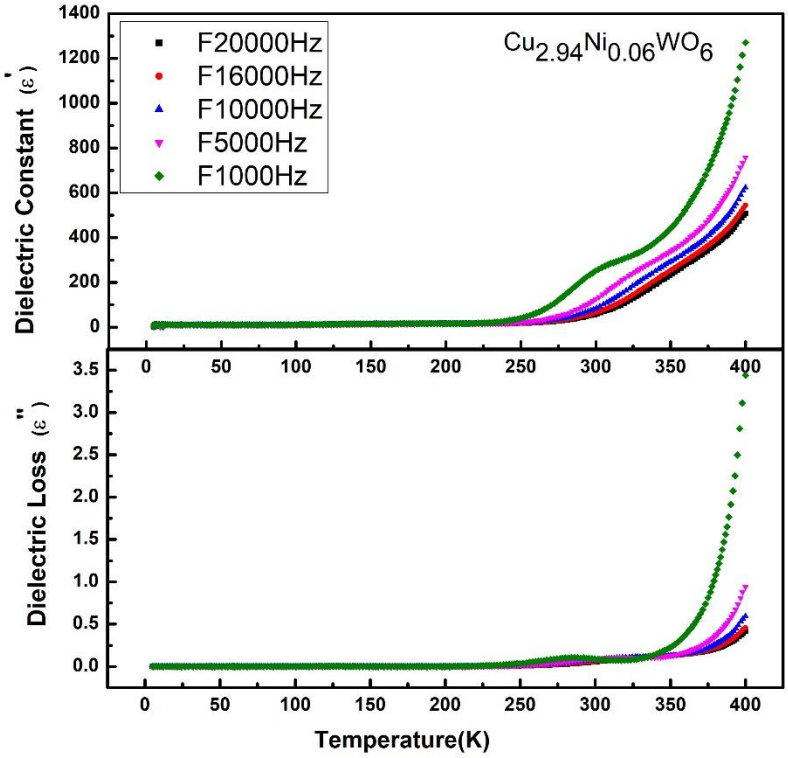

Fig. 4.15 Dielectric constant ε' and dielectric loss ε'' of $Cu_{2.94}Ni_{0.06}WO_6$.

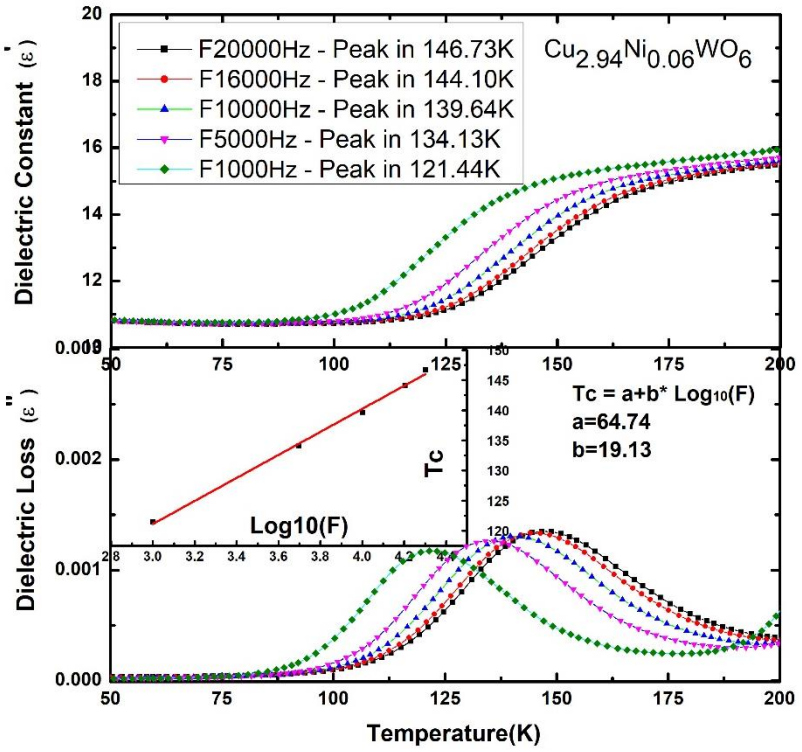

Fig. 4.16 1st phase transition of $Cu_{2.94}Ni_{0.06}WO_6$.

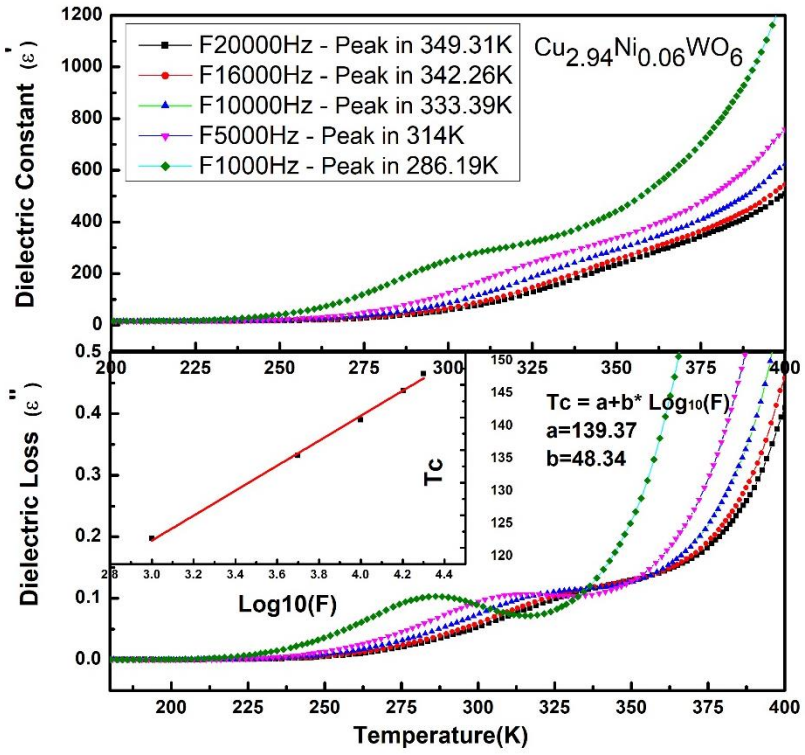

Fig. 4.17 2nd phase transition of $Cu_{2.94}Ni_{0.06}WO_6$.

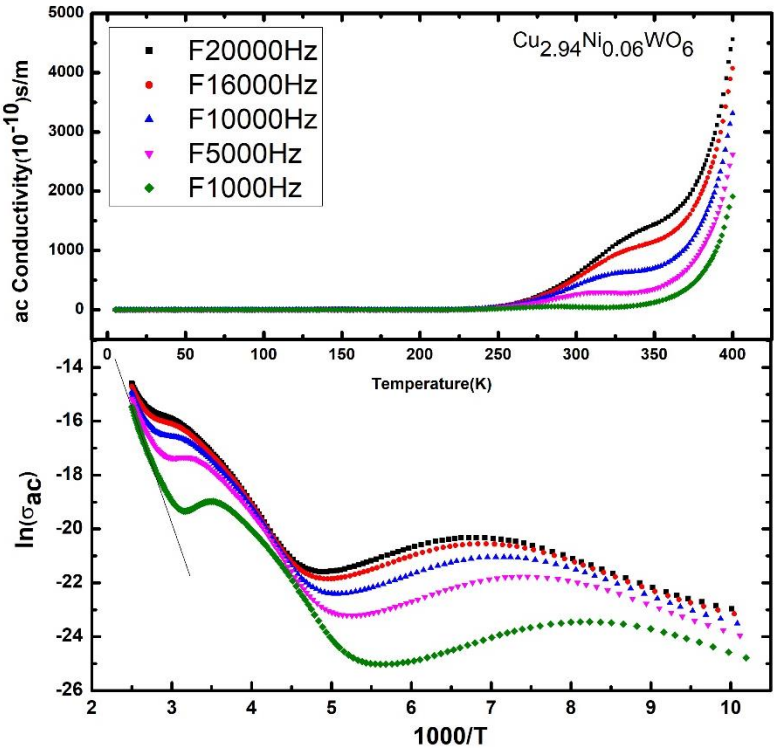

Fig. 4.18 Ac conductivity σ_{ac} ($\ln\sigma_{ac}$) vs. temperature (10^3/T) of $Cu_{2.94}Ni_{0.06}WO_6$.

Table 4.1 At 400K, the range of the dielectric constant ε', the dielectric loss ε'', ac conductivity σ_{ac} and activation energy E_a with the f = 20k Hz.

$Cu_{3-x}Ni_xWO_6$	**ε'**	**ε''**	**$\sigma_{ac}(10^{-10}s/m)$**	**E_a(eV)**
① x=0	13.3	0.01	111	0.7±0.011
② x=0.01	31.0	0.05	558	0.65±0.011
③ x=0.02	146.8	0.27	3000	0.52±0.013
④ x=0.03	368.8	0.58	6447	0.35±0.016
⑤ x=0.06	508.6	0.41	4557	0.22±0.011

Table 4.2 At 400K, the range of the dielectric constant ε', the dielectric loss ε'', ac conductivity σ_{ac} and activation energy E_a with the f = 1k Hz.

$Cu_{3-x}Ni_xWO_6$	**ε'**	**ε''**	**$\sigma_{ac}(10^{-10}s/m)$**	**E_a(eV)**
① x=0	23.7	0.20	110.7	0.84±0.006
② x=0.01	99.7	0.79	439	0.73±0.015
③ x=0.02	412.8	2.73	1168	0.63±0.010
④ x=0.03	1400	6.22	3462	0.67±0.006
⑤ x=0.06	1270	3.43	1912	0.6±0.008

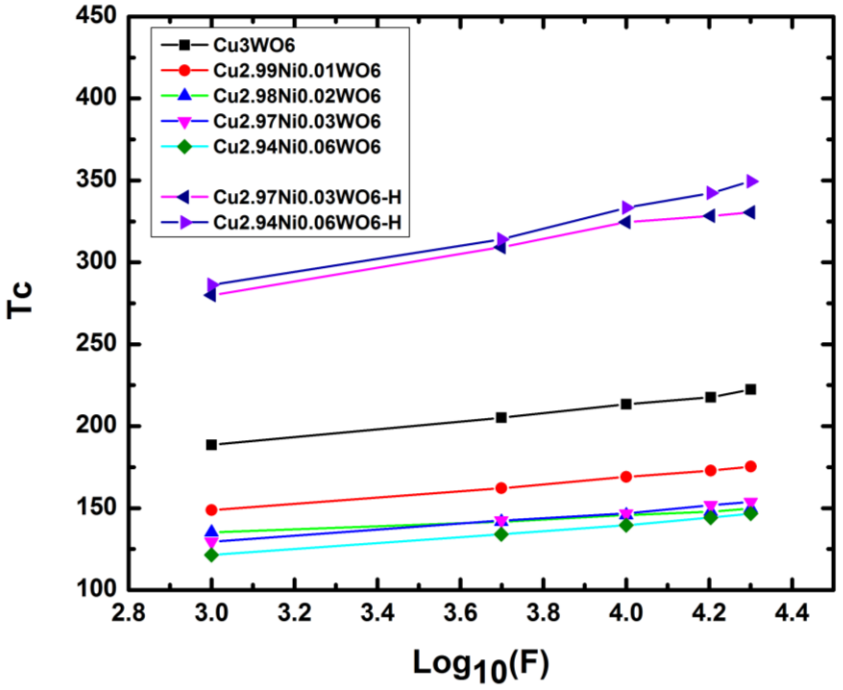

Fig. 4.19 T vs. $\log_{10}$(F) for each phase transition of $Cu_{3-x}Ni_xWO_6$ (x=0 to 0.06).

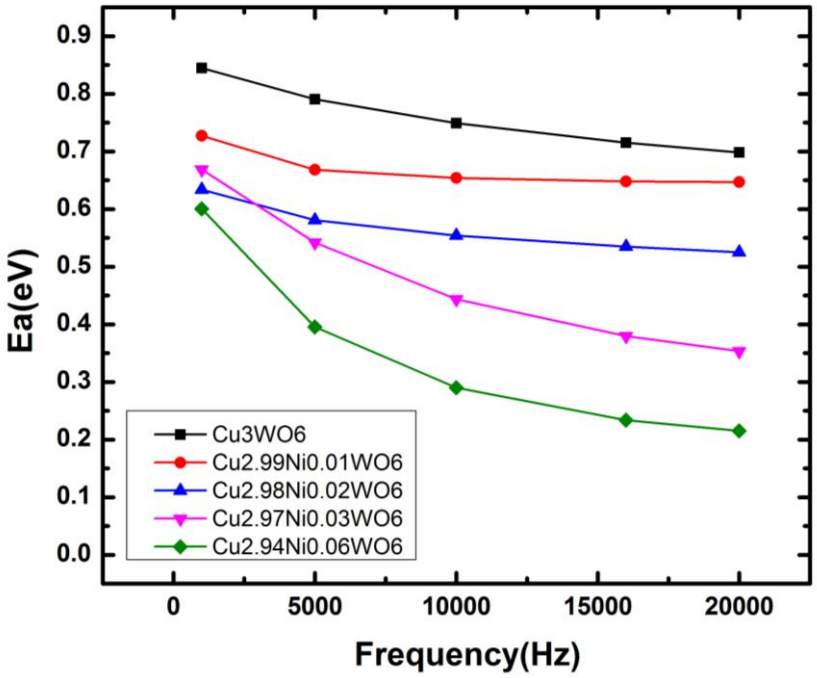

Fig. 4.20 Activation energy Ea vs. frequency for $Cu_{3-x}Ni_xWO_6$ (x=0 to 0.1).

Chapter 5

Conclusion

Using powder XRD and the Rietveld analysis, the crystal structure of Cu_3WO_6 was determined to be a cubic crystal with a lattice parameter equal to 9.7962(3) Å and with the space group $Pa\bar{3}(T_h^6)$. The Ni and W doped compounds showed no distortion on the crystal structure. As the ionic radii of Ni is less than that of Cu and, that of Mo is less than W, then doping of these elements can act as a negative pressure on the lattice parameter of Cu_3WO_6. It was found that neither Ni nor Mo completely substitute Cu or W, respectively. Some excess of copper oxide CuO as well as $CuWO_4$ are left in the solid solution. Using the Rietveld analysis, the content of different phases in each sample were calculated.

In the study of magnetic property, Cu_3WO_6 undergoes an antiferromagnetic phase transition at the Néel temperature $T_N = 130.2K$. The value of the effective magnetic moment μ_{eff} is $3.72\mu_B$ is calculated from experimental results. This value is close to the total theoretical calculation for $\mu_{eff} = 3\mu_B$ for Cu in Cu_3WO_6. With an increasing Ni doping, the maximum of the susceptibility χ was increased and the Néel temperature decreased to lower temperatures. By substituting Ni for Cu, we are inducing a chemical pressure on $Cu_{3-x}Ni_xWO_6$ hence it resulted in a reduction in the antiferromagnetic Heisenberg exchange interaction. After removing the effect of CuO and $Cu_{1-\delta}Ni_\delta WO_4$ on susceptibility χ, the value of the Curie Constant C and the Weiss Constant θ for each compound were calculated. The magnitude of μ_{eff} (exp) increases from $3.72\mu_B$ of Cu_3WO_6 to $4.27\mu_B$ of $Cu_{2.94}Ni_{0.06}WO_6$. This growth is contributed by orbit angular moment. At low

temperatures, the existence of the spin-singlet ground state with an energy gap for all the samples was investigated. The calculated energy gap **Δ** decreases from 6.80 meV (x=0) to 6.63 meV (x=0.06) as the concentration of Ni increases.

The results of the complex permittivity in all samples of $Cu_{3-x}Ni_xWO_6$ indicate a change of the slope in ε' and a peak in ε'' as a function of temperatures between 150 K to 260 K. The peaks in dielectric loss ε'' shifts from 188.5 K for Cu_3WO_6 to 121.44 K for $Cu_{2.94}Ni_{0.06}WO_6$ for f = 1 kHz. There is an anamoly that appeared at high temperatures, which shifts from 279.89K of $Cu_{2.97}Ni_{0.03}WO_6$ to 286.19K of $Cu_{2.94}Ni_{0.06}WO_6$ at f =1 kHz which might be due to an impurity phase in higher doped compounds or a structural instability caused by the Ni doping in Cu_3WO_6. The peak temperature in ε'' shows a linear relation as a function of $\log_{10}(f\text{erquency})$. The conductivity activation energies E_a for each compound decreases with the increasing concentration of Ni.

As we complete this work, we think it would be interesting to carry-out future studies on optical measurements, the Raman spectroscopy, as a funcation of temperature and study magnetization as a function of pressures that would enhance the exact nature of the properties observed in present studies of Cu_3WO_6.

Appendix

1. X-Ray report of Cu_3WO_6

Measurement conditions

X-Ray	40 kV , 30 mA	Scan speed / Duration time	3.6000 sec.
Goniometer	SmartLab(In-plane)	Step width	0.0110 deg
Attachment	Standard	Scan axis	Theta/2-Theta
Filter	Cu_K-beta	Scan range	10.0000 - 89.9920 deg
CBO selection slit	BB	Incident slit	0.663deg
Diffracted beam mono.	None	Length limiting slit	2.0mm
Detector	SC-70	Receiving slit #1	0.663deg
Scan mode	STEP	Receiving slit #2	0.300mm

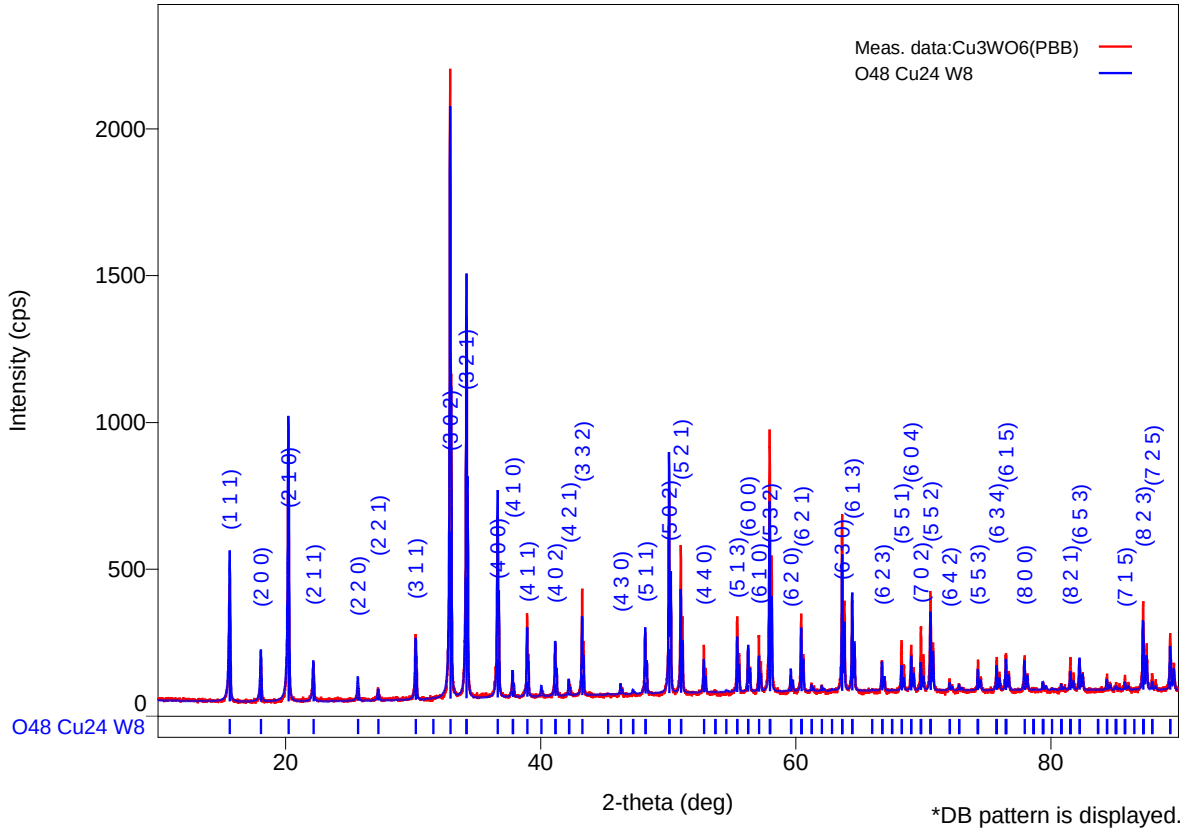

*DB pattern is displayed.

Peak list

No.	2-theta(deg)	d(ang.)	Height(cps)	FWHM(deg)	Int. I(cps deg)	Int. W(deg)	Asym. factor
1	15.6277(14)	5.6658(5)	312(8)	0.080(2)	41.2(3)	0.132(5)	1.06(8)
2	18.074(3)	4.9041(7)	119(5)	0.068(4)	11.9(2)	0.100(6)	1.1(2)
3	20.2326(14)	4.3855(3)	673(12)	0.079(2)	82.6(6)	0.123(3)	1.40(11)
4	22.191(4)	4.0027(7)	99(5)	0.097(6)	14.7(2)	0.147(9)	1.8(3)
5	25.683(6)	3.4658(8)	34(3)	0.073(8)	4.4(2)	0.129(16)	1.4(5)
6	27.266(10)	3.2681(11)	27(2)	0.104(17)	4.8(2)	0.18(2)	1.7(10)
7	30.212(2)	2.95577(19)	200(7)	0.090(3)	25.6(3)	0.128(6)	1.37(15)
8	32.9218(10)	2.71843(8)	2004(21)	0.0711(11)	214.1(12)	0.1068(17)	1.30(10)
9	34.1955(11)	2.62003(8)	1191(16)	0.0800(13)	149.7(9)	0.126(2)	1.23(9)
10	36.6385(16)	2.45074(11)	561(11)	0.089(2)	76.9(6)	0.137(4)	1.30(13)
11	37.811(3)	2.3774(2)	83(4)	0.075(4)	9.8(2)	0.118(9)	1.3(3)
12	38.9530(18)	2.31029(10)	263(8)	0.0686(19)	27.4(3)	0.104(4)	1.07(14)
13	40.075(9)	2.2482(5)	18(2)	0.074(12)	2.2(2)	0.12(2)	1.5(7)
14	41.154(3)	2.19166(13)	166(6)	0.084(3)	19.7(3)	0.119(6)	1.3(2)
15	42.218(5)	2.1389(2)	52(3)	0.074(6)	6.1(2)	0.116(12)	1.0(4)

16	43.2653(12)	2.08948(5)	346(9)	0.0686(14)	35.6(3)	0.103(3)	1.11(9)
17	46.276(2)	1.96029(8)	36(3)	0.054(6)	2.85(19)	0.078(11)	0.6(3)
18	48.209(2)	1.88611(7)	202(7)	0.0830(18)	23.2(3)	0.115(5)	1.14(13)
19	50.0862(11)	1.81974(4)	687(12)	0.0803(11)	80.2(5)	0.117(3)	1.36(9)
20	51.0003(11)	1.78925(4)	499(10)	0.0763(12)	55.0(4)	0.110(3)	1.12(7)
21	52.8121(17)	1.73206(5)	159(6)	0.072(2)	16.3(2)	0.102(5)	1.22(13)
22	55.4261(14)	1.65640(4)	259(8)	0.0803(15)	28.8(3)	0.111(4)	1.19(9)
23	56.289(2)	1.63304(5)	152(6)	0.087(2)	18.3(3)	0.120(6)	2.1(3)
24	57.1186(18)	1.61127(5)	193(6)	0.0738(19)	18.5(3)	0.096(5)	0.64(8)
25	57.9657(10)	1.58972(2)	870(14)	0.0817(11)	105.2(5)	0.121(3)	1.14(6)
26	59.631(5)	1.54925(13)	50(3)	0.089(6)	5.8(3)	0.115(13)	1.7(5)
27	60.4400(17)	1.53043(4)	256(7)	0.0866(17)	30.7(3)	0.120(5)	1.13(10)
28	61.265(10)	1.5118(2)	24(2)	0.098(12)	3.0(3)	0.12(2)	2.7(19)
29	62.065(7)	1.49421(16)	22(2)	0.078(11)	2.3(2)	0.11(2)	2.5(7)
30	63.6516(10)	1.46073(2)	602(11)	0.0819(11)	71.1(4)	0.118(3)	1.05(6)
31	64.4380(14)	1.44478(3)	310(8)	0.0858(16)	38.2(3)	0.123(4)	1.10(8)
32	66.778(4)	1.39972(7)	96(5)	0.092(4)	12.2(3)	0.128(9)	1.4(2)
33	68.3036(19)	1.37213(3)	176(6)	0.080(2)	19.8(3)	0.112(5)	0.88(9)
34	69.060(2)	1.35894(4)	149(6)	0.084(3)	18.8(3)	0.126(7)	0.77(11)
35	69.828(2)	1.34586(3)	217(7)	0.084(2)	25.6(3)	0.118(5)	1.03(11)
36	70.5741(15)	1.33345(2)	330(8)	0.0880(17)	43.1(4)	0.131(4)	0.95(8)
37	72.061(7)	1.30954(11)	37(3)	0.092(7)	4.2(3)	0.113(15)	0.6(2)
38	72.831(7)	1.29759(11)	19(2)	0.081(10)	1.9(2)	0.10(2)	2.7(11)
39	74.308(3)	1.27541(4)	96(5)	0.084(4)	12.4(2)	0.128(9)	1.9(4)
40	75.767(4)	1.25444(5)	108(5)	0.093(4)	15.1(3)	0.139(9)	1.2(2)
41	76.492(3)	1.24434(4)	124(5)	0.094(3)	16.6(3)	0.134(8)	1.24(17)
42	77.931(3)	1.22492(4)	110(5)	0.084(4)	13.1(3)	0.118(8)	0.52(11)
43	79.384(5)	1.20611(6)	24(2)	0.101(8)	2.54(19)	0.107(18)	0.85(17)
44	80.100(18)	1.1971(2)	4.5(10)	0.09(5)	0.5(3)	0.10(8)	0.7(16)
45	80.844(5)	1.18797(6)	24(2)	0.037(12)	1.9(2)	0.077(17)	2(2)
46	81.547(3)	1.17950(4)	110(5)	0.086(3)	13.6(3)	0.123(8)	1.10(19)
47	82.254(3)	1.17115(4)	106(5)	0.095(4)	14.3(3)	0.135(9)	0.78(14)
48	84.392(6)	1.14684(6)	47(3)	0.082(5)	4.8(3)	0.102(12)	0.7(2)
49	85.117(4)	1.13892(4)	21(2)	0.099(13)	2.6(3)	0.12(2)	0.9(5)
50	85.819(8)	1.13139(8)	42(3)	0.091(9)	5.3(3)	0.127(16)	0.9(4)
51	87.2480(17)	1.116497(18	289(8)	0.0967(18)	41.4(4)	0.143(5)	1.19(10)
52	87.945(3)	1.10944(3)	51(3)	0.101(5)	6.4(2)	0.127(13)	0.71(9)
53	89.369(2)	1.09542(2)	188(6)	0.093(3)	26.1(3)	0.139(7)	0.92(11)

Crystal Structure Analysis Results

Indexing

Phase name	Formula	Figure of merit	Phase reg. detail	DB card number
Copper Tungsten Oxide	O48 Cu24 W8	0.527	ICDD (PDF2.DAT)	01-071-2208

Quantitative analysis results

	Phase name	Content(%)
	Copper Tungsten Oxide	100.0(5)

Lattice information

Phase name	a(A)	b(A)	c(A)	alpha(deg)	beta(deg)	gamma(deg)	V(A^3)
Copper	9.7962(3)	9.7962(3)	9.7962(3)	90.000000	90.000000	90.000000	940.09(5)

Phase name	Space group	Z	Z'	Calc. density(g/cm^3)
Copper Tungsten	205 : Pa-3	1	0.042	6.645

Refinement

Measurement range: 10.0000-89.9920deg Refinement range: 10.0000-89.9920deg (1.09 A)
Number of refined parameters: 30

Phase name	Atomic coords	# of indep. reflns
Copper Tungsten Oxide	Fractional coords	128

Rwp = 5.81% S = 1.1076

2. X-Ray Report of $Cu_{2.99}Ni_{0.01}WO_6$

Measurement Conditions

X-Ray	40 kV , 30 mA	Scan speed / Duration time	3.5700 sec.
Goniometer	SmartLab(In-plane)	Step width	0.0100 deg
Attachment	Standard	Scan axis	Theta/2-Theta
Filter	Cu_K-beta	Scan range	10.0000 - 90.0000 deg
CBO selection slit	BB	Incident slit	0.663deg
Diffracted beam mono.	None	Length limiting slit	2.0mm
Detector	SC-70	Receiving slit #1	0.663deg
Scan mode	STEP	Receiving slit #2	0.300mm

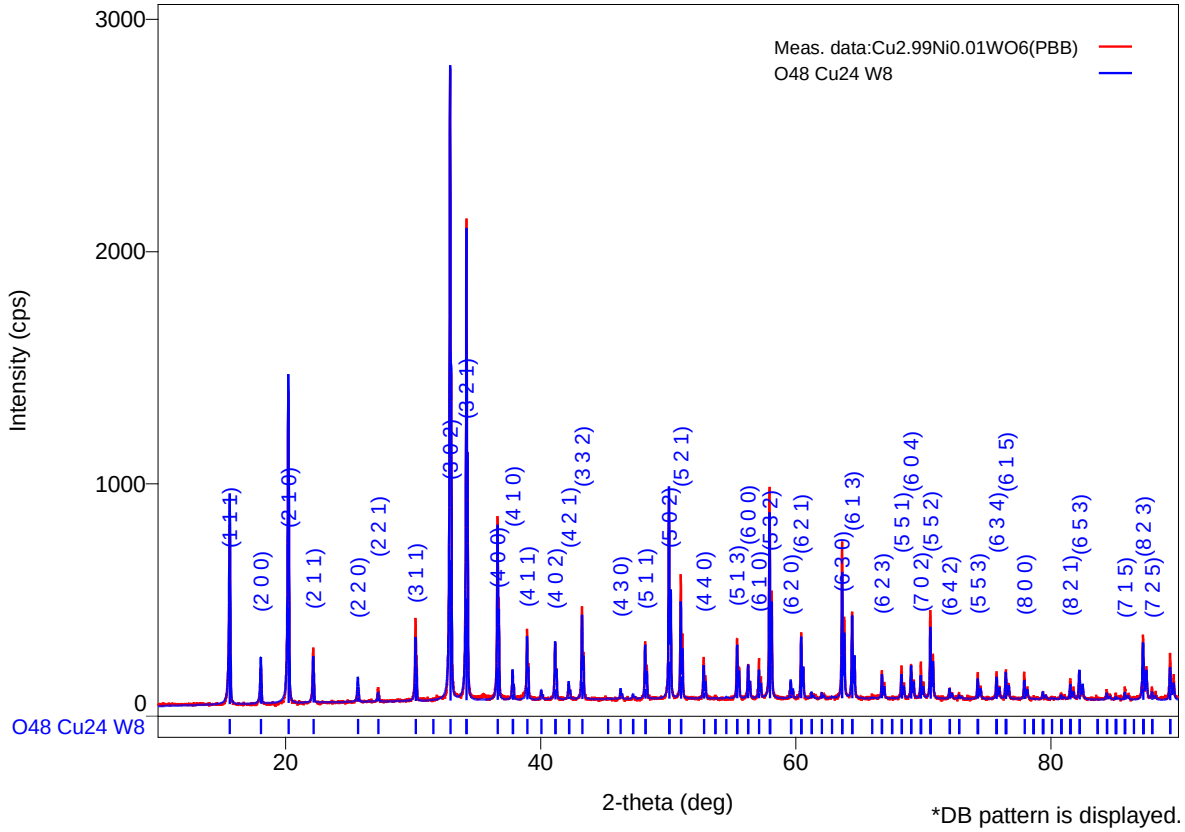

Peak List

No.	2-theta(deg)	d(ang.)	Height(cps)	FWHM(deg)	Int. I(cps deg)	Int. W(deg)	Asym. factor
1	15.6330(18)	5.6639(7)	622(13)	0.075(3)	75.0(8)	0.121(4)	1.24(14)
2	18.068(3)	4.9058(7)	125(6)	0.072(4)	13.5(3)	0.109(8)	0.77(13)
3	20.226(3)	4.3870(6)	1072(17)	0.087(3)	130.8(13)	0.122(3)	1.27(17)
4	22.191(2)	4.0027(4)	189(7)	0.086(3)	21.9(3)	0.116(6)	1.9(2)
5	25.686(7)	3.4654(9)	48(4)	0.096(8)	5.7(3)	0.117(15)	2.4(8)
6	27.274(8)	3.2672(9)	46(4)	0.102(8)	5.3(3)	0.116(16)	2.2(7)
7	30.2091(16)	2.95607(15)	326(10)	0.080(2)	36.6(4)	0.112(5)	1.22(12)
8	32.9153(15)	2.71895(12)	2534(27)	0.0756(16)	276(2)	0.109(2)	1.29(12)
9	34.1968(13)	2.61994(9)	1936(23)	0.0786(14)	215.1(16)	0.111(2)	1.31(10)
10	35.52(4)	2.526(3)	15(2)	0.39(10)	12.6(14)	0.8(2)	1.4(7)
11	36.6340(12)	2.45103(8)	756(15)	0.0770(13)	85.7(6)	0.113(3)	1.01(8)
12	37.810(4)	2.3775(3)	111(6)	0.077(4)	13.4(3)	0.120(9)	1.3(4)
13	38.955(3)	2.31016(19)	281(9)	0.080(4)	36.2(6)	0.129(6)	1.6(4)
14	40.080(8)	2.2479(5)	23(3)	0.11(3)	4.3(4)	0.19(4)	2.8(12)
15	41.149(2)	2.19190(12)	234(8)	0.073(3)	25.1(4)	0.107(5)	0.90(14)
16	41.810(12)	2.1588(6)	6.7(14)	0.05(3)	0.5(2)	0.08(5)	2(4)
17	42.220(5)	2.1388(2)	64(4)	0.081(4)	6.5(3)	0.101(11)	1.8(5)
18	43.2607(16)	2.08969(7)	398(11)	0.0768(14)	41.5(4)	0.104(4)	1.16(11)

19	46.271(3)	1.96051(11)	28(3)	0.066(8)	2.4(2)	0.085(16)	0.6(4)
20	48.211(2)	1.88606(8)	246(8)	0.0788(19)	25.2(4)	0.103(5)	1.42(18)
21	50.0821(12)	1.81988(4)	850(15)	0.0794(10)	92.0(7)	0.108(3)	1.23(8)
22	50.9972(14)	1.78935(4)	527(12)	0.0781(12)	56.0(5)	0.106(3)	1.14(9)
23	52.800(3)	1.73242(9)	171(7)	0.077(3)	18.4(4)	0.107(7)	1.3(2)
24	55.425(2)	1.65644(6)	262(9)	0.0862(19)	29.2(4)	0.112(5)	1.37(15)
25	56.284(3)	1.63317(9)	148(6)	0.086(3)	16.8(4)	0.113(8)	1.5(3)
26	57.132(3)	1.61091(7)	161(7)	0.071(3)	16.1(4)	0.100(6)	1.5(3)
27	57.9660(10)	1.58971(3)	900(16)	0.0822(10)	102.2(6)	0.113(3)	1.23(7)
28	59.626(5)	1.54937(13)	66(4)	0.086(5)	7.0(3)	0.107(12)	1.5(4)
29	60.165(7)	1.53676(16)	9.6(16)	0.033(19)	0.4(2)	0.04(3)	1.27(13)
30	60.440(2)	1.53043(5)	274(9)	0.083(2)	30.1(5)	0.110(5)	1.27(13)
31	61.245(14)	1.5122(3)	24(3)	0.089(14)	2.6(3)	0.11(3)	1.1(9)
32	62.058(7)	1.49434(16)	27(3)	0.071(10)	2.6(3)	0.10(2)	1.5(6)
33	63.6466(12)	1.46083(2)	678(14)	0.0798(13)	75.6(6)	0.112(3)	1.01(7)
34	64.4419(16)	1.44471(3)	369(10)	0.0820(16)	40.7(4)	0.110(4)	1.49(13)
35	66.769(3)	1.39988(6)	120(6)	0.083(4)	13.1(3)	0.110(8)	1.2(2)
36	68.301(3)	1.37218(6)	132(6)	0.089(4)	15.6(4)	0.118(8)	1.05(18)
37	69.060(3)	1.35894(5)	149(6)	0.083(3)	17.2(3)	0.115(7)	0.98(15)
38	69.822(3)	1.34596(5)	144(6)	0.087(3)	16.8(4)	0.116(8)	1.3(2)
39	70.5703(16)	1.33351(3)	377(10)	0.0858(17)	44.2(4)	0.117(4)	1.04(8)
40	72.069(8)	1.30942(13)	43(3)	0.097(8)	4.9(3)	0.115(17)	1.1(4)
41	72.807(14)	1.2980(2)	23(3)	0.093(14)	2.2(4)	0.10(3)	1.0(6)
42	74.284(4)	1.27576(5)	102(5)	0.089(4)	11.4(3)	0.112(9)	1.04(17)
43	75.756(4)	1.25459(6)	108(5)	0.098(4)	13.2(4)	0.123(10)	1.14(19)
44	76.486(4)	1.24442(5)	125(6)	0.092(4)	14.9(4)	0.119(9)	1.18(19)
45	77.9253(13)	1.225000(17	109(6)	0.088(4)	12.3(4)	0.113(9)	0.52(13)
46	79.400(3)	1.20591(4)	24(3)	0.077(11)	2.2(3)	0.09(2)	3(4)
47	80.834(15)	1.18810(18)	19(2)	0.114(15)	2.4(3)	0.12(3)	1.7(10)
48	81.535(4)	1.17964(5)	89(5)	0.088(5)	10.9(3)	0.122(10)	0.79(18)
49	82.249(4)	1.17120(4)	114(6)	0.090(4)	13.8(4)	0.120(9)	0.95(17)
50	84.377(2)	1.14701(2)	40(3)	0.098(6)	4.5(2)	0.114(15)	0.51(18)
51	84.558(19)	1.1450(2)	3.7(10)	0.07(5)	0.32(18)	0.09(7)	0.51(18)
52	85.112(10)	1.13897(10)	21(2)	0.081(13)	2.5(3)	0.12(3)	1.9(12)
53	85.822(9)	1.13136(9)	47(4)	0.088(9)	5.8(3)	0.125(17)	0.9(4)
54	87.236(2)	1.11662(2)	274(9)	0.097(2)	38.8(4)	0.142(6)	0.96(10)
55	87.938(8)	1.10951(8)	46(4)	0.093(9)	6.0(3)	0.129(17)	0.7(3)
56	89.358(3)	1.09552(3)	195(7)	0.094(3)	27.2(5)	0.140(8)	0.83(13)

Crystal Structure analysis results

Indexing

Phase name	Formula	Figure of merit	Phase reg. detail	DB card number
Copper Tungsten	O48 Cu24 W8	0.406	ICDD (PDF2.DAT)	01-071-2208

Lattice information

Phase name	a(A)	b(A)	c(A)	alpha(deg)	beta(deg)	gamma(deg)	V(A^3)
Copper	9.7959(2)	9.7959(2)	9.7959(2)	90.000000	90.000000	90.000000	940.02(4)

Phase name	Space group	Z	Z'	Calc. density(g/cm^3)
Copper Tungsten	205 : Pa-3	1	0.042	6.645

Refinement

Measurement range: 10.0000-90.0000deg Refinement range: 10.0000-90.0000deg (1.09 A)
Number of refined parameters: 30

Phase name	Atomic coords	# of indep. reflns
Copper Tungsten Oxide	Fractional coords	128

Rwp = 5.76% S = 1.0943

3. X-Ray report of $Cu_{2.975}Ni_{0.025}WO_6$

Measurement conditions

X-Ray	40 kV , 44 mA	Scan speed / Duration time	2.3800 sec.
Goniometer	SmartLab(In-plane)	Step width	0.0100 deg
Attachment	RxRy	Scan axis	Theta/2-Theta
Filter	Cu_K-beta	Scan range	10.0000 - 90.0000 deg
CBO selection slit	BB	Incident slit	0.663deg
Diffracted beam mono.	None	Length limiting slit	2.0mm
Detector	SC-70	Receiving slit #1	0.663deg
Scan mode	STEP	Receiving slit #2	0.300mm

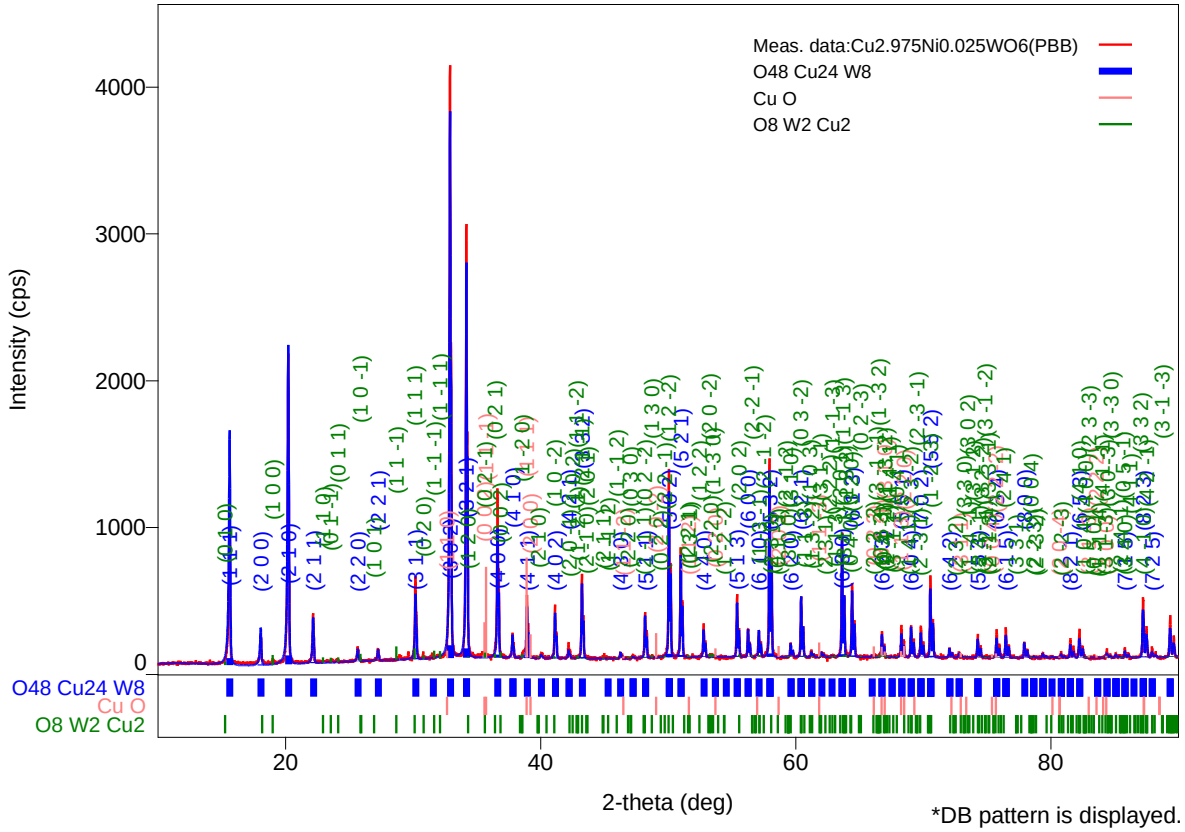

*DB pattern is displayed.

Peak list

No.	2-theta(deg)	d(ang.)	Height(cps)	FWHM(deg)	Int. I(cps deg)	Int. W(deg)	Asym. factor
1	15.627(2)	5.6662(7)	751(18)	0.084(3)	102.4(11)	0.136(5)	1.52(17)
2	18.059(4)	4.9080(10)	153(8)	0.075(8)	21.0(5)	0.137(11)	1.0(3)
3	19.001(13)	4.667(3)	12(2)	0.11(4)	1.5(6)	0.12(7)	0.8(15)
4	20.2229(15)	4.3876(3)	1754(27)	0.073(3)	197.0(18)	0.112(3)	1.19(11)
5	22.173(2)	4.0059(4)	280(11)	0.076(3)	31.4(6)	0.113(6)	0.83(11)
6	25.660(3)	3.4689(4)	77(6)	0.076(11)	11.0(5)	0.143(17)	0.5(3)
7	27.249(7)	3.2701(8)	70(5)	0.088(9)	8.1(4)	0.116(15)	0.8(3)
8	29.640(6)	3.0115(6)	34(4)	0.063(17)	3.3(5)	0.10(3)	0.9(9)
9	30.205(2)	2.9564(2)	494(14)	0.087(3)	58.2(9)	0.118(5)	1.6(2)
10	30.810(15)	2.8998(14)	31(4)	0.062(18)	2.9(4)	0.09(2)	3(5)
11	32.9123(15)	2.71919(12)	3663(39)	0.0852(16)	415(4)	0.113(2)	1.72(13)
12	34.1922(14)	2.62027(11)	2686(34)	0.0856(15)	305(3)	0.114(2)	1.70(13)
13	36.6336(14)	2.45106(9)	1109(22)	0.0709(15)	115.7(10)	0.104(3)	1.11(11)
14	37.805(4)	2.3777(2)	155(8)	0.073(4)	15.4(5)	0.099(9)	1.0(3)
15	38.951(4)	2.3104(2)	390(13)	0.082(4)	50.7(10)	0.130(7)	1.7(4)
16	40.061(6)	2.2489(3)	35(4)	0.092(15)	4.4(5)	0.13(3)	0.8(7)
17	41.149(2)	2.19195(12)	325(12)	0.081(2)	35.0(6)	0.108(6)	1.4(2)
18	42.205(5)	2.1395(2)	103(7)	0.076(4)	9.6(4)	0.094(10)	0.9(3)

19	43.2591(18)	2.08977(8)	545(15)	0.0810(16)	60.9(7)	0.112(4)	1.39(15)
20	44.992(11)	2.0132(5)	14(2)	0.09(5)	2.0(5)	0.15(6)	5(12)
21	45.781(10)	1.9804(4)	8.6(19)	0.03(3)	0.3(3)	0.04(4)	1(3)
22	46.268(5)	1.96061(19)	41(4)	0.076(7)	3.6(3)	0.088(16)	0.9(2)
23	48.211(3)	1.88604(10)	318(12)	0.083(2)	34.5(6)	0.108(6)	1.8(3)
24	50.0793(12)	1.81998(4)	1251(23)	0.0816(10)	135.1(10)	0.108(3)	1.30(8)
25	50.9963(16)	1.78938(5)	726(17)	0.0851(13)	80.0(8)	0.110(4)	1.31(11)
26	51.917(11)	1.7598(4)	13(2)	0.09(3)	1.2(5)	0.09(6)	0.8(13)
27	52.796(3)	1.73256(10)	216(10)	0.076(4)	23.4(6)	0.108(7)	1.1(2)
28	53.335(11)	1.7163(3)	17(3)	0.14(3)	2.5(6)	0.15(6)	0.5(4)
29	53.644(9)	1.7072(3)	11(2)	0.06(3)	0.8(3)	0.07(4)	0.5(4)
30	55.4186(19)	1.65660(5)	406(13)	0.0811(18)	43.6(6)	0.107(5)	1.09(11)
31	56.270(3)	1.63355(9)	198(9)	0.082(3)	21.8(5)	0.110(8)	0.98(18)
32	57.126(4)	1.61109(10)	183(9)	0.086(4)	20.9(6)	0.115(9)	1.4(3)
33	57.9665(11)	1.58970(3)	1349(24)	0.0830(10)	152.0(9)	0.113(3)	1.41(8)
34	59.614(6)	1.54964(13)	91(6)	0.085(6)	9.3(5)	0.103(12)	0.9(3)
35	60.4355(18)	1.53053(4)	400(13)	0.0820(18)	43.2(6)	0.108(5)	0.99(9)
36	61.269(15)	1.5117(3)	31(4)	0.088(17)	3.2(5)	0.10(3)	3(6)
37	62.049(15)	1.4945(3)	42(4)	0.070(18)	5.0(5)	0.12(2)	1.1(11)
38	63.6486(13)	1.46079(3)	828(19)	0.0855(13)	95.1(8)	0.115(4)	1.17(8)
39	64.4371(18)	1.44480(4)	487(14)	0.0827(18)	55.0(7)	0.113(5)	1.26(12)
40	66.775(4)	1.39978(7)	158(8)	0.086(4)	18.9(5)	0.119(9)	1.4(3)
41	68.294(3)	1.37230(5)	219(10)	0.081(3)	24.4(5)	0.111(7)	0.70(13)
42	69.069(3)	1.35879(4)	213(9)	0.089(3)	23.6(5)	0.111(7)	1.41(18)
43	69.821(3)	1.34598(5)	211(9)	0.090(3)	24.0(6)	0.113(8)	0.99(15)
44	70.5740(17)	1.33345(3)	521(15)	0.0868(17)	61.2(7)	0.118(5)	1.09(9)
45	72.076(9)	1.30931(15)	55(5)	0.101(9)	6.6(5)	0.12(2)	1.3(5)
46	72.825(14)	1.2977(2)	33(4)	0.073(14)	3.1(5)	0.09(2)	1.2(10)
47	74.298(4)	1.27556(6)	142(8)	0.089(5)	16.4(6)	0.116(10)	1.7(4)
48	75.760(3)	1.25453(5)	180(9)	0.091(4)	21.2(5)	0.118(9)	1.04(17)
49	76.483(4)	1.24447(6)	187(9)	0.089(4)	22.4(6)	0.120(9)	0.90(18)
50	77.949(5)	1.22468(7)	105(7)	0.099(5)	13.1(5)	0.124(13)	1.4(3)
51	79.383(11)	1.20612(14)	25(3)	0.116(15)	3.2(4)	0.12(3)	0.9(3)
52	80.822(12)	1.18824(15)	33(4)	0.088(11)	3.1(4)	0.10(2)	1.1(6)
53	81.539(5)	1.17959(6)	136(8)	0.082(6)	16.8(5)	0.123(11)	0.8(2)
54	82.257(4)	1.17111(5)	179(9)	0.086(5)	22.7(6)	0.127(9)	0.9(2)
55	84.406(5)	1.14669(6)	53(5)	0.076(10)	6.6(5)	0.13(2)	1.6(5)
56	85.101(4)	1.13908(4)	35(4)	0.075(14)	3.9(4)	0.11(2)	0.6(5)
57	85.816(7)	1.13142(7)	66(5)	0.099(7)	7.8(5)	0.119(17)	0.7(2)
58	87.2421(19)	1.11656(2)	412(13)	0.0961(19)	55.3(6)	0.134(6)	0.94(8)
59	87.942(8)	1.10947(8)	61(5)	0.090(9)	7.0(5)	0.116(18)	0.6(3)
60	89.373(3)	1.09537(3)	273(11)	0.090(3)	35.5(6)	0.130(7)	1.09(16)

Quantitative analysis results (RIR)

Phase name	Content(%)
Copper Tungsten Oxide	90(2)
Copper Oxide	3.4(12)
Copper Tungsten Oxide	6.6(6)

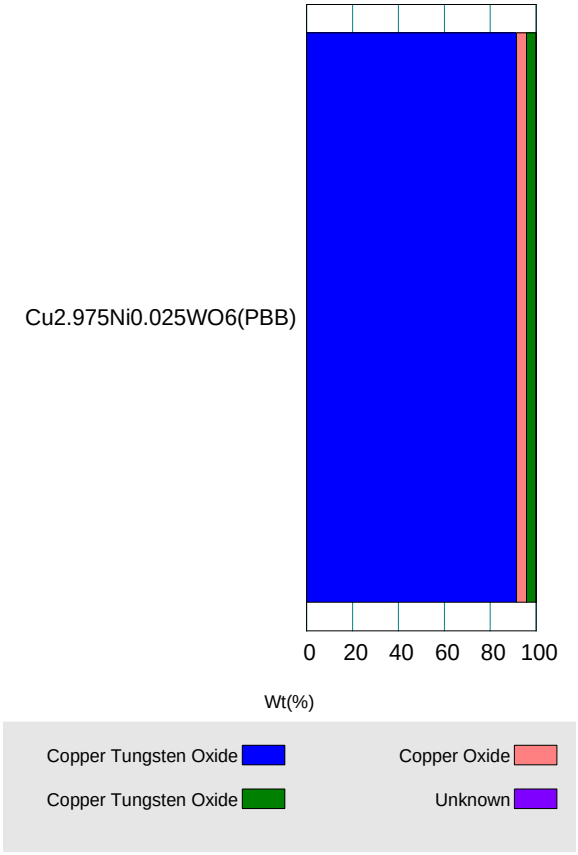

Crystal structure analysis results

Indexing

Phase name	Formula	Figure of merit	Phase reg. detail	DB card number
Copper Tungsten	O48 Cu24 W8	0.573	ICDD (PDF2.DAT)	01-071-2208
Copper Oxide	Cu O	3.537	ICDD (PDF2.DAT)	01-074-1021
Copper Tungsten	O8 W2 Cu2	3.057	ICDD (PDF2.DAT)	01-072-0616

Quantitative analysis results

Lattice information

Phase name	a(A)	b(A)	c(A)	alpha(deg)	beta(deg)	gamma(deg)	V(A^3)
Copper	9.79564(19	9.79564(19	9.79564(19	90.000000	90.000000	90.000000	939.94(3)
Copper	4.95(2)	3.364(6)	4.94(2)	90.000000	99.73(9)	90.000000	81.1(5)
Copper	4.704(3)	5.8391(16)	4.848(4)	91.59(6)	92.14(5)	83.36(6)	132.12(14)

Phase name	Space group	Z	Z'	Calc. density(g/cm^3)
Copper Tungsten	205 : Pa-3	1	0.042	6.645
Copper Oxide	15 : C12/c1,unique-b,cell-1	1	0.125	6.608
Copper Tungsten	2 : P-1	1	0.500	7.790

Refinement

Measurement range: 10.0000-90.0000deg Refinement range: 10.0000-90.0000deg (1.09 A)
Number of refined parameters: 79

Phase name	Atomic coords	# of indep. reflns
Copper Tungsten Oxide	Fractional coords	128
Copper Oxide	Fractional coords	33
Copper Tungsten Oxide	Fractional coords	217

Rwp = 5.94% S = 1.1288

4. X-Ray report of $Cu_{2.95}Ni_{0.05}WO_6$

Measurement conditions

X-Ray	40 kV , 30 mA	Scan speed / Duration time	4.2200 sec.
Goniometer	SmartLab(In-plane)	Step width	0.0100 deg
Attachment	RxRy	Scan axis	Theta/2-Theta
Filter	Cu_K-beta	Scan range	10.0000 - 90.0000 deg
CBO selection slit	BB	Incident slit	0.663deg
Diffracted beam mono.	None	Length limiting slit	2.0mm
Detector	SC-70	Receiving slit #1	0.663deg
Scan mode	STEP	Receiving slit #2	0.300mm

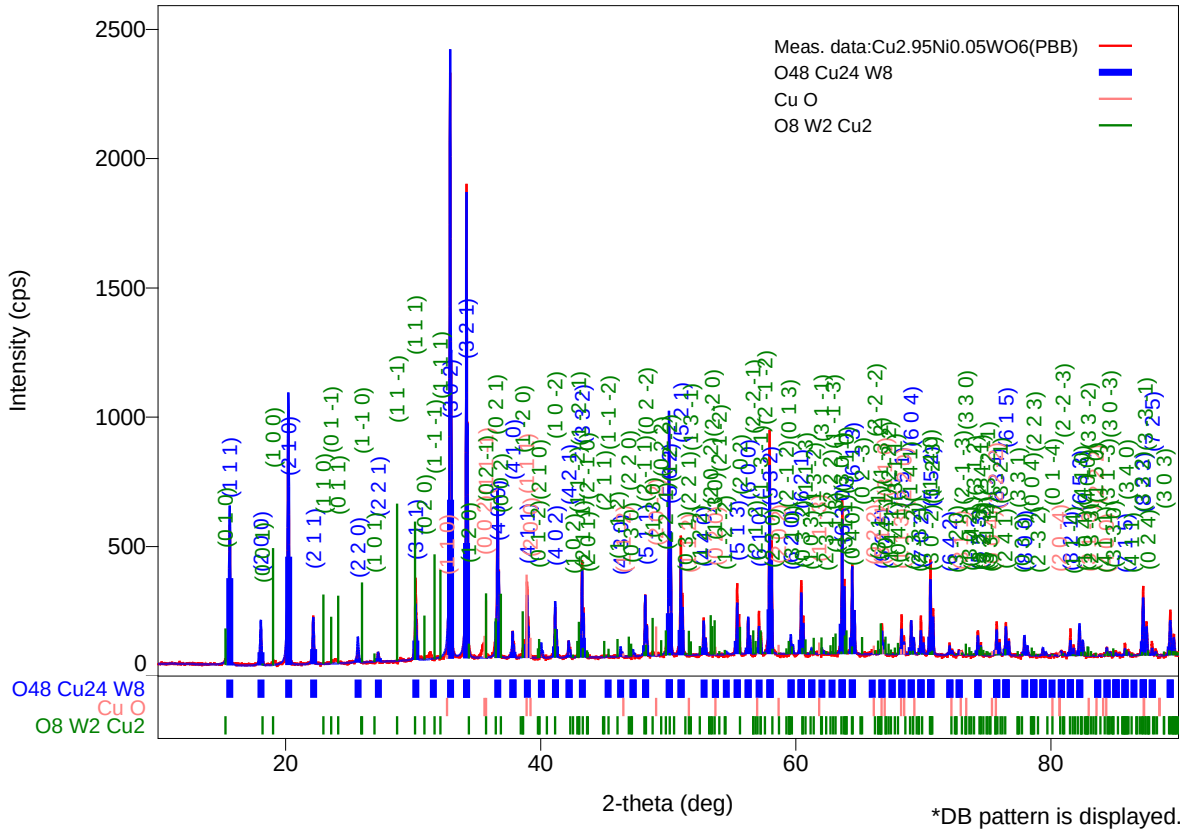

*DB pattern is displayed.

Peak list

No.	2-theta(deg)	d(ang.)	Height(cps)	FWHM(deg)	Int. I(cps deg)	Int. W(deg)	Asym. factor
1	15.6361(14)	5.6628(5)	434(10)	0.074(2)	53.5(4)	0.123(4)	1.28(10)
2	18.074(4)	4.9041(10)	101(5)	0.077(7)	12.6(3)	0.125(9)	1.5(4)
3	19.110(14)	4.641(3)	8.2(14)	0.20(4)	1.8(4)	0.22(9)	1.1(11)
4	20.2267(18)	4.3868(4)	797(14)	0.078(3)	90.3(8)	0.113(3)	1.16(12)
5	22.182(3)	4.0043(5)	152(6)	0.076(4)	16.5(3)	0.108(6)	1.03(18)
6	25.675(3)	3.4669(4)	49(3)	0.068(7)	6.1(2)	0.127(13)	0.9(2)
7	27.256(11)	3.2692(13)	29(3)	0.097(11)	3.1(3)	0.105(19)	0.9(4)
8	30.226(2)	2.9545(2)	268(8)	0.083(3)	32.7(5)	0.122(6)	2.5(4)
9	31.31(3)	2.855(3)	11.9(17)	0.91(8)	15.9(9)	1.3(3)	2.5(4)
10	32.9172(13)	2.71880(10)	2106(22)	0.0766(14)	226.2(17)	0.107(2)	1.21(9)
11	34.1995(10)	2.61973(7)	1721(20)	0.0743(11)	179.5(11)	0.1043(19)	1.30(8)
12	35.532(15)	2.5245(11)	38(3)	0.23(3)	13.6(6)	0.36(4)	2.0(9)
13	36.421(4)	2.4649(3)	31(3)	0.070(11)	3.1(4)	0.10(2)	1.29(10)
14	36.6394(13)	2.45068(8)	610(12)	0.0784(13)	68.9(6)	0.113(3)	1.29(10)
15	37.818(4)	2.3770(2)	105(5)	0.072(4)	11.0(3)	0.105(8)	1.3(4)
16	38.697(6)	2.3250(4)	45(3)	0.157(17)	10.2(7)	0.22(3)	1.17(14)
17	38.9531(19)	2.31028(11)	281(8)	0.0766(19)	30.8(7)	0.109(6)	1.17(14)
18	40.065(14)	2.2487(8)	18(2)	0.097(14)	1.9(3)	0.11(3)	1.7(11)
19	40.921(8)	2.2036(4)	8.1(14)	0.04(2)	0.4(2)	0.05(3)	1.16(17)
20	41.155(2)	2.19164(12)	185(7)	0.078(2)	19.7(4)	0.107(6)	1.16(17)
21	42.213(5)	2.1391(3)	62(4)	0.080(4)	5.9(3)	0.096(11)	0.9(3)
22	43.2648(17)	2.08950(8)	377(9)	0.0735(15)	37.5(4)	0.100(4)	1.16(12)
23	46.282(9)	1.9601(3)	27(3)	0.078(7)	2.2(3)	0.083(17)	1.3(6)
24	48.216(2)	1.88586(8)	234(7)	0.0775(19)	24.1(4)	0.103(5)	1.53(19)
25	48.78(4)	1.8653(15)	10.5(16)	0.19(6)	2.8(5)	0.27(8)	1.1(12)
26	49.865(4)	1.82729(14)	27(3)	0.058(11)	2.0(4)	0.08(2)	1.26(7)
27	50.0867(10)	1.81972(3)	882(14)	0.0771(9)	89.3(7)	0.101(2)	1.26(7)
28	51.0015(16)	1.78921(5)	459(10)	0.0762(16)	49.3(5)	0.107(4)	1.16(11)
29	52.800(3)	1.73242(9)	141(6)	0.082(3)	15.6(4)	0.111(7)	1.10(19)
30	53.43(3)	1.7135(8)	8.9(15)	0.17(7)	2.1(6)	0.24(10)	4(5)
31	53.70(3)	1.7056(8)	8.9(15)	0.16(7)	2.0(6)	0.22(11)	4(5)
32	55.4248(19)	1.65643(5)	276(8)	0.0798(19)	30.1(4)	0.109(5)	0.94(10)
33	56.281(3)	1.63325(7)	146(6)	0.074(3)	15.1(3)	0.103(6)	1.20(19)
34	56.919(9)	1.6164(2)	9.1(15)	0.05(2)	0.6(2)	0.06(3)	1.00(13)
35	57.131(2)	1.61095(6)	162(6)	0.076(2)	15.0(4)	0.093(6)	1.00(13)
36	57.9696(11)	1.58962(3)	864(14)	0.0788(11)	95.1(6)	0.110(3)	1.19(7)
37	59.631(6)	1.54925(14)	55(4)	0.090(5)	5.3(3)	0.096(12)	1.2(3)
38	60.4460(17)	1.53029(4)	297(8)	0.0782(18)	30.2(4)	0.102(4)	1.13(11)
39	61.262(14)	1.5119(3)	19(2)	0.076(18)	2.1(3)	0.11(3)	1.6(16)
40	62.047(5)	1.49459(10)	23(2)	0.074(18)	2.6(3)	0.11(2)	0.5(6)
41	63.6555(12)	1.46064(3)	585(12)	0.0804(13)	63.9(5)	0.109(3)	1.13(7)
42	64.4408(14)	1.44473(3)	337(9)	0.0787(15)	37.2(4)	0.110(4)	1.12(9)
43	66.00(3)	1.4144(6)	11.6(17)	0.20(6)	4.7(5)	0.41(10)	0.7(7)
44	66.774(3)	1.39981(6)	113(5)	0.080(4)	12.7(3)	0.113(8)	0.99(18)
45	68.309(3)	1.37204(5)	150(6)	0.081(3)	17.3(3)	0.116(7)	1.06(17)
46	69.065(3)	1.35885(5)	126(5)	0.093(3)	15.0(3)	0.119(8)	0.96(12)

47	69.821(3)	1.34598(5)	146(6)	0.082(3)	16.0(4)	0.110(7)	0.69(13)
48	70.5757(16)	1.33342(3)	362(9)	0.0859(17)	42.6(4)	0.118(4)	0.86(7)
49	72.068(3)	1.30943(4)	46(3)	0.076(7)	4.5(3)	0.098(14)	0.7(3)
50	72.808(3)	1.29794(5)	26(2)	0.079(11)	2.5(3)	0.10(2)	0.5(3)
51	74.301(4)	1.27552(6)	93(5)	0.090(4)	10.5(3)	0.113(9)	1.3(2)
52	75.767(3)	1.25444(4)	124(5)	0.085(3)	14.3(3)	0.115(7)	1.4(2)
53	76.492(3)	1.24435(4)	128(5)	0.087(3)	15.8(3)	0.124(8)	1.02(17)
54	77.947(6)	1.22471(8)	70(4)	0.096(6)	8.8(4)	0.126(13)	1.2(3)
55	79.376(5)	1.20622(6)	19(2)	0.087(15)	1.8(3)	0.09(3)	0.5(4)
56	80.841(11)	1.18801(13)	19(2)	0.107(18)	2.8(3)	0.15(3)	1.7(7)
57	81.549(4)	1.17948(5)	94(5)	0.082(4)	10.6(3)	0.113(9)	1.1(3)
58	82.259(4)	1.17109(5)	106(5)	0.100(4)	14.5(3)	0.137(10)	0.90(16)
59	84.402(12)	1.14672(14)	27(3)	0.112(13)	3.7(3)	0.14(3)	1.0(5)
60	85.117(19)	1.1389(2)	16(2)	0.13(2)	2.3(4)	0.14(4)	2.1(14)
61	85.816(7)	1.13142(7)	47(3)	0.091(6)	5.1(3)	0.108(14)	0.57(19)
62	87.248(2)	1.11649(2)	265(8)	0.094(2)	36.1(4)	0.136(6)	1.07(11)
63	87.941(3)	1.10948(3)	43(3)	0.094(8)	4.8(4)	0.111(17)	0.5(2)
64	89.376(3)	1.09535(3)	170(6)	0.099(3)	23.0(4)	0.135(8)	1.08(16)

Quantitative analysis results (RIR)

Phase name	Content(%)
Copper Tungsten Oxide	83(699557)
Copper Oxide	5(499479)
Copper Tungsten Oxide	10(77877)

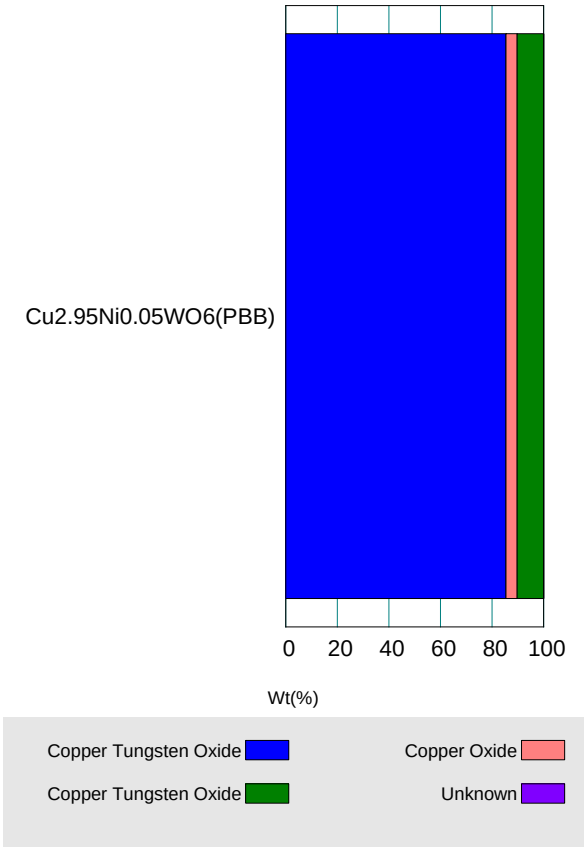

Crystal structure analysis results

Indexing

Phase name	Formula	Figure of merit	Phase reg. detail	DB card number
Copper Tungsten	O48 Cu24 W8	0.644	ICDD (PDF2.DAT)	01-071-2208
Copper Oxide	Cu O	1.399	ICDD (PDF2.DAT)	01-074-1021
Copper Tungsten	O8 W2 Cu2	2.968	ICDD (PDF2.DAT)	01-070-1732

Quantitative analysis results

Lattice information

Phase name	a(A)	b(A)	c(A)	alpha(deg)	beta(deg)	gamma(deg)	V(A^3)
Copper	9.79532(17	9.79532(17	9.79532(17	90.000000	90.000000	90.000000	939.84(3)
Copper	4.6832(8)	3.4281(5)	5.1339(8)	90.000000	99.422(9)	90.000000	81.31(2)
Copper	5.149(15)	5(53)	4.78(4)	102(24)	95(19)	87(708)	131(1260)

Phase name	Space group	Z	Z'	Calc. density(g/cm^3)
Copper Tungsten	205 : Pa-3	1	0.042	6.645
Copper Oxide	15 : C12/c1,unique-b,cell-1	1	0.125	6.608
Copper Tungsten	2 : P-1	1	0.500	7.821

Refinement

Measurement range: 10.0000-90.0000deg Refinement range: 10.0000-90.0000deg (1.09 A)
Number of refined parameters: 95

Phase name	Atomic coords	# of indep. reflns
Copper Tungsten Oxide	Fractional coords	128
Copper Oxide	Fractional coords	35
Copper Tungsten Oxide	Fractional coords	229

Rwp = 5.53% S = 1.1554

5. X-Ray report of $Cu_{2.9}Ni_{0.1}WO_6$

Measurement conditions

X-Ray	40 kV , 40 mA	Scan speed / Duration time	2.9200 sec.
Goniometer	SmartLab(In-plane)	Step width	0.0110 deg
Attachment	RxRy	Scan axis	Theta/2-Theta
Filter	Cu_K-beta	Scan range	10.0000 - 89.9920 deg
CBO selection slit	BB	Incident slit	0.663deg
Diffracted beam mono.	None	Length limiting slit	2.0mm
Detector	SC-70	Receiving slit #1	0.663deg
Scan mode	STEP	Receiving slit #2	0.300mm

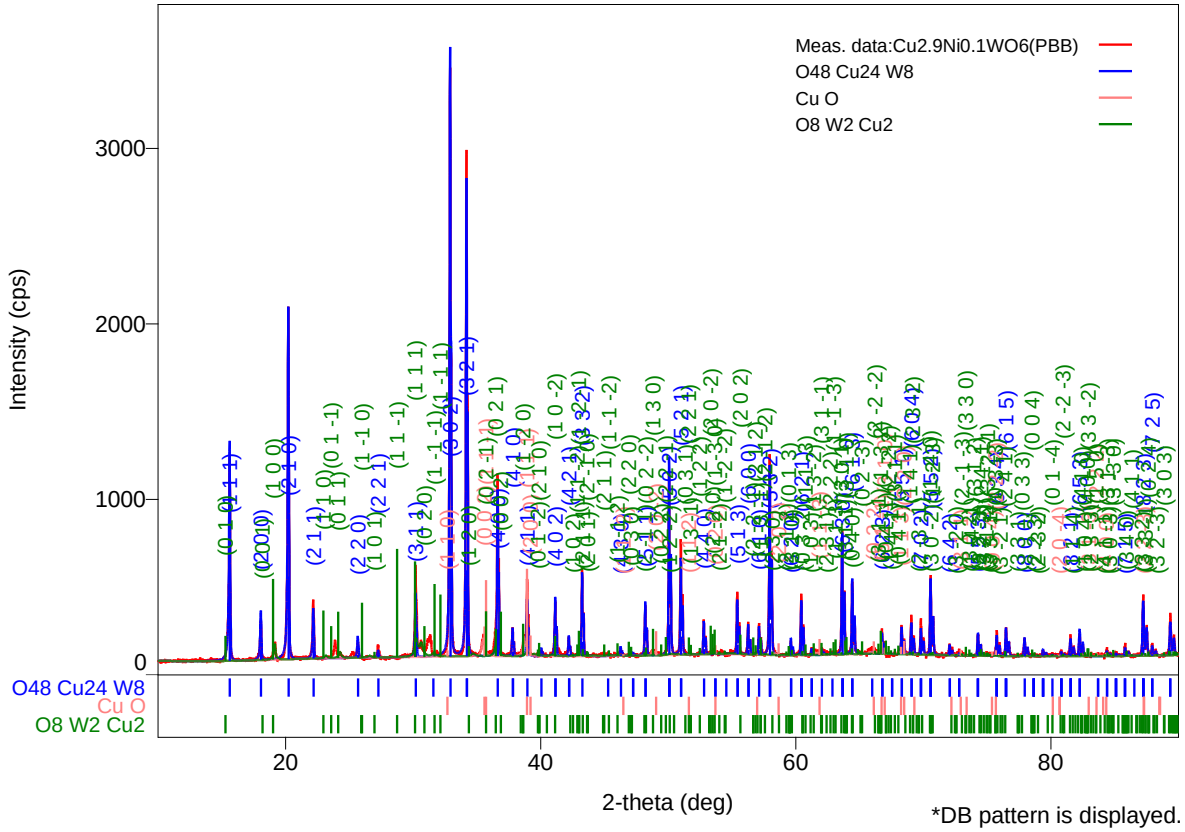

*DB pattern is displayed.

Peak list

No.	2-theta(deg)	d(ang.)	Height(cps)	FWHM(deg)	Int. I(cps deg)	Int. W(deg)	Asym. factor
1	12.5(8)	7.1(4)	1.1(6)	1(2)	1.50386	1.4(8)	1(5)
2	13.3(3)	6.65(12)	1.4(7)	0.2(7)	0.239707	0.18(9)	1(5)
3	15.6358(19)	5.6629(7)	902(18)	0.079(3)	114.991	0.127(2)	1.9(2)
4	15.90(3)	5.569(11)	3.1(10)	0.1(2)	0.293305	0.10(3)	4(122)
5	18.076(4)	4.9035(11)	160(7)	0.093(5)	19.4691	0.122(6)	2.3(5)
6	18.17(6)	4.879(17)	9.8(19)	0.12(8)	1.5638	0.16(3)	2.3(5)
7	19.156(6)	4.6294(14)	66(5)	0.098(16)	9.6211	0.146(10)	0.6(5)
8	19.62(17)	4.52(4)	2.4(9)	0.1(9)	0.187406	0.08(3)	1(17)
9	20.2274(13)	4.3866(3)	1654(24)	0.0791(16)	192.143	0.1162(17)	1.38(11)
10	20.42(4)	4.346(9)	8.5(17)	0.09(13)	1.11053	0.13(3)	1.38(11)
11	20.968(17)	4.233(3)	5.5(14)	0.03(4)	0.161045	0.029(7)	1(6)
12	22.001(10)	4.0368(19)	14(2)	0.03(2)	0.596594	0.041(6)	0.61(8)
13	22.1704(12)	4.0064(2)	276(10)	0.075(3)	29.4203	0.107(4)	0.61(8)
14	22.335(8)	3.9773(14)	14(2)	0.02(3)	0.471735	0.034(5)	0.61(8)
15	23.306(19)	3.814(3)	5.5(14)	0.04(5)	0.310108	0.057(14)	2.3(4)
16	23.69(3)	3.753(4)	12(2)	0.16(6)	2.66907	0.22(4)	2.3(4)
17	23.911(5)	3.7185(8)	71(5)	0.130(9)	12.6753	0.179(12)	2.3(4)
18	24.292(12)	3.6610(18)	17(2)	0.13(3)	3.18501	0.18(3)	2.3(4)

19	25.309(13)	3.5162(17)	20(3)	0.22(4)	5.00753	0.25(3)	3.7(11)
20	25.694(6)	3.4644(8)	64(5)	0.116(8)	8.57065	0.134(10)	3.7(11)
21	25.83(5)	3.446(7)	4.0(12)	0.0(2)	0.215631	0.054(16)	3.7(11)
22	26.277(12)	3.3888(15)	4.5(12)	0.02(5)	0.107322	0.024(7)	4(42)
23	26.40(3)	3.373(4)	8.1(17)	0.02(3)	0.202758	0.025(5)	4(42)
24	27.252(3)	3.2698(4)	60(5)	0.071(10)	5.81183	0.097(7)	0.7(5)
25	29.15(6)	3.061(7)	4.1(12)	0.04(7)	0.167615	0.040(12)	1(7)
26	29.35(13)	3.041(13)	1.6(7)	0.1(2)	0.127605	0.08(4)	1(7)
27	29.51(5)	3.024(5)	3.4(11)	0.02(7)	0.0822779	0.024(8)	1(7)
28	30.213(3)	2.9557(3)	424(12)	0.093(4)	57.9323	0.137(4)	1.6(3)
29	30.638(17)	2.9157(16)	48(4)	0.14(3)	8.81323	0.184(16)	2.0(9)
30	31.29(3)	2.856(3)	62(5)	0.33(4)	26.6863	0.43(3)	2.0(9)
31	32.9164(19)	2.71886(15)	2959(32)	0.0848(18)	334.647	0.1131(12)	1.65(16)
32	34.12(3)	2.626(2)	309(10)	0.142(5)	47.6404	0.154(5)	1.27(6)
33	34.1974(9)	2.61989(6)	2526(29)	0.0731(10)	200.788	0.0795(9)	1.27(6)
34	34.306(19)	2.6118(14)	107(6)	0.12(4)	14.376	0.134(8)	1.27(6)
35	35.482(17)	2.5279(12)	62(5)	0.209(16)	13.7566	0.223(17)	0.9(3)
36	35.83(7)	2.504(5)	2.0(8)	0.04(18)	0.0822231	0.041(17)	0.9(3)
37	36.54(3)	2.457(2)	105(6)	0.23(4)	27.984	0.265(15)	1.37(13)
38	36.6391(14)	2.45070(9)	831(17)	0.078(3)	74.6226	0.0898(18)	1.37(13)
39	36.75(3)	2.4439(18)	54(4)	0.13(6)	8.08119	0.150(12)	1.37(13)
40	37.64(3)	2.3876(16)	7.0(16)	0.12(7)	0.899722	0.13(3)	1.3(3)
41	37.811(5)	2.3774(3)	125(7)	0.088(4)	11.6947	0.094(5)	1.3(3)
42	38.709(6)	2.3243(3)	82(5)	0.140(12)	16.5024	0.200(13)	1.7(2)
43	38.955(2)	2.31016(14)	396(12)	0.084(3)	47.5956	0.120(4)	1.7(2)
44	40.07(2)	2.2486(12)	22(3)	0.09(2)	2.17087	0.097(12)	1.0(10)
45	40.795(4)	2.2101(2)	17(2)	0.014(17)	0.309316	0.018(3)	2.0(5)
46	41.145(18)	2.1921(9)	109(6)	0.11(2)	15.0298	0.138(8)	2.0(5)
47	41.169(8)	2.1909(4)	196(8)	0.069(17)	17.1911	0.088(4)	2.0(5)
48	41.305(10)	2.1840(5)	13(2)	0.04(3)	0.706917	0.055(9)	2.0(5)
49	41.450(7)	2.1767(4)	28(3)	0.09(2)	3.16833	0.112(12)	2.0(5)
50	41.940(11)	2.1524(5)	7.5(16)	0.03(4)	0.329709	0.044(9)	2.0(5)
51	42.211(5)	2.1392(3)	91(6)	0.075(8)	9.82414	0.108(7)	0.8(3)
52	42.368(11)	2.1316(5)	12(2)	0.03(3)	0.48823	0.042(7)	0.8(3)
53	42.51(2)	2.1247(10)	6.1(14)	0.02(5)	0.197893	0.033(8)	0.8(3)
54	42.71(5)	2.115(2)	2.6(9)	0.02(10)	0.0873482	0.034(13)	0.8(3)
55	43.2606(11)	2.08970(5)	467(13)	0.082(7)	47.6513	0.102(3)	1.12(17)
56	43.45(3)	2.0812(14)	7.0(16)	0.18(8)	1.59154	0.23(5)	1.12(17)
57	43.7(6)	2.07(3)	3.5(11)	0.0(16)	0.115538	0.033(10)	1.12(17)
58	43.98(13)	2.057(6)	1.3(7)	0.1(3)	0.119086	0.09(5)	1.12(17)
59	44.187(19)	2.0480(8)	6.3(15)	0.05(5)	0.41811	0.066(15)	1.12(17)
60	44.93(3)	2.0157(12)	6.9(16)	0.17(9)	1.24217	0.18(4)	4(13)
61	45.333(7)	1.9989(3)	16(2)	0.026(18)	0.521894	0.032(5)	0.6(19)
62	45.6(2)	1.989(10)	0.4(4)	0.2(6)	0.109255	0.2(2)	0.6(19)
63	45.812(14)	1.9791(6)	7.0(16)	0.03(3)	0.228549	0.033(7)	0.6(19)
64	46.18(6)	1.964(2)	1.6(7)	0.05(12)	0.111257	0.07(3)	0.5(7)
65	46.266(6)	1.9607(3)	29(3)	0.068(19)	2.72984	0.094(10)	0.5(7)
66	48.1995(18)	1.88647(7)	290(10)	0.065(3)	28.0108	0.097(3)	0.52(8)
67	48.65(14)	1.870(5)	2.0(8)	0.1(5)	0.2583	0.13(6)	1.3(9)
68	48.800(19)	1.8646(7)	22(3)	0.11(3)	3.63949	0.16(2)	1.3(9)

69	50.0817(16)	1.81989(5)	1013(19)	0.0804(14)	105.649	0.1043(19)	1.22(10)
70	50.336(15)	1.8113(5)	21(3)	0.05(5)	1.91254	0.090(11)	2(6)
71	50.9966(19)	1.78937(6)	633(15)	0.0799(17)	66.4283	0.105(2)	1.11(11)
72	51.19(2)	1.7830(7)	16(2)	0.08(6)	1.71467	0.111(16)	1.11(11)
73	52.52(3)	1.7410(10)	7.5(16)	0.11(7)	0.946881	0.13(3)	0.8(2)
74	52.701(13)	1.7355(4)	19(3)	0.06(3)	1.21692	0.064(9)	0.8(2)
75	52.794(4)	1.73261(12)	186(8)	0.080(5)	16.4915	0.089(4)	0.8(2)
76	53.373(16)	1.7152(5)	9.9(18)	0.06(4)	0.66033	0.067(12)	0.8(2)
77	53.604(17)	1.7083(5)	14(2)	0.12(4)	1.88809	0.13(2)	0.8(2)
78	54.08(9)	1.694(3)	3.0(10)	0.1(2)	0.246245	0.08(3)	0.8(2)
79	54.163(14)	1.6920(4)	20(3)	0.07(3)	1.57566	0.077(10)	0.8(2)
80	54.93(4)	1.6701(11)	15(2)	0.09(4)	1.46968	0.095(14)	1.0(19)
81	55.428(3)	1.65636(7)	337(11)	0.085(2)	36.199	0.107(3)	1.29(17)
82	55.716(17)	1.6485(5)	6.9(15)	0.02(4)	0.164891	0.024(5)	1(20)
83	56.15(6)	1.6366(17)	9.1(18)	0.13(9)	1.33458	0.15(3)	0.87(17)
84	56.274(4)	1.63344(10)	170(8)	0.079(3)	14.9097	0.088(4)	0.87(17)
85	57.133(4)	1.61090(11)	171(8)	0.082(4)	16.1854	0.095(4)	1.5(3)
86	57.74(4)	1.5955(10)	10.2(19)	0.11(8)	1.41523	0.14(3)	1.17(8)
87	57.90(14)	1.591(4)	88(5)	0.13(3)	13.7188	0.157(10)	1.17(8)
88	57.9688(12)	1.58965(3)	1054(19)	0.0815(15)	104.734	0.0994(18)	1.17(8)
89	58.24(3)	1.5829(8)	8.9(17)	0.12(9)	1.23911	0.14(3)	1(4)
90	59.622(10)	1.5495(2)	64(5)	0.080(9)	5.63678	0.089(7)	0.9(5)
91	60.4374(11)	1.53049(2)	332(11)	0.088(2)	33.6157	0.101(3)	0.96(14)
92	60.58(4)	1.5272(10)	6.9(15)	0.17(13)	1.37611	0.20(4)	0.96(14)
93	61.26(2)	1.5119(5)	28(3)	0.08(2)	2.71624	0.096(11)	0.9(11)
94	61.78(8)	1.5003(18)	4.5(12)	0.4(2)	1.8915	0.42(12)	0.96(14)
95	62.058(9)	1.49436(19)	22(3)	0.08(2)	2.01012	0.092(11)	0.96(14)
96	62.82(4)	1.4780(8)	4.3(12)	0.10(9)	0.472388	0.11(3)	0.96(14)
97	63.20(2)	1.4701(5)	5.2(13)	0.02(7)	0.12454	0.024(6)	1(6)
98	63.6531(18)	1.46069(4)	692(15)	0.0844(17)	76.8323	0.111(2)	1.18(11)
99	64.33(6)	1.4470(12)	11(2)	0.11(5)	1.47965	0.13(2)	1.14(10)
100	64.4390(19)	1.44476(4)	396(12)	0.0857(17)	40.1331	0.101(3)	1.14(10)
101	64.75(2)	1.4385(5)	19(3)	0.04(2)	0.907047	0.047(6)	1(3)
102	65.93(9)	1.4156(17)	15(2)	0.37(9)	6.01838	0.39(6)	1.0(3)
103	66.27(14)	1.409(3)	2.0(8)	0.1(3)	0.171609	0.09(4)	1.0(3)
104	66.3(5)	1.408(9)	4.9(13)	0.16(18)	0.822382	0.17(4)	1.0(3)
105	66.773(7)	1.39982(12)	117(6)	0.092(6)	11.5548	0.098(5)	1.1(3)
106	68.07(4)	1.3762(8)	7.4(16)	0.10(11)	0.786811	0.11(2)	0.9(2)
107	68.27(6)	1.3728(10)	23(3)	0.25(14)	5.95788	0.26(3)	0.9(2)
108	68.304(5)	1.37212(9)	124(7)	0.078(9)	10.3443	0.083(4)	0.9(2)
109	68.577(10)	1.36732(18)	12(2)	0.03(2)	0.35221	0.029(5)	0.9(2)
110	69.067(3)	1.35882(5)	209(8)	0.089(3)	21.2104	0.101(4)	1.08(14)
111	69.823(4)	1.34595(7)	194(8)	0.091(4)	20.2195	0.104(4)	1.1(2)
112	70.585(2)	1.33327(4)	450(12)	0.088(2)	49.9261	0.111(3)	1.54(18)
113	70.879(11)	1.32845(18)	5.9(14)	0.02(6)	0.119943	0.020(5)	1(18)
114	70.99(6)	1.3266(9)	2.7(10)	0.02(13)	0.0714066	0.027(9)	1(18)
115	71.81(3)	1.3135(4)	8.2(17)	0.03(4)	0.232951	0.029(6)	5(289)
116	72.073(9)	1.30935(14)	62(5)	0.087(9)	6.57398	0.107(8)	1.0(5)
117	72.43(9)	1.3038(15)	4.8(13)	0.09(9)	0.470556	0.10(3)	1(3)
118	72.812(17)	1.2979(3)	31(3)	0.108(15)	3.59768	0.116(12)	0.8(6)

119	73.60(5)	1.2859(8)	3.4(11)	0.14(15)	0.525987	0.15(5)	1(4)
120	74.053(16)	1.2792(2)	4.3(12)	0.06(4)	0.269787	0.063(18)	1.73(6)
121	74.302(2)	1.27550(3)	112(6)	0.085(4)	10.6165	0.095(5)	1.73(6)
122	74.48(8)	1.2729(12)	5.5(14)	0.4(2)	2.33825	0.43(11)	1.73(6)
123	74.95(13)	1.2660(19)	2.6(9)	0.2(3)	0.61385	0.24(9)	1.73(6)
124	75.045(10)	1.26471(15)	8.3(17)	0.05(4)	0.420308	0.050(10)	1.73(6)
125	75.25(2)	1.2617(3)	4.0(12)	0.02(4)	0.106343	0.027(8)	1.73(6)
126	75.603(10)	1.25675(15)	14(2)	0.06(3)	1.05959	0.074(11)	1.9(6)
127	75.773(5)	1.25436(7)	136(7)	0.091(6)	16.0823	0.118(6)	1.9(6)
128	76.495(4)	1.24430(6)	113(6)	0.076(8)	9.1762	0.081(4)	1.3(4)
129	76.51(2)	1.2441(3)	40(4)	0.18(4)	7.8623	0.195(18)	1.3(4)
130	77.816(5)	1.22645(7)	20(3)	0.045(12)	0.944558	0.048(6)	1.4(2)
131	77.947(4)	1.22471(5)	88(5)	0.103(5)	9.68077	0.110(7)	1.4(2)
132	78.68(2)	1.2151(3)	6.8(15)	0.08(7)	0.578675	0.085(19)	1(3)
133	79.40(2)	1.2059(3)	22(3)	0.11(2)	2.46304	0.113(14)	1.0(9)
134	80.10(5)	1.1971(6)	4.0(12)	0.15(16)	0.621978	0.16(5)	1(2)
135	80.36(4)	1.1939(5)	4.2(12)	0.08(11)	0.350073	0.08(2)	1(2)
136	80.83(2)	1.1882(3)	25(3)	0.10(2)	2.62286	0.104(12)	1.6(17)
137	81.349(16)	1.18187(19)	9.4(18)	0.04(4)	0.419954	0.045(9)	1.0(3)
138	81.545(2)	1.17953(2)	107(6)	0.087(6)	10.7673	0.101(6)	1.0(3)
139	81.692(13)	1.17777(16)	12(2)	0.06(4)	0.812778	0.066(11)	1.0(3)
140	82.10(4)	1.1729(5)	5.7(14)	0.12(11)	0.719285	0.13(3)	1.1(5)
141	82.261(6)	1.17106(7)	114(6)	0.101(13)	12.3109	0.108(6)	1.1(5)
142	82.37(3)	1.1698(3)	17(2)	0.08(7)	1.50481	0.087(12)	1.1(5)
143	82.87(4)	1.1640(5)	3.3(11)	0.02(6)	0.0788251	0.024(8)	1(7)
144	83.07(4)	1.1617(4)	5.4(14)	0.03(4)	0.15552	0.029(7)	1(7)
145	83.505(16)	1.15675(18)	5.5(14)	0.03(6)	0.340795	0.062(15)	5(21)
146	83.721(13)	1.15431(15)	11(2)	0.04(4)	0.804427	0.072(13)	5(21)
147	84.40(2)	1.1467(3)	28(3)	0.11(2)	3.2367	0.114(13)	1.0(9)
148	85.12(2)	1.1389(2)	21(3)	0.08(2)	1.89695	0.092(12)	1.3(14)
149	85.818(12)	1.13140(12)	50(4)	0.095(10)	5.10713	0.102(8)	0.9(4)
150	87.248(3)	1.11649(3)	334(11)	0.101(3)	44.4299	0.133(4)	1.15(13)
151	87.586(10)	1.11305(10)	19(3)	0.01(5)	0.194235	0.0104(14)	1(16476)
152	87.952(4)	1.10937(4)	55(4)	0.096(10)	5.82652	0.105(8)	0.8(4)
153	89.373(4)	1.09537(4)	219(9)	0.104(4)	29.5328	0.135(5)	0.92(15)

Quantitative analysis results (RIR)

Phase name	Content(%)
Copper Tungsten Oxide	80.816068
Copper Oxide	6.529748
Copper Tungsten Oxide	12.714184

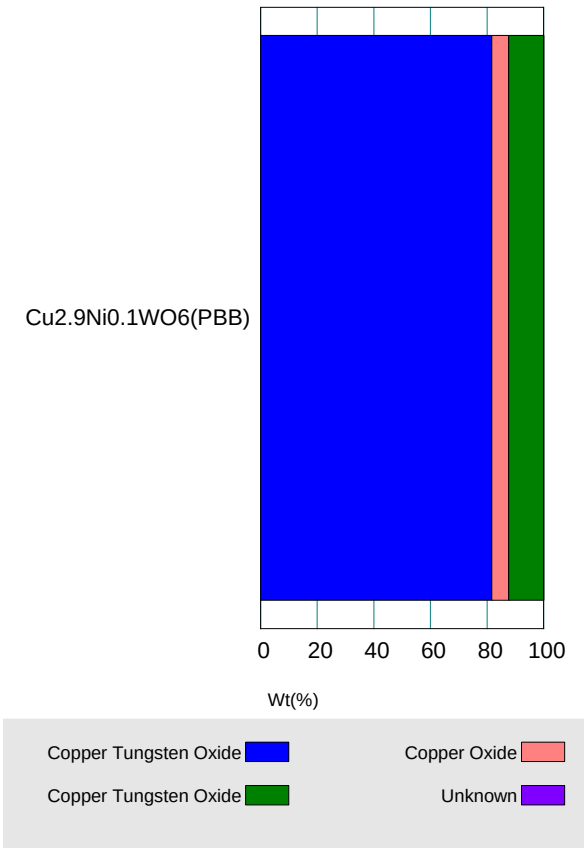

Crystal structure analysis results

Indexing

Phase name	Formula	Figure of merit	Phase reg. detail	DB card number
Copper Tungsten	O48 Cu24 W8	0.569	ICDD (PDF2.DAT)	01-071-2208
Copper Oxide	Cu O	1.480	ICDD (PDF2.DAT)	01-074-1021
Copper Tungsten	O8 W2 Cu2	6.975	ICDD (PDF2.DAT)	01-070-1732

Quantitative analysis results

Lattice information

Phase name	a(A)	b(A)	c(A)	alpha(deg)	beta(deg)	gamma(deg)	V(A^3)
Copper	9.7944(2)	9.7944(2)	9.7944(2)	90.000000	90.000000	90.000000	939.58(4)
Copper	4.6813(18)	3.4252(12)	5.1270(19)	90.000000	99.451(19)	90.000000	81.09(5)
Copper	4.6745(7)	5.660(2)	4.5774(12)	93.47(3)	86.29(2)	82.34(2)	119.48(6)

Phase name	Space group	Z	Z'	Calc. density(g/cm^3)
Copper Tungsten	205 : Pa-3	1	0.042	6.645
Copper Oxide	15 : C12/c1,unique-b,cell-1	1	0.125	6.608
Copper Tungsten	2 : P-1	1	0.500	7.821

Refinement

Measurement range: 10.0000-89.9920deg Refinement range: 10.0000-89.9920deg (1.09 A)
Number of refined parameters: 95

Phase name	Atomic coords	# of indep. reflns
Copper Tungsten Oxide	Fractional coords	128
Copper Oxide	Fractional coords	35
Copper Tungsten Oxide	Fractional coords	193

Rwp = 5.58% S = 1.1546

6. X-Ray report of $Cu_3W_{0.99}Mo_{0.01}O_6$

Measurement conditions

X-Ray	40 kV , 40 mA	Scan speed / Duration time	2.5300 sec.
Goniometer	SmartLab(In-plane)	Step width	0.0110 deg
Attachment	RxRy	Scan axis	Theta/2-Theta
Filter	Cu_K-beta	Scan range	10.0000 - 89.9920 deg
CBO selection slit	BB	Incident slit	0.663deg
Diffracted beam mono.	None	Length limiting slit	2.0mm
Detector	SC-70	Receiving slit #1	0.663deg
Scan mode	STEP	Receiving slit #2	0.300mm

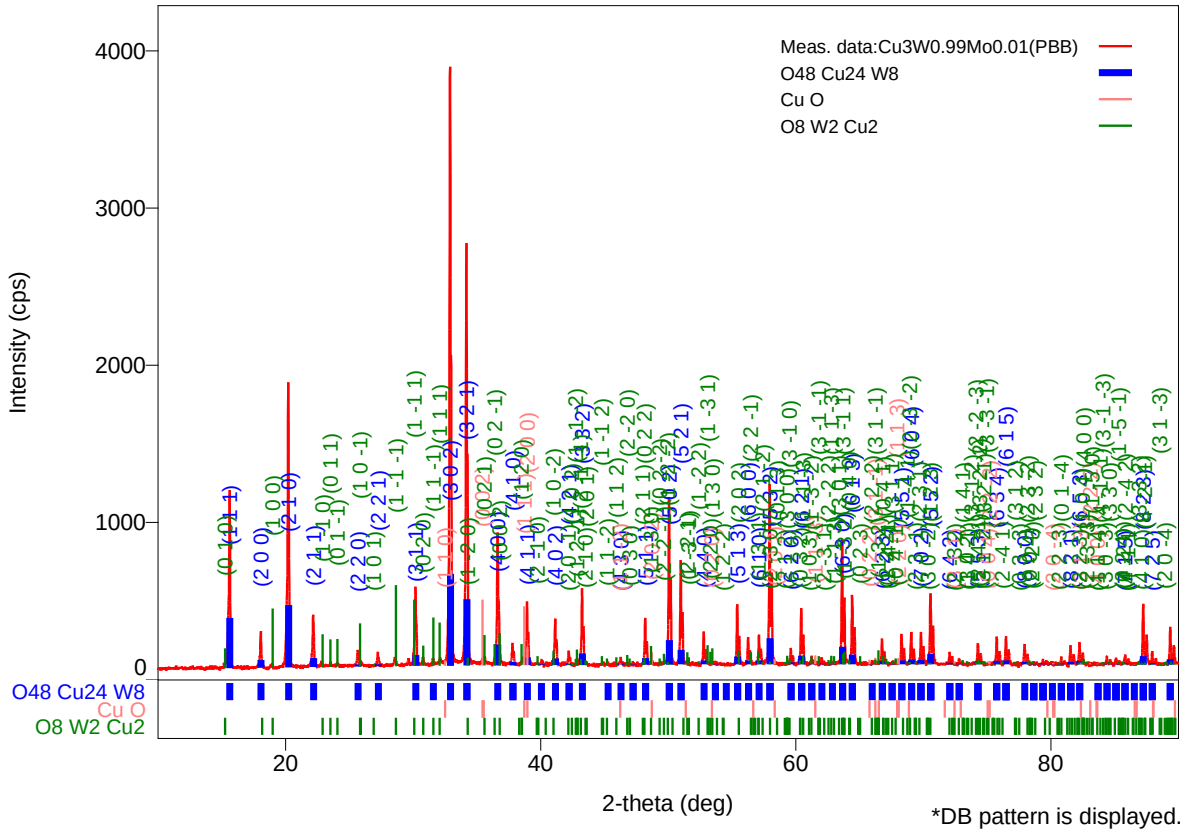

*DB pattern is displayed.

Peak list

No.	2-theta(deg)	d(ang.)	Height(cps)	FWHM(deg)	Int. I(cps deg)	Int. W(deg)	Asym. factor
1	15.6232(13)	5.6674(5)	908(19)	0.075(2)	111.1(9)	0.122(4)	1.16(8)
2	18.070(3)	4.9052(9)	185(9)	0.065(6)	20.0(5)	0.108(8)	1.5(5)
3	18.934(10)	4.683(2)	17(3)	0.08(3)	2.0(4)	0.12(4)	0.6(7)
4	20.220(2)	4.3881(4)	1520(25)	0.077(3)	180(2)	0.119(3)	1.11(13)
5	22.175(3)	4.0056(5)	271(10)	0.082(5)	34.0(6)	0.125(7)	1.11(18)
6	23.52(7)	3.779(11)	12(2)	0.31(13)	7.6(13)	0.7(2)	0.6(3)
7	25.688(6)	3.4651(8)	80(6)	0.094(9)	11.2(4)	0.139(15)	2.9(11)
8	25.918(6)	3.4350(7)	28(3)	0.08(2)	4.3(4)	0.15(3)	0.7(6)
9	27.256(3)	3.2693(4)	79(6)	0.065(8)	9.3(4)	0.117(13)	2.1(4)
10	28.580(10)	3.1208(11)	43(4)	0.111(19)	8.2(4)	0.19(3)	0.9(5)
11	29.644(8)	3.0111(8)	29(3)	0.08(2)	3.4(5)	0.12(3)	1.5(16)
12	30.201(2)	2.9568(2)	442(13)	0.082(3)	55.7(8)	0.126(6)	1.3(2)
13	30.79(2)	2.9013(18)	27(3)	0.14(4)	6.7(6)	0.25(5)	1.5(15)
14	31.577(15)	2.8310(13)	31(4)	0.100(18)	4.0(4)	0.13(3)	1.8(15)
15	32.133(14)	2.7833(12)	24(3)	0.10(4)	3.8(8)	0.15(5)	2(2)
16	32.9124(15)	2.71919(12)	3527(37)	0.0809(16)	387(3)	0.110(2)	1.59(14)
17	34.1918(13)	2.62031(10)	2469(31)	0.0787(14)	270(2)	0.109(2)	1.46(11)
18	35.58(5)	2.521(3)	31(3)	0.34(8)	18.8(12)	0.61(11)	2(2)
19	36.635(2)	2.45096(13)	760(17)	0.085(2)	94.5(10)	0.124(4)	1.25(15)
20	37.807(5)	2.3776(3)	128(7)	0.077(5)	15.4(5)	0.120(10)	1.3(4)
21	38.949(5)	2.3105(3)	343(12)	0.084(6)	46.2(12)	0.134(8)	1.6(5)
22	40.092(4)	2.2472(2)	30(3)	0.07(2)	4.0(4)	0.13(3)	5(6)
23	41.152(3)	2.19179(15)	282(11)	0.080(3)	30.6(6)	0.109(6)	1.3(2)
24	42.208(6)	2.1393(3)	77(6)	0.077(6)	7.8(4)	0.101(13)	0.9(4)
25	43.256(2)	2.08990(9)	461(14)	0.0757(19)	49.0(6)	0.106(4)	1.08(13)
26	46.280(10)	1.9601(4)	39(4)	0.070(13)	3.8(4)	0.10(2)	0.9(6)
27	48.209(3)	1.88612(10)	295(11)	0.080(2)	29.8(7)	0.101(6)	1.4(2)
28	50.0787(12)	1.82000(4)	1045(20)	0.0797(10)	109.3(8)	0.105(3)	1.15(7)
29	50.9931(17)	1.78949(6)	643(16)	0.0802(15)	67.8(8)	0.106(4)	1.04(10)
30	52.787(3)	1.73282(10)	200(9)	0.072(4)	19.0(7)	0.095(8)	0.73(16)
31	53.085(15)	1.7238(4)	14(2)	0.09(3)	1.7(5)	0.12(6)	0.73(16)
32	55.425(2)	1.65643(6)	366(12)	0.081(2)	37.6(7)	0.103(5)	1.30(16)
33	56.274(3)	1.63345(9)	168(8)	0.075(3)	17.3(4)	0.103(8)	1.0(2)
34	57.126(3)	1.61107(9)	181(8)	0.077(4)	19.1(5)	0.106(8)	1.2(2)
35	57.9663(12)	1.58971(3)	1165(21)	0.0806(11)	126.6(9)	0.109(3)	1.20(7)
36	59.613(6)	1.54966(13)	91(6)	0.076(6)	8.7(5)	0.096(12)	0.8(3)
37	60.438(2)	1.53047(5)	358(12)	0.081(2)	39.2(6)	0.110(5)	1.19(15)
38	61.245(7)	1.51223(15)	31(4)	0.10(3)	5.5(6)	0.18(4)	0.6(7)
39	62.042(6)	1.49470(12)	30(3)	0.078(16)	3.1(5)	0.11(3)	0.6(6)
40	63.6500(12)	1.46076(2)	789(18)	0.0830(12)	88.2(7)	0.112(3)	1.18(7)
41	64.4350(18)	1.44484(4)	429(13)	0.0833(19)	48.1(6)	0.112(5)	1.08(10)
42	66.775(4)	1.39979(8)	156(8)	0.080(5)	18.7(5)	0.120(9)	1.2(3)
43	68.300(3)	1.37219(6)	191(9)	0.082(3)	21.7(5)	0.113(8)	0.91(16)
44	69.061(3)	1.35892(6)	200(9)	0.089(3)	23.2(5)	0.116(8)	0.86(14)
45	69.832(3)	1.34580(6)	200(9)	0.081(4)	22.0(6)	0.110(8)	1.7(3)
46	70.5746(19)	1.33344(3)	455(13)	0.088(2)	54.3(7)	0.119(5)	1.13(10)

47	72.072(7)	1.30937(11)	68(5)	0.078(7)	7.0(4)	0.103(14)	0.9(4)
48	72.807(11)	1.29796(17)	33(4)	0.077(10)	2.8(4)	0.08(2)	0.9(5)
49	74.285(4)	1.27575(6)	134(7)	0.088(4)	15.3(5)	0.114(10)	0.82(17)
50	75.760(4)	1.25453(6)	165(8)	0.084(4)	19.1(5)	0.116(9)	1.0(2)
51	76.486(4)	1.24442(5)	171(8)	0.088(4)	19.9(5)	0.117(9)	0.98(18)
52	77.945(4)	1.22473(5)	122(7)	0.092(4)	14.3(5)	0.117(10)	1.2(2)
53	79.395(16)	1.2060(2)	28(3)	0.079(16)	2.6(5)	0.09(3)	2(2)
54	80.819(13)	1.18828(16)	32(4)	0.089(12)	3.1(5)	0.09(2)	0.7(4)
55	81.552(5)	1.17944(6)	107(7)	0.103(5)	13.2(5)	0.123(12)	1.3(3)
56	82.260(4)	1.17107(5)	134(7)	0.095(4)	17.2(4)	0.128(10)	1.3(2)
57	84.408(9)	1.14666(9)	50(4)	0.074(11)	5.9(4)	0.117(18)	1.3(9)
58	85.128(14)	1.13879(15)	28(3)	0.107(14)	3.2(5)	0.11(3)	1.7(9)
59	85.838(9)	1.13119(10)	56(5)	0.105(10)	7.8(5)	0.14(2)	1.7(7)
60	87.246(2)	1.11652(2)	381(12)	0.088(2)	48.8(6)	0.128(6)	1.07(12)
61	87.960(4)	1.10929(4)	70(5)	0.087(7)	8.3(4)	0.118(15)	1.4(3)
62	89.367(4)	1.09543(4)	233(10)	0.094(4)	32.1(7)	0.138(8)	0.89(17)

Quantitative analysis results (RIR)

Phase name	Content(%)
Copper Tungsten Oxide	85.8(14)
Tenorite, syn	4.8(6)
Scheelite (Cu-exchanged) - synthetic	9.3(8)

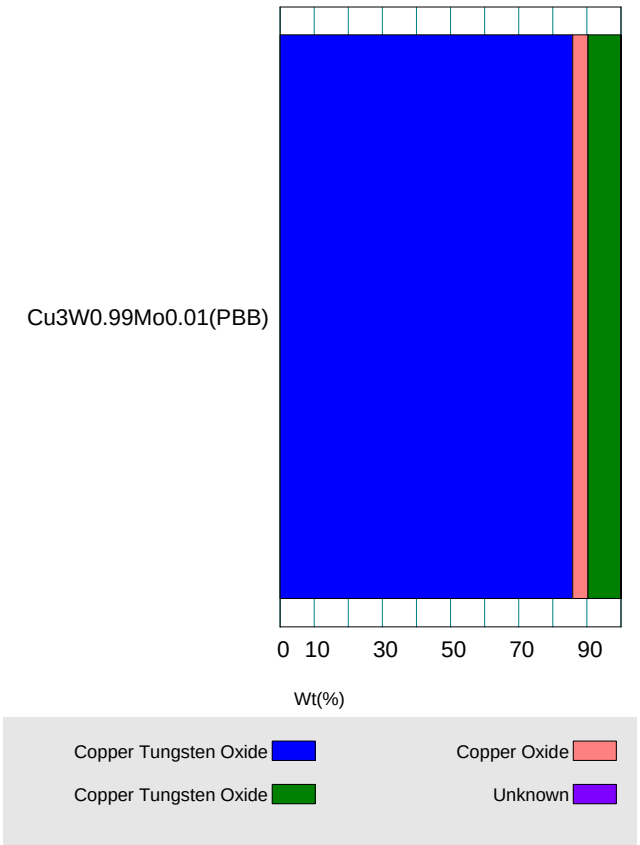

Crystal structure analysis results

Indexing

Phase name	Formula	Figure of merit	Phase reg. detail	DB card number
Copper Tungsten	O48 Cu24 W8	0.455	ICDD (PDF2.DAT)	01-071-2208
Tenorite, syn	Cu O	2.712	ICDD (PDF2.DAT)	00-045-0937
Scheelite (Cu-	O8 W2 Cu2	1.513	ICDD (PDF2.DAT)	01-088-0269

Quantitative analysis results

Lattice information

Phase name	a(A)	b(A)	c(A)	alpha(deg)	beta(deg)	gamma(deg)	V(A^3)
Copper	9.79439(15	9.79439(15	9.79439(15	90.000000	90.000000	90.000000	939.58(3)
Tenorite,	4.676(2)	3.4014(14)	5.117(2)	90.000000	99.79(3)	90.000000	80.19(6)
Scheelite	4.7057(11)	5.842(2)	4.870(2)	88.24(2)	92.783(19)	97.256(18)	132.59(8)

Phase name	Space group	Z	Z'	Calc. density(g/cm^3)
Copper Tungsten	205 : Pa-3	1	0.042	6.645
Tenorite, syn	15 : C12/c1,unique-b,cell-1	1	0.125	6.506
Scheelite (Cu-	2 : P-1	1	0.500	7.760

Refinement

Measurement range: 10.0000-89.9920deg Refinement range: 10.0000-89.9920deg (1.09 A)
Number of refined parameters: 87

Phase name	Atomic coords	# of indep. reflns
Copper Tungsten Oxide	Fractional coords	128
Tenorite, syn	Fractional coords	34
Scheelite (Cu-exchanged) -	Fractional coords	219

Rwp = 7.78% S = 1.4568

7. X-Ray report of $Cu_3W_{0.975}Mo_{0.025}O_6$

Measurement conditions

X-Ray	40 kV , 44 mA	Scan speed / Duration time	2.5300 sec.
Goniometer	SmartLab(In-plane)	Step width	0.0100 deg
Attachment	RxRy	Scan axis	Theta/2-Theta
Filter	Cu_K-beta	Scan range	10.0000 - 90.0000 deg
CBO selection slit	BB	Incident slit	0.663deg
Diffracted beam mono.	None	Length limiting slit	2.0mm
Detector	SC-70	Receiving slit #1	0.663deg
Scan mode	STEP	Receiving slit #2	0.300mm

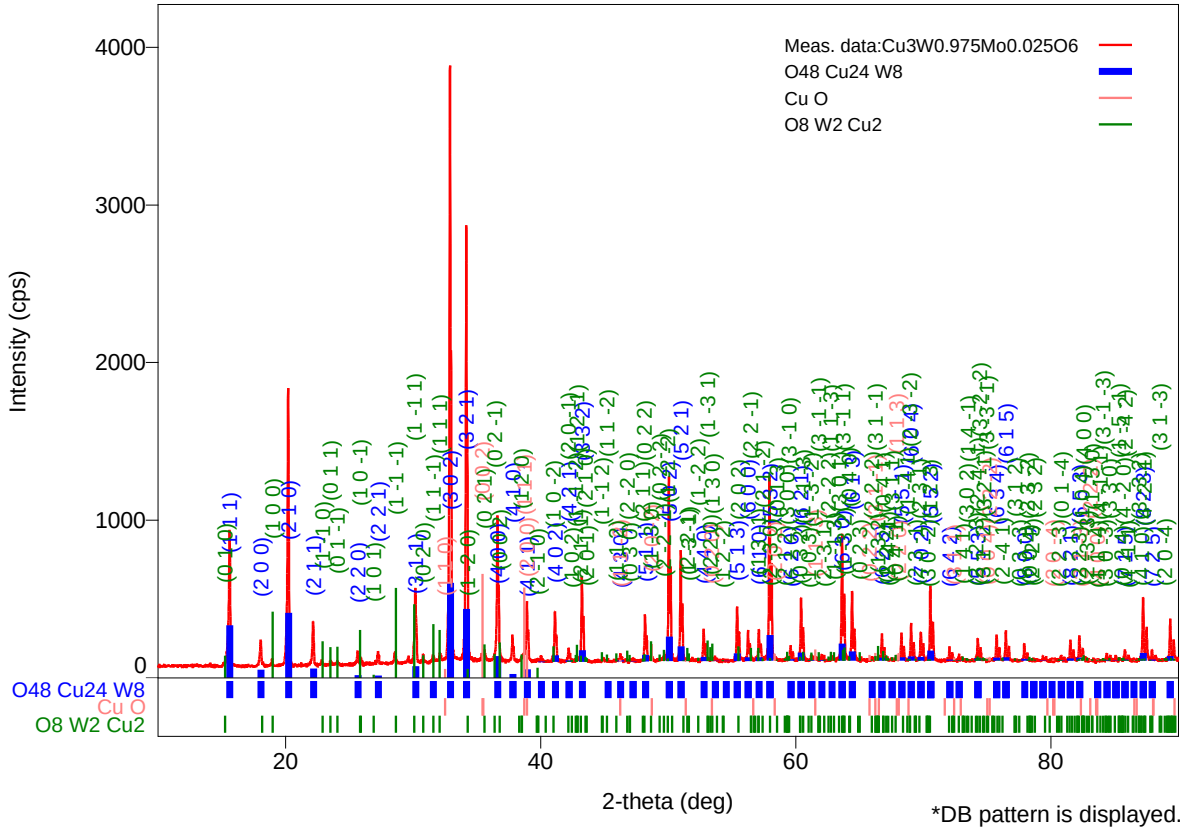

Peak list

No.	2-theta(deg)	d(ang.)	Height(cps)	FWHM(deg)	Int. I(cps deg)	Int. W(deg)	Asym. factor
1	15.6191(17)	5.6689(6)	671(16)	0.083(3)	91.0(9)	0.136(5)	1.17(10)
2	18.069(7)	4.9054(19)	114(7)	0.114(5)	15.2(6)	0.133(13)	2.2(6)
3	18.244(7)	4.8587(18)	16(3)	0.045(19)	0.9(3)	0.05(3)	2.2(6)
4	18.948(4)	4.6798(10)	34(4)	0.057(12)	2.3(3)	0.068(17)	0.6(5)
5	20.2098(15)	4.3904(3)	1490(24)	0.074(2)	164.6(16)	0.110(3)	0.87(8)
6	22.179(4)	4.0049(8)	219(9)	0.093(5)	25.2(6)	0.115(8)	1.7(3)
7	22.83(2)	3.893(4)	20(3)	0.08(3)	1.7(4)	0.09(3)	1.0(11)
8	23.533(9)	3.7774(15)	19(3)	0.051(16)	1.4(3)	0.07(3)	1.6(11)
9	25.669(7)	3.4677(10)	67(5)	0.081(10)	7.5(4)	0.113(15)	1.9(8)
10	25.930(4)	3.4333(5)	35(4)	0.050(10)	2.2(4)	0.064(17)	0.7(9)
11	27.266(7)	3.2680(9)	64(5)	0.091(9)	7.6(4)	0.118(16)	2.7(13)
12	28.597(5)	3.1190(6)	60(5)	0.092(10)	8.5(4)	0.141(19)	2.2(5)
13	29.674(10)	3.0082(10)	30(3)	0.102(17)	4.2(4)	0.14(3)	5(3)
14	30.088(3)	2.9677(3)	87(6)	0.083(9)	9.4(12)	0.11(2)	1.39(15)
15	30.2027(17)	2.95668(16)	423(13)	0.081(2)	44.0(15)	0.104(7)	1.39(15)
16	30.795(7)	2.9012(6)	45(4)	0.081(12)	5.9(4)	0.13(2)	1.3(6)
17	31.548(7)	2.8336(6)	33(4)	0.11(3)	7.0(5)	0.21(4)	0.6(5)
18	32.115(12)	2.7849(10)	34(4)	0.10(4)	4.1(10)	0.12(4)	1.1(13)
19	32.9085(16)	2.71950(13)	3556(37)	0.0772(17)	382(4)	0.107(2)	1.35(13)

20	34.1865(13)	2.62070(9)	2560(32)	0.0809(14)	282(2)	0.110(2)	1.38(10)
21	35.59(2)	2.5204(14)	44(4)	0.31(5)	21.8(11)	0.49(7)	2.4(17)
22	36.634(2)	2.45106(14)	830(18)	0.081(2)	104.9(11)	0.126(4)	1.5(2)
23	37.799(4)	2.3781(3)	149(8)	0.075(5)	17.8(5)	0.119(9)	1.0(3)
24	38.954(5)	2.3103(3)	338(12)	0.089(6)	50.6(12)	0.150(9)	2.2(7)
25	39.778(14)	2.2643(8)	15(2)	0.09(5)	1.9(4)	0.13(5)	1.8(12)
26	40.065(6)	2.2487(3)	28(3)	0.086(14)	3.4(5)	0.12(3)	1.8(12)
27	41.144(3)	2.19217(13)	318(11)	0.078(2)	34.4(6)	0.108(6)	1.4(2)
28	42.211(6)	2.1392(3)	88(6)	0.074(5)	8.9(4)	0.101(12)	1.1(4)
29	43.2511(19)	2.09013(9)	527(14)	0.0766(18)	56.2(7)	0.107(4)	1.04(12)
30	44.88(4)	2.0179(15)	13(2)	0.13(5)	2.3(5)	0.17(7)	0.6(7)
31	46.272(10)	1.9604(4)	43(4)	0.074(14)	4.8(4)	0.11(2)	1.9(12)
32	47.24(3)	1.9225(10)	15(2)	0.06(3)	1.1(4)	0.07(4)	0.9(16)
33	48.202(2)	1.88638(9)	284(11)	0.083(2)	31.0(5)	0.109(6)	1.24(17)
34	48.639(9)	1.8705(3)	21(3)	0.13(2)	2.9(5)	0.14(4)	0.6(4)
35	50.0747(12)	1.82013(4)	1142(21)	0.0807(10)	120.3(9)	0.105(3)	1.16(7)
36	50.9944(13)	1.78944(4)	698(17)	0.0808(11)	74.1(7)	0.106(3)	1.26(9)
37	52.797(4)	1.73251(11)	197(9)	0.076(3)	20.2(6)	0.102(7)	1.3(3)
38	55.424(2)	1.65645(6)	348(12)	0.0853(19)	36.7(6)	0.106(5)	1.39(16)
39	56.271(4)	1.63352(9)	182(8)	0.076(4)	20.0(5)	0.110(8)	1.1(2)
40	57.128(3)	1.61102(8)	190(9)	0.080(3)	20.1(5)	0.106(7)	1.6(3)
41	57.9611(11)	1.58984(3)	1176(22)	0.0843(10)	132.9(8)	0.113(3)	1.19(6)
42	59.615(6)	1.54962(14)	89(6)	0.086(6)	9.3(5)	0.104(13)	1.1(3)
43	60.431(2)	1.53062(5)	399(13)	0.0835(19)	43.2(6)	0.108(5)	0.99(10)
44	61.237(18)	1.5124(4)	21(3)	0.15(3)	5.3(7)	0.25(7)	0.7(3)
45	62.056(12)	1.4944(3)	36(4)	0.072(16)	3.7(5)	0.10(2)	0.9(8)
46	63.6459(12)	1.46084(2)	806(18)	0.0874(12)	93.1(7)	0.115(3)	1.15(7)
47	64.4321(19)	1.44490(4)	424(13)	0.0878(18)	48.6(6)	0.115(5)	1.20(11)
48	65.986(11)	1.4146(2)	17(3)	0.11(4)	3.2(6)	0.19(6)	0.5(6)
49	66.772(5)	1.39983(8)	154(8)	0.083(5)	18.8(6)	0.122(10)	1.4(3)
50	68.303(3)	1.37214(5)	167(8)	0.086(3)	18.9(4)	0.113(8)	1.23(18)
51	69.060(3)	1.35894(5)	214(9)	0.088(3)	23.8(5)	0.111(7)	0.93(12)
52	69.819(3)	1.34601(6)	185(9)	0.088(3)	20.2(6)	0.109(8)	1.15(18)
53	70.5737(18)	1.33345(3)	475(14)	0.0903(18)	55.2(7)	0.116(5)	1.19(10)
54	72.061(8)	1.30955(13)	63(5)	0.089(8)	6.1(5)	0.097(16)	0.9(3)
55	72.823(4)	1.29772(6)	44(4)	0.035(8)	3.2(3)	0.073(15)	1.1(5)
56	74.285(4)	1.27575(5)	142(7)	0.087(4)	16.4(4)	0.115(9)	0.90(17)
57	75.7695(16)	1.25440(2)	166(8)	0.079(2)	17.8(5)	0.107(8)	2.6(2)
58	76.490(3)	1.24437(4)	174(8)	0.091(3)	19.7(5)	0.113(8)	1.20(16)
59	77.9305(17)	1.22493(2)	103(6)	0.079(5)	11.1(5)	0.108(11)	0.6(2)
60	79.401(5)	1.20589(6)	26(3)	0.070(14)	2.3(4)	0.09(3)	3(5)
61	80.816(15)	1.18832(18)	28(3)	0.085(14)	2.5(5)	0.09(3)	0.8(5)
62	81.540(5)	1.17958(6)	121(7)	0.092(5)	13.8(5)	0.114(11)	0.92(19)
63	82.254(4)	1.17114(5)	157(8)	0.086(4)	19.9(5)	0.127(10)	0.85(19)
64	84.411(6)	1.14663(6)	44(4)	0.097(9)	5.3(4)	0.12(2)	2.1(6)
65	85.094(5)	1.13916(5)	30(3)	0.086(15)	3.3(4)	0.11(3)	0.5(4)
66	85.823(8)	1.13134(9)	62(5)	0.107(8)	8.3(5)	0.134(19)	1.0(3)
67	87.250(2)	1.11647(2)	410(13)	0.094(2)	55.1(7)	0.134(6)	1.42(16)
68	87.948(7)	1.10941(7)	66(5)	0.095(7)	8.3(5)	0.125(17)	1.0(3)
69	89.370(3)	1.09540(3)	251(10)	0.095(3)	34.8(6)	0.139(8)	0.98(15)

Quantitative analysis results (RIR)

Phase name	Content(%)
Copper Tungsten Oxide	93(2)
Tenorite, syn	2.4(4)
Scheelite (Cu-exchanged) - synthetic	4.6(11)

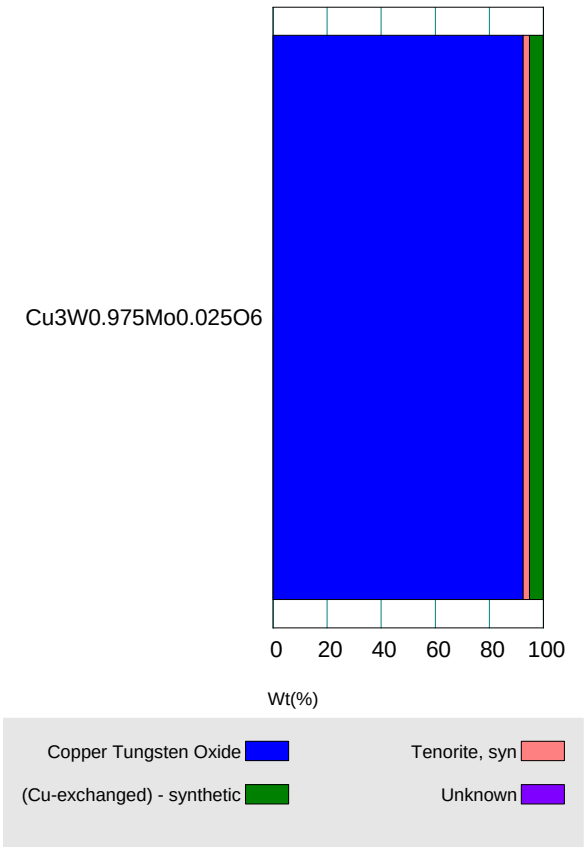

Crystal structure analysis results

Indexing

Phase name	Formula	Figure of merit	Phase reg. detail	DB card number
Copper Tungsten	O48 Cu24 W8	0.568	ICDD (PDF2.DAT)	01-071-2208
Tenorite, syn	Cu O	2.755	ICDD (PDF2.DAT)	00-045-0937
Scheelite (Cu-	O8 W2 Cu2	1.556	ICDD (PDF2.DAT)	01-088-0269

Quantitative analysis results

Lattice information

Phase name	a(A)	b(A)	c(A)	alpha(deg)	beta(deg)	gamma(deg)	V(A^3)
Copper	9.7936(2)	9.7936(2)	9.7936(2)	90.000000	90.000000	90.000000	939.36(4)
Tenorite,	4.75(5)	3.19(4)	5.51(7)	90.000000	106.3(8)	90.000000	80.1(16)
Scheelite	4.7085(11)	5.8327(10)	4.8734(9)	88.41(2)	92.668(13)	97.283(16)	132.58(5)

Phase name	Space group	Z	Z'	Calc. density(g/cm^3)

Copper Tungsten	205 : Pa-3	1	0.042	6.645
Tenorite, syn	15 : C12/c1,unique-b,cell-1	1	0.125	6.506
Scheelite (Cu-	2 : P-1	1	0.500	7.760

Refinement

Measurement range: 10.0000-90.0000deg Refinement range: 40.0000-90.0000deg(1.09 A)
Number of refined parameters: 87

Phase name	Atomic coords	# of indep. reflns
Copper Tungsten Oxide	Fractional coords	128
Tenorite, syn	Fractional coords	34
Scheelite (Cu-exchanged) -	Fractional coords	220

Rwp = 5.47% S = 1.0492

8. X-Ray report of $Cu_3W_{0.95}Mo_{0.05}O_6$

Measurement conditions

X-Ray	40 kV , 44 mA	Scan speed / Duration time	2.6000 sec.
Goniometer	SmartLab(In-plane)	Step width	0.0090 deg
Attachment	RxRy	Scan axis	Theta/2-Theta
Filter	Cu_K-beta	Scan range	10.0000 - 89.9920 deg
CBO selection slit	BB	Incident slit	0.663deg
Diffracted beam mono.	None	Length limiting slit	2.0mm
Detector	SC-70	Receiving slit #1	0.663deg
Scan mode	STEP	Receiving slit #2	0.300mm

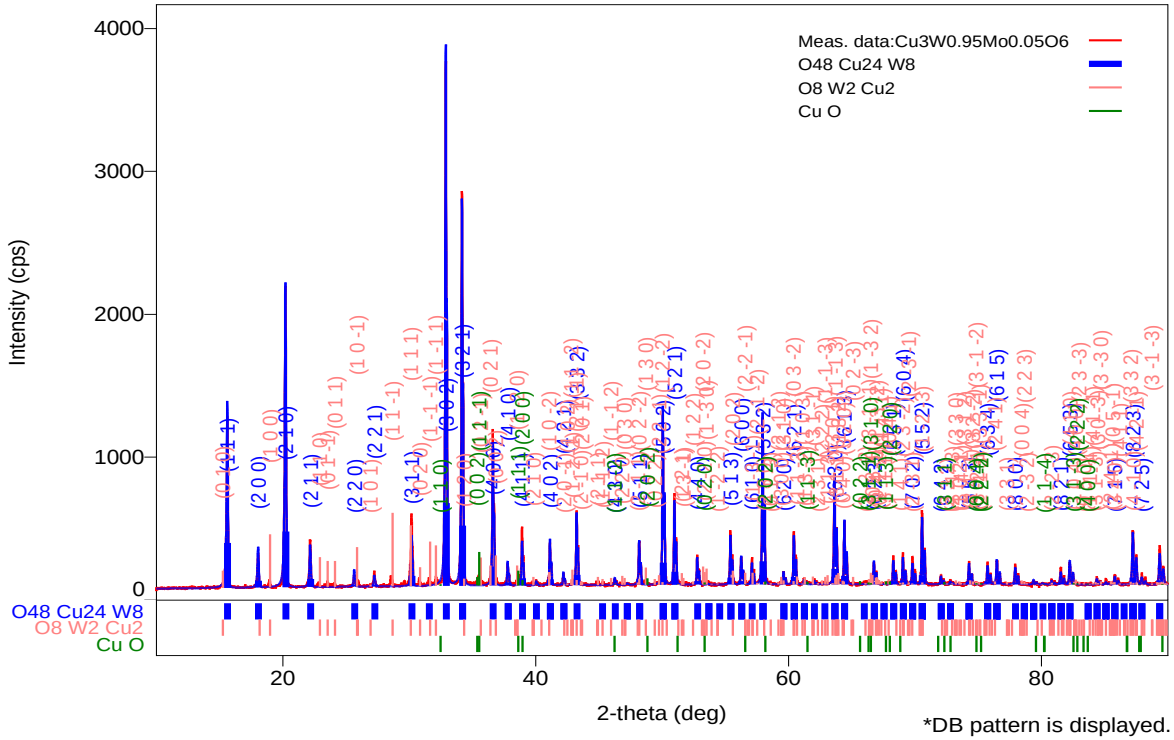

*DB pattern is displayed.

Peak list

No.	2-theta(deg)	d(ang.)	Height(cps)	FWHM(deg)	Int. I(cps deg)	Int. W(deg)	Asym. factor
1	15.6224(15)	5.6677(5)	947(19)	0.079(2)	121.9(10)	0.129(4)	1.41(12)
2	18.052(4)	4.9101(10)	178(8)	0.091(5)	23.6(4)	0.132(8)	1.1(2)
3	18.228(4)	4.8629(10)	27(3)	0.047(11)	1.8(2)	0.068(17)	1.1(2)
4	18.959(13)	4.677(3)	39(4)	0.09(2)	5.5(4)	0.14(2)	1.7(11)
5	20.2078(15)	4.3908(3)	1789(26)	0.077(2)	208.6(19)	0.117(3)	0.93(8)
6	22.173(2)	4.0058(4)	272(10)	0.085(4)	33.2(4)	0.122(6)	1.49(19)
7	22.851(17)	3.888(3)	23(3)	0.08(2)	2.9(3)	0.13(3)	3(5)
8	23.534(7)	3.7772(12)	35(4)	0.040(13)	3.0(4)	0.085(19)	1.6(15)
9	24.074(15)	3.694(2)	23(3)	0.07(3)	2.8(4)	0.12(3)	2(4)
10	25.651(6)	3.4701(9)	66(5)	0.096(10)	8.6(4)	0.132(17)	0.8(3)
11	25.926(6)	3.4339(8)	40(4)	0.078(12)	4.3(3)	0.107(18)	0.8(3)
12	27.250(5)	3.2700(6)	79(6)	0.082(8)	9.3(4)	0.117(14)	1.2(4)
13	28.567(4)	3.1222(4)	57(5)	0.105(15)	9.1(4)	0.16(2)	0.8(4)
14	29.619(9)	3.0137(9)	24(3)	0.09(3)	2.6(5)	0.11(4)	1.3(12)
15	30.1909(19)	2.95781(18)	442(13)	0.085(3)	59.6(8)	0.135(6)	1.02(11)
16	30.806(8)	2.9001(7)	47(4)	0.072(10)	5.0(4)	0.105(17)	1.7(10)
17	31.566(13)	2.8320(12)	38(4)	0.08(2)	5.8(5)	0.16(3)	0.7(6)
18	32.128(8)	2.7837(7)	39(4)	0.08(2)	4.7(8)	0.12(3)	0.8(9)
19	32.9046(15)	2.71981(12)	3315(36)	0.0824(16)	376(3)	0.113(2)	1.57(13)
20	34.1848(11)	2.62082(8)	2558(31)	0.0796(12)	281.6(19)	0.110(2)	1.34(9)
21	35.53(4)	2.525(3)	46(4)	0.28(3)	20.4(10)	0.45(6)	1.3(8)
22	36.6252(18)	2.45160(11)	996(20)	0.0739(18)	113.1(10)	0.114(3)	1.10(13)
23	37.799(5)	2.3781(3)	133(7)	0.081(5)	16.4(5)	0.123(10)	1.2(4)
24	38.949(5)	2.3105(3)	338(11)	0.090(6)	50.2(12)	0.148(9)	2.1(7)
25	40.074(14)	2.2482(7)	16(2)	0.18(4)	6.0(8)	0.37(11)	4(7)
26	41.139(2)	2.19244(11)	273(10)	0.082(2)	31.8(5)	0.117(6)	1.00(14)
27	42.210(3)	2.13926(15)	71(5)	0.083(4)	6.8(3)	0.096(11)	1.2(2)
28	43.2516(18)	2.09011(8)	491(14)	0.0757(19)	54.8(6)	0.112(4)	1.21(14)
29	46.052(15)	1.9693(6)	8.4(18)	0.07(3)	0.6(3)	0.07(5)	1.7(10)
30	46.278(11)	1.9602(4)	38(4)	0.083(9)	3.3(5)	0.09(2)	1.7(10)
31	47.226(8)	1.9231(3)	11(2)	0.06(2)	0.7(3)	0.06(4)	0.8(13)
32	48.207(3)	1.88620(9)	299(11)	0.080(2)	31.7(6)	0.106(6)	1.8(3)
33	50.0717(10)	1.82023(3)	1169(21)	0.0795(8)	123.0(8)	0.105(3)	1.14(6)
34	50.9916(15)	1.78953(5)	637(16)	0.0804(13)	68.1(7)	0.107(4)	1.25(10)
35	52.792(3)	1.73266(10)	196(9)	0.076(3)	19.8(5)	0.101(7)	1.2(3)
36	53.55(3)	1.7099(9)	12(2)	0.21(9)	3.9(7)	0.33(12)	1.1(13)
37	55.417(2)	1.65665(6)	367(12)	0.0805(19)	39.6(6)	0.108(5)	1.15(13)
38	56.273(3)	1.63345(9)	185(8)	0.085(3)	19.6(7)	0.105(8)	1.2(2)
39	56.520(12)	1.6269(3)	14(2)	0.09(3)	1.4(5)	0.11(5)	1.2(2)
40	57.125(3)	1.61109(8)	182(8)	0.079(4)	19.5(5)	0.108(8)	1.7(3)
41	57.9593(9)	1.58988(2)	1162(21)	0.0836(8)	132.4(7)	0.114(3)	1.23(5)
42	59.613(6)	1.54966(13)	85(6)	0.084(6)	8.9(4)	0.105(12)	0.9(3)
43	60.433(2)	1.53058(5)	366(12)	0.0869(19)	41.2(6)	0.113(5)	1.19(12)
44	61.267(3)	1.51173(8)	40(4)	0.096(11)	4.8(5)	0.12(2)	5(4)
45	62.066(18)	1.4942(4)	21(3)	0.13(4)	5.4(6)	0.26(6)	4(5)
46	63.6442(12)	1.46088(3)	764(17)	0.0882(12)	90.5(7)	0.119(4)	1.25(8)

47	64.4312(18)	1.44492(4)	422(13)	0.0882(18)	48.6(6)	0.115(5)	1.08(9)
48	66.770(4)	1.39987(7)	155(8)	0.085(4)	20.3(4)	0.131(9)	1.3(3)
49	68.297(3)	1.37224(5)	187(8)	0.083(3)	21.2(5)	0.113(8)	0.96(15)
50	69.058(3)	1.35897(5)	207(9)	0.086(3)	23.0(5)	0.111(7)	0.90(13)
51	69.818(3)	1.34603(5)	187(8)	0.088(3)	21.1(5)	0.113(8)	1.04(15)
52	70.5721(17)	1.33348(3)	500(14)	0.0864(17)	57.5(6)	0.115(4)	1.15(9)
53	72.071(7)	1.30939(10)	64(5)	0.086(7)	6.1(4)	0.096(14)	1.1(3)
54	72.800(5)	1.29807(8)	27(3)	0.103(16)	3.0(5)	0.11(3)	0.6(4)
55	74.286(4)	1.27573(6)	137(7)	0.089(4)	15.6(5)	0.114(10)	0.93(19)
56	75.755(3)	1.25461(5)	152(8)	0.090(3)	18.1(4)	0.119(9)	1.05(16)
57	76.482(3)	1.24448(4)	161(8)	0.092(3)	17.6(5)	0.109(8)	0.89(13)
58	77.947(5)	1.22472(6)	119(7)	0.089(5)	13.7(5)	0.116(11)	1.3(3)
59	79.411(15)	1.20577(19)	24(3)	0.092(17)	2.4(5)	0.10(3)	3(3)
60	80.810(3)	1.18839(4)	36(4)	0.075(9)	3.0(4)	0.084(19)	0.5(3)
61	81.551(5)	1.17945(6)	114(7)	0.088(5)	13.0(5)	0.114(11)	1.6(4)
62	82.254(4)	1.17114(5)	148(8)	0.094(4)	18.5(5)	0.126(10)	0.92(17)
63	84.401(10)	1.14674(11)	46(4)	0.098(10)	5.3(4)	0.12(2)	1.3(6)
64	85.108(4)	1.13901(4)	32(4)	0.072(13)	3.4(4)	0.11(2)	0.9(7)
65	85.818(7)	1.13139(8)	70(5)	0.090(9)	9.2(5)	0.132(17)	0.9(4)
66	87.242(2)	1.11656(2)	387(12)	0.098(2)	53.3(6)	0.138(6)	0.97(10)
67	87.940(2)	1.10948(2)	71(5)	0.088(7)	8.5(5)	0.120(16)	0.5(2)
68	89.375(3)	1.09535(3)	261(10)	0.101(3)	38.4(5)	0.147(8)	1.21(15)

Quantitative analysis results (RIR)

Phase name	Content(%)
Copper Tungsten Oxide	91(3)
Tenorite	3.3(19)
Copper Tungsten Oxide	5.7(11)

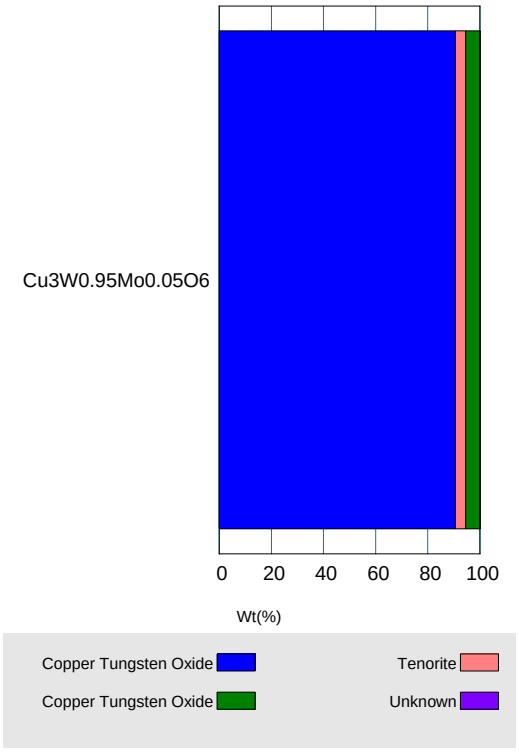

Crystal structure analysis results

Indexing

Phase name	Formula	Figure of merit	Phase reg. detail	DB card number
Copper Tungsten	O48 Cu24 W8	0.399	ICDD (PDF2.DAT)	01-071-2208
Tenorite	Cu O	2.792	ICDD (PDF2.DAT)	01-072-0629
Copper Tungsten	O8 W2 Cu2	1.221	ICDD (PDF2.DAT)	01-080-1918

Quantitative analysis results

Lattice information

Phase name	a(A)	b(A)	c(A)	alpha(deg)	beta(deg)	gamma(deg)	V(A^3)
Copper	9.7933(2)	9.7933(2)	9.7933(2)	90.000000	90.000000	90.000000	939.26(4)
Tenorite	4.6621(5)	3.40614(13	5.1125(5)	90.000000	99.758(8)	90.000000	80.011(12)
Copper	4.7138(10)	5.8425(11)	4.8791(11)	91.635(18)	92.647(12)	82.597(13)	133.07(5)

Phase name	Space group	Z	Z'	Calc. density(g/cm^3)
Copper Tungsten	205 : Pa-3	1	0.042	6.645
Tenorite	15 : C12/c1,unique-b,cell-1	1	0.125	6.515
Copper Tungsten	2 : P-1	1	0.500	7.816

Refinement

Measurement range: 10.0000-89.9920deg Refinement range: 40.0000-89.9920deg(1.09 A)
Number of refined parameters: 87

Phase name	Atomic coords	# of indep. reflns
Copper Tungsten Oxide	Fractional coords	128
Tenorite	Fractional coords	34
Copper Tungsten Oxide	Fractional coords	220

Rwp = 5.53% S = 1.0738

Bibliography

[1] Alexander Krimmel, *Electronically highly correlated ternary transition metal oxides*, (2003)

[2] Van Uitert, L.G. Rubin, J.J. and W.A.J. Bonner, *Am. Ceram. Soc.* 46(1963) 512

[3] Clark, G.M. and Doyle, W.P. *Spectrochim. Acta* 22(1966) 1441

[4] Conroy, L.E. and Sienko, M.J. J.*Am.Chem.Soc.* 79(1957) 4048

[5] Sienko, M.J. and Weller, P.F. *Inorg.Chem*. 1(1962)324

[6] E. Gebert and L. Kihlborg, *Acta Chem. Sand.* 23(1969)*221*

[7] F.A. Benko, C.L. MacLaurin, and F.P. Koffyberg, *Materials Research Bulletin*, V17.133-136(1982)

[8] M. Hase, K. Uchinokura, *Phys. Rev.* B215(1995)325

[9] Y. Fudamoto, M. Hase, and K. Uchinokura, G.M. Luke, *Phys. Rev.* B65(2002) 174428

[10] H. Kuroe, private communication

[11] J.C. Bonner, L.Kihlborg, *Acta Chem. Scand.* 13(1969) 221

[12] www.rigaku.com, Intelligent X-ray diffraction (XRD) system – Chapter 2

[13] *Introduction Solid Physics*, Charles Kittel, 299

[14] *Introduction Solid Physics*, Charles Kittel, 305

[15] www.nde-ed.org, Education Resources, *The Hysteresis Loop and Magnetic Properties*

[16] *Introduction Solid Physics*, Charles Kittel, 342

[17] P. Pissis, A. Kyritsis, *Solid State Ionics 97, 105* (1997)

[18] M. K. Ram, S. Annapoorni, S. S. Pandey, B. D,Malhotra, *Polymer 39, 3399* (1998)

[19] R. I. Mohamed, *Journal of Physics and Chemistry of Solids 61, 1357* (2000)

[20] A. Tataroglu, S. Altındal, M. M. Bulbul, *Microelectronic Engineering, 81,140* (2005)

[21] I. Chaabane, F. Hlel, K. Guidara, *Ionics, 16, 371* (2010)

[22] E. H. Rhoderick, R. H. Williams, *Metal– Semiconductor Contacts, second ed., Oxford University Press, Oxford,* (1988)

[23] E. H. Nicollian, A. Goetzberger, *Appl. Phys. Lett. 7, 216* (1965)

[24] K. Prabakar, S. K. Narayandass, D. Mangalaraj, *Phys.Status Solidi A, 199, 507* (2003)

[25] http://shodhganga.inflibnet.ac.in/bitstream/10603/48048/16/16_chapter%206.pdf

[26] A Junod et al, *Journal of Physics: Condensed Matter*, Volume 1, 43,8021-8034(1989)

[27] Joseph E. Yourey, Joshua B. Kurta, and Bart M. Bartlett, *Inorganic Chemistry*, 2012,51,10394-10401(2012)